Master's thesis

NTNU
Norwegian University of Science and Technology
Faculty of Natural Sciences
Department of Physics

Johannes Røsok Eskilt

Triplet Proximity Effect in Heterostructures with Spin-Orbit Coupling and Precessing Magnetic Fields

Master's thesis in Applied Physics and Mathematics
Supervisor: Jacob Linder
June 2019

NTNU
Norwegian University of
Science and Technology

Johannes Røsok Eskilt

Triplet Proximity Effect in Heterostructures with Spin-Orbit Coupling and Precessing Magnetic Fields

Master's thesis in Applied Physics and Mathematics
Supervisor: Jacob Linder
June 2019

Norwegian University of Science and Technology
Faculty of Natural Sciences
Department of Physics

NTNU
Norwegian University of
Science and Technology

Abstract

We will use the quasiclassical theory of superconductivity in the diffusive limit to look at two different research projects. The first project looks at a lateral Josephson junction with intrinsic Rashba type spin-orbit coupling which we show is able to carry a long-ranged supercurrent in a strongly polarized ferromagnet. This setup has focused on being experimentally feasible, and only an in-plane rotation of the magnetic field is needed to effectively turn off the long-ranged supercurrent. For some parameters, the in-plane rotation can also cause $0-\pi$ transitions which means there exists an angle of the in-plane rotation where the current is zero.

The next project looks at heterostructures where a ferromagnet has a precessing magnetic field. These systems are driven out of equilibrium, and we have created a framework for calculating observables by finding the Green's functions and distribution functions in a frame where the magnetic field is stationary. With this framework, we show how the superconductive ordering changes the results compared to a precessing magnetic field in a ferromagnet in proximity to only normal state materials. We are also able to show that a Josephson junction with a non-zero precession and non-zero macroscopic phase difference may experience charge accumulation which drives a resistive current. The resistive current can be tuned by the angular frequency of the magnetic field, and there may exist a frequency where the charge accumulation is zero. This charge accumulation is also present in the superconductors and therefore induces a voltage difference across the junction. We therefore conclude that the phase difference will change over time due to this voltage difference.

Sammendrag

Vi vil bruke den kvasiklassiske teorien om superledere i det diffuse grensesjiktet for å gjennomføre to forskjellige forskningsprosjekt. Det første prosjektet ser på et sidestilt Josephson-kobling med iboende, Rashba-type spinn-bane kobling som vi viser kan bære en langtrekkende superstrøm i en sterkt polarisert ferromagnet. Dette oppsettet har fokusert på å være eksperimentelt gjennomførbart, og bare en rotasjon av magnetfeltet i planet trengs for å effektivt skru av den langt-trekkende superstrømmen. For noen parametere kan rotasjonen i planet også forårsake en $0-\pi$-transisjon som betyr at det finnes en vinkel i planet hvor strømmen er null.

Det neste prosjektet ser på heterostrukturerer hvor en ferromagnet har et preseserende magnetfelt. Disse systemene er drevet ut av likevekt, og vi har laget et rammeverk for å regne ut observabler ved å finne Greens-funksjoner og fordelingsfunksjoner i en ramme der det magnetiske feltet er stasjonært. Med dette rammeverket viser vi hvordan superledende orden endrer resultatet sammenlignet med et preseserende magnetfelt i en ferromagnet i nærheten av bare metaller i normal tilstand. Vi viser også at en Josephson-kobling med en presesjon og makroskopisk faseforskjell ulik null kan erfare en ladningsakkumulering som driver en resistiv strøm. Den resistive strømmen kan bli stilt inn av den angulære frekvensen til magnetfeltet, og det kan finnes en frekvens hvor ladningsakkumuleringen er null. Denne ladningsakkumuleringen finnes også sted i superlederne som induserer en spenningsforskjell over koblingen. Vi konkluderer derfor at faseforskjellen vil endre seg over tid på grunn av denne spenningsforskjellen.

Preface

The submission of this thesis concludes my five-year study for the master's degree in Applied Physics and Mathematics at the Norwegian University of Science and Technology. I would especially thank my supervisor Jacob Linder for all the help he has given me. Thank you for your patience, our weekly meetings, your letters of recommendation and answering e-mails almost faster than I can type them. I also want to thank Jabir Ali Ouassou for his tips and tricks in making the numerical calculations go faster.

I also want to thank all my friends at the Student Society in Trondheim (Studentersamfundet i Trondhjem) for all the great memories and friendships. My time in Trondheim would not be anywhere near as joyful without you.

This master's thesis is the continuation of the last semester's specialization project. Much of my time last semester went into deriving the quasiclassical approximation and the Usadel equation in the dirty limit, and that is why I have not derived them in this thesis, nor gone into the microscopic theory of magnetization and superconductivity. I have rather spent time on subjects I did not fully understand at the beginning of the semester. The projects entailed a lot of programming in Matlab, but I have chosen to not supplement this thesis with the programming code. The code will be handed out upon request.

Johannes Røsok Eskilt

Trondheim, Norway

June, 2019

Notation

Throughout this thesis we will use SI units, but we will allows ourselves to set the reduced Planck's constant equal to 1, $\hbar = 1$, to reduce the immense amount of typing this would bring. We set e equal to the charge of the electron, $e = -|e|$.

The size of the matrices in this thesis will be symbolized as following:

$$\dim(\underline{A}) = 2 \times 2, \tag{1}$$

$$\dim(\hat{A}) = 4 \times 4, \tag{2}$$

$$\dim(\check{A}) = 8 \times 8. \tag{3}$$

If matrices of different sizes are multiplied or summed that should be interpreted as the smaller matrix being repeated along the diagonal. For example:

$$\hat{A}\check{B} = \mathrm{diag}(\hat{A}, \hat{A})\check{B}. \tag{4}$$

The Pauli matrices are given as

$$\underline{\sigma}_1 = \begin{bmatrix} 0 & 1 \\ 1 & 0 \end{bmatrix} \quad \underline{\sigma}_2 = \begin{bmatrix} 0 & -i \\ i & 0 \end{bmatrix} \quad \underline{\sigma}_3 = \begin{bmatrix} 1 & 0 \\ 0 & -1 \end{bmatrix}. \tag{5}$$

In spin-Nambu space, we will also for $n \in \{1, 2, 3\}$ define the matrices

$$\hat{\sigma}_n = \mathrm{diag}(\underline{\sigma}_n, \underline{\sigma}_n^*). \tag{6}$$

We may write these matrices as vectors which should be interpreted as $\underline{\boldsymbol{\sigma}} = (\underline{\sigma}_1, \underline{\sigma}_2, \underline{\sigma}_3)$ and $\hat{\boldsymbol{\sigma}} = (\hat{\sigma}_1, \hat{\sigma}_2, \hat{\sigma}_3)$.

We will also generalize the Pauli matrices to a 4×4 dimensional space,

$$\hat{\tau}_1 = \begin{bmatrix} 0 & 0 & 0 & 1 \\ 0 & 0 & 1 & 0 \\ 0 & 1 & 0 & 0 \\ 1 & 0 & 0 & 0 \end{bmatrix} \quad \hat{\tau}_2 = \begin{bmatrix} 0 & 0 & 0 & -i \\ 0 & 0 & -i & 0 \\ 0 & i & 0 & 0 \\ i & 0 & 0 & 0 \end{bmatrix} \quad \hat{\tau}_3 = \begin{bmatrix} 1 & 0 & 0 & 0 \\ 0 & 1 & 0 & 0 \\ 0 & 0 & -1 & 0 \\ 0 & 0 & 0 & -1 \end{bmatrix}. \tag{7}$$

We will write the identity matrix as the 0-th component of these matrices depending on its size, i.e. $\underline{\sigma}_0 = \mathrm{diag}(1, 1)$ and $\hat{\tau}_0 = \mathrm{diag}(1, 1, 1, 1)$.

The following notation to differ between the different directions in three dimensional space will be used:

$$\boldsymbol{e}_x = (1, 0, 0) \qquad \boldsymbol{e}_y = (0, 1, 0) \qquad \boldsymbol{e}_z = (0, 0, 1). \tag{8}$$

For two arbitrary matrices $\hat{A}$ and $\hat{B}$ we will use the following notation for the commutator and the anti-commutator:

$$[A, B]_- = AB - BA \qquad [A, B]_+ = AB + BA. \tag{9}$$

Contents

Preface **1**

1 Introduction **5**
1.1 Structure of Thesis 6

2 Fundamental Concepts **7**
2.1 Superconductivity 7
2.2 Josephson Effect 7
2.3 Proximity Effect 8
2.4 Andreev Reflection 9
2.5 Transforming Singlet Cooper Pairs to Triplet Pairs 9
2.6 Precessing Magnetic Field in Superconducting Hybrid Structure 12
2.7 Applications 13

3 Theory **14**
3.1 Green's Functions 14
3.2 Quasiclassical Approximation 16
3.3 Diffusion Equation 17
3.4 Boundary Condition 18
3.5 Bulk Superconductor and Normal State Metal Solutions 19
3.6 Numerical Calculations 19
3.6.1 Theta-Parameterization 19
3.6.2 Riccati-Parameterization 20
3.7 Spin-Orbit Coupling 21
3.8 Precessing Magnetization 22
3.8.1 Gauge-Invariant Phase Difference 23
3.8.2 Green's Function Transformation 24

4 Observables **27**
4.1 Gap Energy 27
4.2 Charge and Spin-Currents 29
4.3 Charge and Spin-Accumulation 31
4.4 Density of States 32

5 Project 1: Precessing Exchange Field in Heterostructures **34**
5.1 Going from the Transformed Frame to the Laboratory Frame 34
5.2 Boundary Condition 36
5.3 Observables 38
5.3.1 Gap Energy 38

5.3.2 Charge and Spin-Currents . . . 38
5.3.3 Charge and Spin-Accumulation . . . 39
5.3.4 Density of States . . . 40
5.4 Weak Proximity Limit . . . 40
5.5 Distribution Function . . . 42
5.6 Numerical Analysis . . . 47
5.6.1 Parameters . . . 49
5.6.2 Charge-Current . . . 49
5.6.3 Spin-Currents . . . 50
5.6.4 Gap Energy . . . 53
5.6.5 Zero Energy Density of States . . . 54
5.6.6 Charge Accumulation . . . 56
5.7 Gauge-Invariant and Time Dependent Phase Difference . . . 59

6 Project 2: Lateral SFS Josephson Junction with Spin-Orbit Coupling 61
6.1 Weak Proximity Approximation . . . 62
6.2 Pure Rashba Coupling and In-Plane Magnetization . . . 66
6.3 Numerical Solutions . . . 68
6.4 Parameters . . . 69

7 Conclusion 72

A Supercurrent in a SNS Josephson Junction 75

B Ring Product 77

C Convolution Identity 78

D Analytical Solutions to Condensate Functions and Distribution Functions 80
D.1 FS Bilayer with a Precessing Exchange Field . . . 80
D.2 SFS Josephson Junction with a Precessing Exchange Field . . . 81
D.3 Distribution Functions in a Precessing Exchange Field . . . 82

E Research Article 83

Bibliography 92

1 | Introduction

The field of spintronics revolves around the spin property of electrons rather than their charge. This has the potential of superseding the classical charge-based computer processing devices in terms of both higher energy and time efficiency [16]. Spintronics has already found its way to current computer hardware: Some hard drives and random access memories are based on the giant magnetoresistive effect (GMR) [17]. When two ferromagnetic layers are placed in contact through a normal metal, the electrical resistance will significant depend on the alignment between the two exchange fields. If they are parallel, the resistance is low, and an anti-parallel alignment gives a much higher resistance. There are however two main challenges with today's development of spintronics devices [18]. The first problem is Joule heating which destroys thin-film layers, and the second is short decay lengths due to spin-flip scattering. The former of these problems can be solved by putting the materials into proximity to superconductors. As we will explain later, the proximity effect happens when a superconductor is placed in proximity to a normal state material and the Cooper pairs leak across the interface and into the adjacent material. Thus, the materials in proximity will start exhibiting superconducting properties which can combat Joule heating. Supercurrents experience zero resistance, and thus Joule heating is greatly minimized. In addition, the symbiosis between magnetic and superconductive order can also enhance effects found in non-superconductive spintronics by several orders of magnitude such as an enhanced spin Hall effect [64], quasiparticle lifetime [65] and thermoelectric currents [66].

The field of superconducting spintronics has emerged to investigate how superconducting order can be used to enhance the effects of spintronics. This field is made possible by taking the conventional, Cooper pairs of electrons with opposite spin, and rotate them into having same spin-projection which makes the pair similar to a boson with a spin-projection equal to $S_z = 1$. This spin-rotation can be made possible with a nonhomogeneous exchange field, either by two or more ferromagnetic layers with noncollinear exchange fields, or one ferromagnet where the exchange field spatially varies [23, 28]. It has also been shown that a time-varying exchange field can create these triplets states [7], and recently, intrinsic spin-orbit coupling of type Rashba and Dresselhaus has been proposed to generate such triplets [29].

Since these triplets can align themselves with the exchange field of a ferromagnet, they will decay over much longer distances than singlet states or triplet states with a zero-projection along the exchange field. This means that a SFS Josephson junction, a ferromagnet sandwiched between two superconductors, with these triplets can carry a supercurrent over longer lengths of the ferromagnetic layer than an ordinary homogeneous ferromagnet would. Triplets with a non-zero spin projection can also carry a current of spin which can have several applications in the future of spintronics devices.

1.1 Structure of Thesis

This thesis is the final product of two different research projects. The first was started last semester during my specialization project, and shows how one can control a long-ranged supercurrent in a lateral Josephson junction with spin-orbit coupling and a ferromagnet as the weak link by making in-plane rotations of the exchange field. The motivation for considering such a setup is that an in-plane magnetization is experimentally more feasible in a lateral structure. In addition, one needs the momentum of the quasiparticles to couple with the spin-orbit coupled field which requires a change in momentum from a z-direction to a x-direction. This research project was not finalized last semester and will therefore be fully covered in this thesis. A research article is currently being written and will be sent for review at Physics Review B. A draft of this article can be found in Appendix E.

The other research project was started on in the beginning of this semester, and this project looks at superconductor hybrid structures with a precessing exchange field. Such a setup will be driven out of equilibrium, and therefore contains a lot more 'physics' than the previous project. A lot more pages have thus been given to this topic.

The next chapter will qualitatively explain the rich physics of Josephson junctions, proximity effect, triplet pairs and their applications. Chapter 3 will then go into the theory behind the diffusive limit and its corresponding diffusion equation in the quasiclassical approximation. We will also go into the specific theories behind the two different research projects. Then in chapter 4, we will show how we can calculate observables like currents, gap energy and density of states with the quasiclassical Green's functions in the diffusive limit. The two next chapter will then focus on the two different research projects. Chapter 5 looks into the physics of heterostructures with a ferromagnet with a precessing exchange field, while chapter 6 will show that a lateral Josephson junction with Rashba type spin-orbit coupling can carry a long-ranged supercurrent and can be controlled by an in-plane rotation of the exchange field. We will then in the last chapter conclude our findings and go into details about future prospects.

2 | Fundamental Concepts

2.1 Superconductivity

The first microscopic theory of superconductivity was made by Bardeen, Cooper and Schrieffer (BCS) in 1957 [51], and the theory stated something that many would deem impossible in metals; there was an effective potential in superconductors which attracted electrons to each other even though their charge repel each other. Cooper first showed the year before [52] that such a hypothetical potential would force two electrons of opposite momentum and spin to bound to each other and reach an energy level less than the Fermi energy. The pair of electrons in this potential became later known as a Cooper pair. But it wasn't until the discovery of the BCS theory that anyone where able to explain what this potential could be. This theory explained that such a potential could be achieved by vibrations in the positive lattice of ions that makes up a metal. This vibration can overcome the electrons' repulsion of each other, but the energy of a Cooper pair is low and can easily be destroyed by thermal energy. Therefore, superconductors can only exist at low temperatures. Such conventional BCS superconductors also have a s-wave symmetry since the electrons of a Cooper pair have opposite momentum, and thus their wavefunctions are symmetric under an exchange of position coordinates.

There does exist another class of superconductors which does not have the s-wave symmetry of conventional, BCS superconductors. These are high-temperature superconductors and are governed by d-wave symmetries. Even though they are superconductive at high temperatures they require a very high purity which makes them difficult to manufacture. Therefore, we are exclusively going to be looking at conventional BCS superconductors.

2.2 Josephson Effect

As a 22 year old PhD student at Cambridge University, Brian Josephson released a paper predicting that two superconductors separated by a thin insulating barrier would be able to carry a zero voltage supercurrent [2][3],

$$I_Q = I_c \sin(\Delta\phi). \tag{2.1}$$

Here, I_c is the maximum current the junction can carry and $\Delta\phi$ is the macroscopic phase difference between the two superconductors. Josephson showed this to be true for an insulator, but the predictions are also true for any type of 'weak link' between two superconductors. This weak link could be a simple normal metal which would be called a SNS-junction or a ferromagnetic material, SFS. His predictions were shortly after shown to be true experimentally, and this young physicist's discovery ended up earning him a Nobel Prize in Physics eleven years later in 1973. Shortly after Josephson released his paper, Ambegaokar and

Baratoff were able to calculate the exact critical current I_c for the same system as Josephson considered, namely two equal superconductors with s-wave symmetry and an insulator in between [4],

$$I_c R_n = \frac{\pi \Delta(T)}{2e} \tanh\left(\frac{\beta \Delta(T)}{2}\right), \tag{2.2}$$

where R_n is the resistance in the normal metal. $\beta = 1/k_B T$ where k_B is the Boltzmann constant and T is the temperature. If the temperature is close to the critical temperature T_c, we can use the well known BCS result $\Delta(T) \propto \sqrt{1 - T/T_c}$ to show that the current is linearly with temperature, $I_c \propto T - T_c$. On the other hand, if $T \to 0$, then Δ becomes constant and independent of temperature, and thus $I_c(0)R_n = \pi\Delta_0/2e$. More advanced microscopic theories for superconductors have shown that the value of $I_c(0)R_n$ are 1.32 and 2 times greater in dirty and clean superconductors, respectively [3]. They all give the same predictions for $I_c(T)R_n$ for temperatures close to T_c.

Josephson also predicted that a voltage difference V across the junction would make the phase difference $\Delta\phi$ change over time

$$\frac{d\Delta\phi}{dt} = \frac{2eV}{\hbar}. \tag{2.3}$$

Zero-voltage would give rise to a DC current, but with a non-zero and constant voltage, the phase difference would be $\Delta\phi = \Delta\phi_0 + 2eVt/\hbar$, and thus the current would become alternating and can now be written as

$$I_Q = I_c \sin(\Delta\phi_0 + 2eVt/\hbar). \tag{2.4}$$

The AC current would have a frequency of $f_J = 2eV/h$. Due to the acceleration of charges, this process emits electromagnetic radiation at the frequency $\omega_J = 2\pi f_J = 2eV/\hbar$ [75]. If one were to send microwave radiation onto the junction, one can elevate the potential to constant intervals $V = n\frac{\hbar}{2e}\omega_J$ which are caused by the absorption of n quanta of microwave radiation. Josephson's theory was shown to be true experimentally a year later by Shapiro [45], and these constant voltage regions in an AC Josephson junction are today called Shapiro steps.

2.3 Proximity Effect

Long before Josephson discoveries, the proximity effect was discovered experimentally by the German physicists Holm and Meissner in 1932 [9], 30 years before Josephson released his papers. They saw that the resistance of normal state metals sandwiched between two superconductors had a drastically lower resistance. 20 years later, Holm's student I. Dietrich continued working on the problem, and she was able to show that the current was in fact dissipationless, and thus a supercurrent [10]. At the time, few physicists seemed to care about their discoveries, which is why Josephson was unaware when doing his calculations in 1962. Josephson did on the other hand solve the problem theoretically for the first time by the use of the 5 year old theory of BCS superconductivity.

When a normal state metal is placed in proximity to a superconductor, the metal starts exhibiting superconductive properties over mesoscopic distances. Due to the non-locality of Cooper pairs, they can not immediately break down when entering the metal. The pair will then loose its coherence as it experience scattering in the metal and soon decay. On the other hand, quasiparticles in the metal with energies less than the gap energy are able to

enter the superconductor which lowers the gap energy and the critical temperature of the superconductor. In addition, if the metal is a ferromagnet, the superconductor can also start exhibiting magnetic ordering in the region close to the interface. This effect is called the inverse proximity effect and with both effects considered they are called the full proximity effect. To explain the proximity effect on a microscopic level we have to understand Andreev reflections.

2.4 Andreev Reflection

If an electron in a normal metal reaches the interface of a superconductor with zero barrier resistance, then the electron can become a quasiparticle in the superconductor as long as $\epsilon > \Delta$ where the energy is measured from the chemical potential μ. If the energy of the electron is less than the gap energy, there are no quasiclassical states for the electron to inhabit. In this case, the Russian physicist Andreev showed in 1964 [5] that the electrons can cross the interface if the transparency of the interface is low and then be reflected as a hole. Two electron charges $2e$ will be transferred across the interface and become a Cooper pair in the superconductor. This transition will conserve momentum, charge, spin and energy, and with a low barrier transparency and $\epsilon \ll \Delta$ most of incident electrons will be Andreev reflected. This effect transfers twice the amount of electrons than if the superconductor was in a normal metal state, and thus the conductance is twice the normal state if the energies of the incident electrons are low. This conductance will converge to the normal state as the temperature moves closer to T_c. The opposite case is also possible where an incident hole from the normal metal is reflected as an electron. This process breaks apart a Cooper pair in the superconductor and $2e$ is also transferred across the interface and into the normal metal. The most important part of the Andreev reflection is the phase coherence between the hole and electron. If the energy of the incoming electron (hole) is equal to the Fermi energy, $\epsilon = 0$, then the reflected hole (electron) will have the exact same energy since the Cooper pair created in the superconductor will have a zero center-of-mass momentum. If however the energy is different from the Fermi energy, the mismatch in momentum will be on the order of $\Delta k = 2\epsilon/\hbar v_f$ where v_f is the Fermi velocity [74]. Thus, the difference in momenta will destroy the coherence between the electron and hole, and in diffusive materials the coherence lengths will be on the order of $\xi_N = \sqrt{\hbar D/\epsilon}$ where D is the diffusion constant. Scattering from impurities will also affect the phase coherence and make the pair decay. The retroflected hole (electron) will then in a SFS junction move to the other superconductor interface, and as long as there is a non-zero phase difference between the two superconductors then there will be differences in preferred retroflection of holes or electrons at the two interfaces, and thus there will be a flow of charge in a certain direction which creates a supercurrent.

2.5 Transforming Singlet Cooper Pairs to Triplet Pairs

Conventional superconductors are well described by the BCS theory. This theory tells us that the two electrons that make up a Cooper pair have a singlet spin state, and that a conventional BCS superconductor can be characterized as a s-wave with even-frequency. s-wave pairing implies that an exchange of spatial coordinates will leave the wave function unchanged, while an even-frequency wave function is invariant under an exchange of time-coordinates. Thus, the Fermi principle is satisfied since the overall wave function switches sign if the two electrons are switched (-1 from spin, +1 from spatial coordinates, and +1

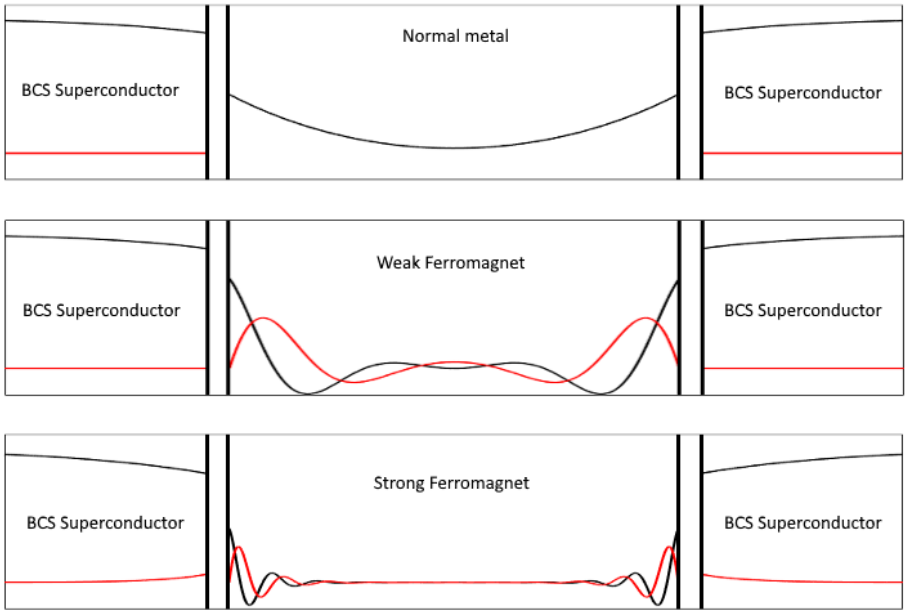

Figure 2.1: SNS and SFS Josephson junctions where the black lines represents singlet states ($\uparrow\downarrow - \downarrow\uparrow$) while the red lines represents triplet states with zero spin-projection along the magnetic field ($\uparrow\downarrow + \downarrow\uparrow$). The figure is adapted from reference [24].

from time coordinates).

We are exclusively going to be looking at diffusive materials, especially diffusive ferromagnets in this thesis. The frequent scattering in such materials forces the change of spatial coordinates to be even under parity. This restriction will be assumed to be strict in this thesis, so the two other wave functions (spin and time coordinates) have to switch sign when multiplied. Thus there are two possibilities: Spin-singlet and even in time coordinate exchange as a conventional BCS superconductor, and the other possibility of being a spin-triplet and be anti-symmetric in time coordinates [23]. Note that this anti-symmetric in time property must mean that such a wave function has to be zero at equal times $t_1 = t_2$. Such parings are called odd-frequency pairings and are realized in diffusive ferromagnets in proximity to superconductors.

When a supercurrent is flowing through a superconductor-normal-superconductor (SNS) Josephson junction, only spin-singlet Cooper pairs will exist in the normal state metal, but if the normal state metal has an exchange field, i.e. is a ferromagnet, then the exchange field will energetically favour one spin direction. This Zeeman effect causes a split in the energy bands and effectively destroys the phase correlation between the two, and thus an exchange field causes the pairs to decay on a length scale comparable to $\xi_F = \sqrt{\hbar D/(\epsilon \pm M)}$ in diffusive materials where D is the diffusion coefficient, ϵ is the energy of the quasiparticle and M is the magnitude of the exchange field. This decay length is normally much shorter than the decay length of singlet pairs in the normal metal in SNS junctions, which has the coherence length $\xi_N = \sqrt{\hbar D/\epsilon}$. The coherence length of a supercurrent flowing through normal state materials will be affected by the decay length of the pair coherence. A supercurrent flowing through a diffusive metal without an exchange field has a decay length of order $\xi_N = \sqrt{\hbar D/k_B T}$, but if the metal has an exchange field, the decay length of the supercurrent is $\xi_F = \sqrt{\hbar D/M}$. The former is normally much longer, and thus a supercurrent can flow over longer lengths in a metal without an exchange field than a ferromagnet. The

Zeeman effect however has an interesting property of converting the singlet states into triplet states with zero spin-projection along the magnetic field. The energy band splitting causes a shift in the momentum of the two electrons to $\boldsymbol{k}_\uparrow = \boldsymbol{k}_f + \boldsymbol{Q}/2$ and $\boldsymbol{k}_\downarrow = \boldsymbol{k}_f - \boldsymbol{Q}/2$ [24], and thus the Cooper pair gains a center-of-mass momentum $\pm\boldsymbol{Q}$. This momentum causes a modulation in the pair amplitude which varies over position $\boldsymbol{R}$,

$$\begin{aligned}(\uparrow\downarrow - \downarrow\uparrow) \rightarrow \left(\uparrow\downarrow\, e^{i\boldsymbol{Q}\cdot\boldsymbol{R}/\hbar} - \downarrow\uparrow\, e^{-i\boldsymbol{Q}\cdot\boldsymbol{R}/\hbar}\right) \\ = (\uparrow\downarrow - \downarrow\uparrow)\cos(\boldsymbol{Q}\cdot\boldsymbol{R}/\hbar) + i\,(\uparrow\downarrow + \downarrow\uparrow)\sin(\boldsymbol{Q}\cdot\boldsymbol{R}/\hbar).\end{aligned} \tag{2.5}$$

Thus, the pair correlations in the ferromagnet will oscillate with the wavenumber $\boldsymbol{Q}/\hbar$ and be a mixture of both singlet and triplet pairs with zero spin-projection along the exchange field, i.e. $S_z = 0$, see figure 2.1. This state is called the FFLO (Fulde–Ferrell–Larkin–Ovchinnikov) phase named after two independent discoveries in 1964; one by the American physicists Fulde and Larkin [25], and the other by the Soviet Russians Larkin and Ovchinnikov [26]. In addition, due to the inverse proximity effect, the triplet states generated in the ferromagnet will leak across the interface and into the superconductor. We see from the equation above that the singlet state can switch sign and become negative in the ferromagnet, $(\uparrow\downarrow - \downarrow\uparrow) \rightarrow -(\uparrow\downarrow - \downarrow\uparrow)$. If two superconductors are separated by a length where the singlet states have opposite signs at the two SF interfaces, we end up with a so-called π state [67]. These states have a lower free energy than the normal 0-states, and thus, in those cases, the system switches its ground state to a π-state. A transition between these two states also gives the current a sign shift at a given phase difference, and is therefore easily detectable in plots of supercurrents. Note that a stable π state is not possible in a conventional SNS Josephson junction since the FFLO phase can not be achieved.

The transition between singlet and zero-projection triplet states is called spin-mixing and is not able to create equal spin pairs that are aligned with the magnetic field. Such pairs generally have more appreciable properties than zero-projection triplets. Firstly, such pairs can not be deteriorated by the exchange field since the pair will not experience any Zeeman split. Thus, equal spin pairs decay in ferromagnets on the same length scale as in normal metals and are thus called long-ranged triplets. SFS Josephson junctions with these long-ranged pairs will thus be able to carry long-ranged currents that decay on the order of $\xi_N = \sqrt{\hbar D/k_B T}$. In addition, these pairs are also able to transport spin since the two spins do not cancel each other out, which is of great importance in the field of superconducting spintronics in which transport of spin can be used to create spin-based electronic devices. Then the question becomes: How do we generate triplet pairs with a non-zero projection?

One way is to take the zero-projection triplet states created by the spin-mixing effect and consider them from a different angle in spin space [24]. The singlet states are invariant under a rotation in spin space since they have a zero spin magnitude, i.e. $|\boldsymbol{S}| = 0$. But a zero projection triplet state in the y-basis $(\uparrow\downarrow + \downarrow\uparrow)_y$ is equal to a the non-zero projection triplet state in the z-basis $i(\uparrow\uparrow + \downarrow\downarrow)_z$. This means that if we have a SFF'-trilayer where the ferromagnet F has an exchange field along the y-axis and while F' points in the z-direction, then F will create opposite spin triplet pairs in the y-basis due to spin-mixing which in F' will be equal spin triplets when viewed with respect to the z-axis. Thus these pairs will be aligned with the exchange field in F' and be long-ranged triplets. This effect is called spin-rotation and can be realized in several ways. One way is as we already mentioned to have two ferromagnetic layers with misaligned magnetic fields. It can also be realized in heterostructures with magnetic interfaces. For example, it is possible to generate such

states carrying long-ranged charge and spin supercurrents in Josephson junctions with a non-magnetic metal as weak link with magnetic insulators as interfaces [27]. Another option of creating long-ranged triplets is to have a single ferromagnet with a nonhomogenous exchange field [28]. It is also possible with a single ferromagnet with a time-varying exchange field [7] which is something we are going to be closely looking at later.

It was commonly believed that only magnetic inhomogenities could spawn long-ranged components, but in 2013 Bergeret and Tokatly [36] showed that there could exist other sources for such triplets and established a universal condition for long-ranged triplets. A year later, the two showed [29] that intrinsic spin-orbit coupling of type Rashba [31] and Dresselhaus [30] satisfied the condition of long-ranged triplets.

Other sources of long-ranged components have been proposed such as inhomogenous distribution functions [37], or unconventional superconductors with intrinsic spin-triplet pairings [38]. But this thesis is only going to focus on two sources of long-ranged triplets, namely the presence of a precessing magnetic field or intrinsic spin-orbit coupling.

2.6 Precessing Magnetic Field in Superconducting Hybrid Structure

When a ferromagnet with a precessing magnetic field is placed in proximity to a normal state metal, the ferromagnet will pump a spin-current polarized in the direction of the precessing axis into the adjacent metal. This effect is known as spin-pumping, and is a well understood phenomena today. The past two decades there has been more focus on the presence of superconductive ordering in a setup with a precessing exchange field both theoretically and experimentally. The presence of a superconductor has shown to suppress these spin-currents at the superconductor interface [77, 78]. There are two ways for a quasiparticle to enter a superconductor: Either it can enter as a quasiparticle, but then it needs an energy above the gap energy, and thus the spin carried by these low-energy quasiparticles are suppressed close to the superconductor interface. The other possibility is for an electron-like quasiparticle to enter through Andreev reflection where it is coupled to the retroflected hole with opposite spin to create a zero-spin Cooper pair in the superconductor, but in this process, no spin is transported into the superconductor. It was however recently showed experimentally that layers with strong spin-orbit coupling added to the superconductors would on the other hand enhance spin-currents [79]. The researchers argued that this was most likely due to the transport of equal-spin triplets and not quasiparticles.

The presence of a spin-current polarized along the precession angle will also alter the tilt angle of the precession. The spin-current will force the magnetic field to align itself more with the axis of precession which in turn will slow down the angular velocity of precession. A precessing magnetic field will have a damping term which over time makes the magnetic field converge to a zero tilt angle. This damping term is called Gilbert damping, and since the spin-current in a precessing exchange field in proximity to a superconductor is weakened, the effective Gilbert damping will be lower than in the normal state case. Interestingly, last year, it was reported that a SFS Josephson junction with a precessing magnetic field induced a large spin-transfer torque at temperatures under the transition temperatures [76]. This effect was not seen in a FS bilayer, and the researchers concluded that this was due to the charge current of equal-spin triplet pairs flowing through the SFS junction which lowered the tilt angle.

2.7 Applications

While getting a fundamental understanding of quasiparticle correlations in heterostructures with superconducting ordering is interesting in its own right, such structures also have real life applications today and possible several future applications. First of all, in the field of measurements, metrology, a voltage applied Josephson junction has been used as a standard of the volt by using the equation previously mentioned $\nu = 2eV/h$. By using the definition of frequency, the cesium standard, and the most precise measurement of the magnetic quantum flux $2h/e$, one can make a standard of one volt. Today, the National Institute of Standards and Technology standard of one volt can be created by having 20208 Josephson junctions in series [46].

Josephson junctions also have the exciting application of representing a quantum bit [47, 48, 49]. This is due to the high non-linearity of the inductance which we can calculate by taking the time derivative of equation (2.1) and entering it into (2.3). The resulting equation is

$$\frac{dI_Q}{dt} = I_c \frac{2eV}{\hbar} \cos(\Delta\phi). \tag{2.6}$$

By using the definition of inductance $V = LdI_Q/dt$, the Josephson inductance becomes

$$L = \frac{\hbar}{2eI_c \cos(\Delta\phi)}, \tag{2.7}$$

which shows the non-linearity in the variable $\Delta\phi$. While conventional circuit elements are linear and therefore have highly degenerate energy levels, the non-linearity of the inductance of a Josephson junctions is crucial since a quantum bit (qubit) is restricted to be in the two lowest energy levels, and the non-linearity allows a bigger spacing between these two energy levels. This non-linearity can even make a single photon increase the inductance by an order of unity and breaks the degeneracy of the energy levels [50].

3 | Theory

3.1 Green's Functions

As a starting point to describe the electrons in our heterostructures we will use the language of Green's functions. These functions act as building blocks as to how electrons correlate to each other, and we will develop differential equations so that we can find numerical values for these functions. With them we can find observable of interest such as currents and density of states.

A Green's function $G(\boldsymbol{r}_1, t_1, \sigma_1; \boldsymbol{r}_2, t_2, \sigma_2)$ can be thought of as a measure of the probability that a particle with the position $\boldsymbol{r}_2$ with spin σ_2 at time t_2 will propagate and exist at position $\boldsymbol{r}_1$ with spin σ_1 at time t_1. These functions will not only describe electrons, but also the absence of electrons called holes, or more generally, they describe quasiparticles. These quasiparticles can be different from electrons in that they may have a different effective mass and charge.

There are two main formalism of Green's functions in quantum condensed matter physics: The Keldysh formalism and Matsubara formalism. The former is the one we are going to be using, but the Matsubara technique can be useful when the system is in equilibrium. This is because the distribution function then will be $\hat{h} = \tanh(\beta\epsilon/2)\hat{\tau}_0$ where β is the inverse temperature and ϵ is the energy of the quasiparticle. When calculating the supercurrent through a metal in a SNS Josepshson junction in the weak proximit limit, we have to integrate over all energies which can easily be done by contour integration. Only $\tanh(\beta\epsilon/2)$ will have zeroes in the upper half-plane when $\epsilon = i(2n+1)\pi k_B T$ where n in any positive integer. Thus, we arrive at an infinite sum as an expression for the supercurrent, see appendix A for an example.

The Keldysh formalism gives us three different components, the first being the retarded component which describes particles propagating forward in time, and the advanced component which describes particle propagating backwards in time. Electrons moving back in time can be though of as holes moving forward in time, and thus one can think of the advanced component as describing the propagation of holes while the retarded component describes electrons. These components only describe equilibrium properties in that they are assumed to begin and return to the initial state over long periods of time, thus they describe only how the processes at times t_1 and t_2 have changed the initial state [34]. This assumption is however wrong if the system does not return to the initial state, and thus the third component of the Keldysh formalism is the Keldysh component. This component does not assume any final state due to the special choice of contour in time utilized by Keldysh, and is thus suitable to describe non-equilibrium phenomena.

Following the notation of J.P. Morten in reference [6], the 8×8 Green's function is in Keldysh space

$$\check{G}(1,2) = \begin{bmatrix} \hat{G}^R(1,2) & \hat{G}^K(1,2) \\ 0 & \hat{G}^A(1,2) \end{bmatrix}, \tag{3.1}$$

where R, A and K denotes the retarded, advanced and Keldysh component, respectively, and the coordinates are $(1) = (\boldsymbol{r}_1, t_1)$. Each of these matrices are 4×4 where the outer 2×2 matrices lie in Nambu space, which describe electron-hole symmetries, and the inner matrices lie in spin-space. The diagonal components in Nambu space are called normal Green's functions $\underline{G}_{\sigma\sigma'}$ and the off-diagonal components are called anomalous Green's functions $\underline{F}_{\sigma\sigma'}$. In Nambu space the retarded and advanced Green's function are [6]

$$\hat{G}^{R(A)}(1,2) = \begin{bmatrix} \underline{G}^{R(A)}(1,2) & \underline{F}^{R(A)}(1,2) \\ \left(\underline{F}^{R(A)}\right)^*(1,2) & \left(\underline{G}^{R(A)}\right)^*(1,2) \end{bmatrix}, \tag{3.2}$$

while the Keldysh component is

$$\hat{G}^K(1,2) = \begin{bmatrix} \underline{G}^K(1,2) & \underline{F}^K(1,2) \\ -\left(\underline{F}^K\right)^*(1,2) & -\left(\underline{G}^K\right)^*(1,2) \end{bmatrix}. \tag{3.3}$$

Each of the components can be written as an average value of the product of creation and annihilation operators for electrons, $\psi^\dagger_{\sigma'}(\boldsymbol{r}', t')$ and $\psi_{\sigma'}(\boldsymbol{r}', t')$. In spin space, the different Green's functions are defined as follows [6]:

$$G^R_{\sigma\sigma'}(1,2) = -i\Theta(t_1 - t_2)\langle\Big[\psi_\sigma(1), \psi^\dagger_{\sigma'}(2)\Big]_+\rangle, \tag{3.4}$$

$$G^A_{\sigma\sigma'}(1,2) = i\Theta(t_2 - t_1)\langle\Big[\psi_\sigma(1), \psi^\dagger_{\sigma'}(2)\Big]_+\rangle, \tag{3.5}$$

$$G^K_{\sigma\sigma'}(1,2) = -i\langle\Big[\psi_\sigma(1), \psi^\dagger_{\sigma'}(2)\Big]_-\rangle, \tag{3.6}$$

where $\Theta(t)$ is the well known Heavyside function. $\langle ... \rangle$ denotes the average value and is defined as $\langle O(t)\rangle = \mathrm{Tr}(\rho O(t))$ in the Heisenberg picture where ρ is the density matrix. The anomalous Green's functions are defined as

$$F^R_{\sigma\sigma'}(1,2) = -i\Theta(t_1 - t_2)\langle[\psi_\sigma(1), \psi_{\sigma'}(2)]_+\rangle, \tag{3.7}$$

$$F^A_{\sigma\sigma'}(1,2) = i\Theta(t_2 - t_1)\langle[\psi_\sigma(1), \psi_{\sigma'}(2)]_+\rangle, \tag{3.8}$$

$$F^K_{\sigma\sigma'}(1,2) = -i\langle[\psi_\sigma(1), \psi_{\sigma'}(2)]_-\rangle. \tag{3.9}$$

As we can see from the definition of the anomalous Green's functions, they describe the correlation of electron pairs. This if especially useful in our case when we are looking at Cooper pairs and pairs of electrons with equal spin projection, namely long-ranged triplets.

3.2 Quasiclassical Approximation

The Green's functions described in the last section oscillates rapidly over the relative coordinates $t = t_1 - t_2$ and $\boldsymbol{r} = \boldsymbol{r}_1 - \boldsymbol{r}_2$, and the oscillations happen over distances comparable to the Fermi wavelength λ_F [6, 16, 34, 39]. We are more interested in longer length scales, both longer materials on the scale of at least 5 nm, and coherence length of superconductors on the length scale of around $\xi_S \approx 25$ nm. These are both much larger than the Fermi wavelength, and thus the fast oscillation does not give us any information of interest. We can therefore choose to focus on the center-of-mass coordinates $\boldsymbol{R} = (\boldsymbol{r}_1 + \boldsymbol{r}_2)/2$ and $T = (t_1 + t_2)/2$. We can thus average out the relative coordinates by taking the Fourier transformation of both relative time and relative position. This yields in the case of relative time the energy of the quasiparticles ϵ and the momentum of the particles $\boldsymbol{p}$ in the case of relative position. This approximation is called the gradient approximation and is the first step of the quasiclassical approximation. The next step is to assume that all the quasiparticles that contribute to any physical observables lie close to the Fermi energy. This is especially true for low temperatures where most states below the Fermi energy are full. This means that we fix the momentum we got from the Fourier transform to be equal to the Fermi momentum $\boldsymbol{p}_f$. Note that we are only fixing the magnitude, and not the direction of the momentum. One can then define the quasiclassical Green's function $\check{g}(\boldsymbol{R}, \boldsymbol{p}_f; T, \epsilon)$ to follow these constraints, and we can define it as

$$\check{g}(\boldsymbol{R}, \boldsymbol{p}_f; T, \epsilon) \equiv \frac{i}{\pi} \int_{-\infty}^{\infty} d\xi_p \check{G}(\boldsymbol{R}, \boldsymbol{p}; T, \epsilon). \tag{3.10}$$

where $\boldsymbol{p}$ is the momentum, and $\boldsymbol{p}_f$ is the Fermi momentum. And $\xi_p = \boldsymbol{p}^2/2m - \mu$ where μ is the chemical potential. This definition is equal to the approximation

$$\check{G}(\boldsymbol{R}, \boldsymbol{p}; T, \epsilon) = -i\pi\delta(\xi_p)\check{g}(\boldsymbol{R}, \boldsymbol{p}_f; T, \epsilon). \tag{3.11}$$

In reality, the integral above diverges as an integral of $1/\xi_p$ for large kinetic energies [6], and thus we either need to introduce a cut-off energy or solve the integral by introducing contour integration. Nevertheless, this approximation changes our normal and anomalous Green's functions, and the retarded quasiclassical Greens' function has the form

$$\hat{g}^R = \begin{bmatrix} \underline{g} & \underline{f} \\ -\underline{\tilde{f}} & -\underline{\tilde{g}} \end{bmatrix}. \tag{3.12}$$

For an arbitrary function of energy $a(\epsilon)$ the definition of the tilde operation is $\tilde{a}(\epsilon) = (a(-\epsilon))^*$. From now on, we will often denote the retarded quasiclassical Green's function as simply $\hat{g}^R = \hat{g}$. With this quasiclassical theory, it is now possible to describe the propagation of quasiparticles in heterostructures by starting with Gorkov's equation or Bogoliubov-de Gennes equation [16, 40, 41] and then deriving the Eilenberger equation [42] first done in 1968. This equation is an effective transport equation for the quasiclassical Green's function and is much more suitable for calculations. Two years later, Usadel discovered [43] that in in diffusive materials, when the mean path ways of quasiparticles are much shorter than any characteristic length scales, the Greens function is mainly isotropic in space. He took advantage of this fact and found an equation of motion for the spherical symmetric Green's function and also showed that it is possible to express the small anisotropic part of Green's function as a function of the spherical symmetric one. The now known Usadel equation has

then become the starting point of most numerical and analytical calculations of heterostructures in diffusive materials. For a full derivation of the Eilenberger and Usadel equation, we suggest the reader to look at the references [6, 19, 34, 39].

3.3 Diffusion Equation

The Usadel equation is given as

$$iD\tilde{\nabla}\cdot\left(\check{g}\circ\tilde{\nabla}\check{g}\right)=\left[\epsilon\hat{\tau}_3+\hat{\Delta}+\boldsymbol{M}\cdot\hat{\boldsymbol{\sigma}}\,\circ,\check{g}\right]_-, \tag{3.13}$$

where the gap energy matrix is

$$\hat{\Delta}=\begin{bmatrix}0&0&0&\Delta\\0&0&-\Delta&0\\0&\Delta^*&0&0\\-\Delta^*&0&0&0\end{bmatrix}, \tag{3.14}$$

and the ring product $\circ$ is defined in Appendix B.

It is easy to show that if $\check{g}$ is a solution to the Usadel equation then so will $\check{g}\circ\check{g}$ and $\check{g}\circ\check{g}\circ\check{g}$ and so on. Seeing that $\check{g}=1$ is a solution we can make the normalization condition

$$\check{g}\circ\check{g}=1. \tag{3.15}$$

This condition can also be showed explicitly in the case of thermal equilibrium and in a spatially homogeneous state [6]. With this condition we get following identities

$$\hat{g}^R\circ\hat{g}^R=\hat{g}^A\circ\hat{g}^A=1, \tag{3.16}$$

$$\hat{g}^R\circ\hat{g}^K+\hat{g}^K\circ\hat{g}^A=0, \tag{3.17}$$

and as a consequence of the last line, we can make the following ansatz [19]:

$$\hat{g}^K=\hat{g}^R\circ\hat{h}-\hat{h}\circ\hat{g}^A, \tag{3.18}$$

where $\hat{h}$ is known as the distribution function. It is immediately clear that this ansatz satisfies the identity in equation (3.17) with the normalization condition in equation (3.16). Note that the distribution function is not unique, and by substituting $\hat{h}\to\hat{h}+\hat{g}^R\circ\hat{A}+\hat{A}\circ\hat{g}^A$ will also satisfy (3.18), where $\hat{A}$ is an arbitrary matrix. The distribution function describes the occupation of states, and in equilibrium this function is simply $\hat{h}=1-2f_0(\epsilon)=\tanh(\beta\epsilon/2)$, where $\beta=1/k_BT$ and $f_0(\epsilon)=1/(e^{\beta\epsilon}+1)$ is the Fermi-Dirac distribution. If a system is out of equilibrium, then certain spin directions might be favoured or electron-hole distribution might change over position in our system, and the distribution function $\hat{h}$ will give us information about this. Using the notation of Schmid and Schön [20], we can parameterize the distribution to be $\hat{h}=h_L\hat{\tau}_0+h_T\hat{\tau}_3$. They denotes h_L as longitudinal and h_T as transverse. This parameterization is useful in cases where a material is subjected to an electric voltage, but useless in the case of a spin-voltage, where the distributions of quasiparticles with different spin directions are unequal which is the case in a system with a precessing ferromagnet. We will therefore instead use a notation similar to that of Ouassou, Vethaak and Linder [21]. They parameterized the distribution function as

$$\hat{h} = \sum_{n=1}^{8} h_n \hat{\rho}_n \tag{3.19}$$

where

$$\begin{aligned} \hat{\rho}_1 &= \hat{\tau}_0\hat{\sigma}_0 \qquad \hat{\rho}_2 = \hat{\tau}_0\hat{\sigma}_1 \qquad \hat{\rho}_3 = \hat{\tau}_0\hat{\sigma}_2 \qquad \hat{\rho}_4 = \hat{\tau}_0\hat{\sigma}_3 \\ \hat{\rho}_5 &= \hat{\tau}_3\hat{\sigma}_0 \qquad \hat{\rho}_6 = \hat{\tau}_3\hat{\sigma}_1 \qquad \hat{\rho}_7 = \hat{\tau}_3\hat{\sigma}_2 \qquad \hat{\rho}_8 = \hat{\tau}_3\hat{\sigma}_3 \end{aligned} \tag{3.20}$$

and $h_n = \mathrm{Tr}(\hat{\rho}_n\hat{h})/4$. The authors also derived equations of motion for these distribution functions by looking at the Keldysh component of the Usadel equation. Thus, we not only need to solve the Usadel equation for the retarded Green's function, but we then also need to solve the differential equation for the distribution functions h_n with the retarded Green's function and the advanced Green's function. The latter can be calculated from the relation $\hat{g}^A = -\hat{\tau}_3\left(\hat{g}^R\right)^\dagger\hat{\tau}_3$. In the case of equilibrium, these equation of motions will conveniently yield constant distribution functions i.e., $\nabla h_n = 0$, and we need to provide the equilibrium solution $h_1 = \tanh(\beta\epsilon/2)$ as a boundary condition in order for the system to yield the equilibrium solution throughout the whole system. This also means that if a system is out-of equilibrium, we need to provide information to the system what the distribution function should be at the boundaries. For example, in the article of Ouassou et.al. [21] the authors had a voltage-biased superconductor which they modelled by having two metal reservoirs on either side of the superconductor. These reservoirs had fixed distribution function with shifted energies in the electron-hole space to model the voltage across the superconductor.

3.4 Boundary Condition

A differential equation can not be solved without a proper set of boundary conditions. Kupriyanov and Lukichev (KL) were the first to formulate a boundary condition in the diffusive limit in 1988 [1], and is given as

$$2\zeta L\check{g}(\epsilon,T)\circ\nabla\check{g}(\epsilon,T) = [\check{g}_L(\epsilon,T)\circ\check{g}_R(\epsilon,T)]_-. \tag{3.21}$$

Here, $\zeta = R_B/R_N$ is the interface transparency and is given as the ratio between the barrier resistance R_B and the normal state material resistance R_N, and L is the length of the material in the direction of propagation. A more general boundary condition for arbitrary transmission channels, but without spin-active interfaces was made by Nazarov eleven years later. With a notation similar that of reference [56], the Nazarov boundary condition is given as

$$\frac{L}{R_N}\check{g}\circ\nabla\check{g} = 2\frac{e^2}{\pi}\sum_n \frac{T_n[\check{g}_L\circ\check{g}_R]_-}{4+T_n\left([\check{g}_L\circ\check{g}_R]_+-2\right)}. \tag{3.22}$$

The transmission eigenvalues T_n give the probability of scattering for different channels n. These eigenvalues can be found from the transmission matrix which characterizes the scattering in a junction [57, 58]. In a tunnel junction, these eigenvalues will be small $T_n \ll 1$, and thus the Nazarov boundary condition can be written as

$$\frac{L}{R_N}\check{g}\circ\nabla\check{g} = \frac{1}{2}\frac{e^2}{\pi}\left(\sum_n T_n\right)[\check{g}_L\circ\check{g}_R]_-. \tag{3.23}$$

The conductance of the barrier is given as the sum of all transmission eigenvalues, and thus the barrier resistance is $R_B = \frac{1}{e^2 \sum_n T_n/\pi}$, and we arrive at the KL boundary condition. We therefore do not need to know all transmission eigenvalues, but instead only a single scalar ζ.

We will throughout this thesis assume that the interfaces are not spin-polarized, and thus the KL boundary condition will be adequate. There has however been made several progresses in deriving more general boundary conditions, and a derivation of a fully generalized boundary condition in the diffusive limit can be found in reference [55]. In addition, boundary conditions for spin-orbit coupled interfaces were very recently derived in reference [80].

3.5 Bulk Superconductor and Normal State Metal Solutions

Deep inside a superconductor we can assume that the Green's function is constant over position, and so the Usadel equation becomes

$$\left[\epsilon\hat{\tau}_3 + \hat{\Delta}, \hat{g}^R\right]_- = 0. \tag{3.24}$$

This equation in itself is not enough to find the bulk BCS Green's function, but it can be shown [6] that the solution will be

$$\hat{g}^R_{BCS} = \begin{bmatrix} \cosh(\theta(\epsilon))\underline{\sigma}_0 & \sinh(\theta(\epsilon))i\underline{\sigma}_2 e^{i\phi} \\ \sinh(\theta(\epsilon))i\underline{\sigma}_2 e^{-i\phi} & -\cosh(\theta(\epsilon))\underline{\sigma}_0, \end{bmatrix} \tag{3.25}$$

where $\theta(\epsilon) = \text{atanh}(|\Delta|/\epsilon)$. This is the BCS solution for a bulk superconductor, and it will be used as a starting point in numerical simulations and will be used as a boundary condition when looking at the weak proximity effect. It is easy to show that this equation both satisfies the Usadel equation and the constraint $\left(\hat{g}^R\right)^2 = \hat{\tau}_0$.

In a normal metal the gap energy is zero and we simple get

$$\hat{g}^R = \begin{bmatrix} 1 & 0 \\ 0 & -1 \end{bmatrix} = \hat{\tau}_3. \tag{3.26}$$

3.6 Numerical Calculations

The Usadel equation for the retarded Green's function is a 4×4 matrix differential equation which yields a total of 16 coupled differential equations. There is absolutely no hope in trying to solve such a problem analytically. It is however possible to make approximations such as the weak proximity approximation, which simply sets $\underline{g} = \underline{\sigma}_0$, and we thus only need to solve the anomalous Green's functions $\underline{f}$. However, if the proximity effect is strong, this approximation can fail to capture essential details of our system. We therefore have to resolve to numerical methods to find our Green's function.

3.6.1 Theta-Parameterization

One way to solve the Usadel equation is to use the so-called theta-parameterization. This is based on using the following parameterization [6]:

$$\underline{g} = \cosh(\theta(x,\epsilon))\underline{\sigma}_0 \tag{3.27}$$

$$\underline{f} = \sinh(\theta(x,\epsilon))e^{i\phi(x,\epsilon)}i\underline{\sigma}_2. \tag{3.28}$$

One would then plug the corresponding retarded Green's function into the Usadel equation and KL boundary condition to solve $\theta(x,\epsilon)$ and $\phi(x,\epsilon)$. Such a parameterization is useful when considering a bulk BCS superconductors. In that case we simply get the BCS solution we mentioned on the last page,

$$\hat{g}^R_{BCS} = \begin{bmatrix} \cosh(\theta(\epsilon))\underline{\sigma}_0 & \sinh(\theta(\epsilon))e^{i\phi(\epsilon)}i\underline{\sigma}_2 \\ \sinh(\theta(\epsilon))e^{-i\phi(\epsilon)}i\underline{\sigma}_2 & -\cosh(\theta(\epsilon))\underline{\sigma}_0 \end{bmatrix}. \tag{3.29}$$

which is independent of position and by using equation (3.26), we find that $\phi(\epsilon) = \phi$ which is simply the macroscopic phase of the superconductor and $\theta(\epsilon) = \text{atanh}(\Delta/\epsilon)$. This parameterization is however not useful when wanting to describe triplet states since the diagonal components of $\underline{f}$ are zero and can only describe singlet states, and thus, this parameterization is useless in our case.

3.6.2 Riccati-Parameterization

The Green's function comes with a great deal of symmetries and constraints which can be satisfied by making the parameterization [8, 73]:

$$\hat{g}^R = \begin{bmatrix} \underline{N}\left(1+\underline{\gamma}\underline{\tilde{\gamma}}\right) & 2\underline{N}\underline{\gamma} \\ -2\underline{\tilde{N}}\underline{\tilde{\gamma}} & -\underline{\tilde{N}}\left(1+\underline{\tilde{\gamma}}\underline{\gamma}\right), \end{bmatrix} \tag{3.30}$$

where the normalization matrix is $\underline{N} = \left(1-\underline{\gamma}\underline{\tilde{\gamma}}\right)^{-1}$, and the tilde conjugation means changing the sign of ϵ and complex conjugating. This parameterization effectively turns the 16 differential into eight differential equations for every element of the matrices $\underline{\gamma}$ and $\underline{\tilde{\gamma}}$. It also has the advantage of being restricted to the interval $\underline{\gamma} \to [0,1]$; when elements of the retarded Green's function goes to zero, then $||\underline{\gamma}|| \to 0$, and if some elements of the Green's function diverges, then $||\gamma|| \to 1$. This gives a high numerical stability when solving the Usadel equation since $\underline{\gamma}$ is bounded to a small interval. With this parameterization, it is possible to derive the Usadel equation for $\underline{\gamma}$ with intrinsic spin-orbit coupling which was first derived by Ouassou in reference [8],

$$\begin{aligned} D\Big[\nabla^2\underline{\gamma} + 2\nabla\underline{\gamma}\underline{\tilde{N}}\underline{\tilde{\gamma}}\nabla\underline{\gamma}\Big] \\ = &-2i\epsilon\underline{\gamma} - \Delta\underline{\sigma}_2 + \underline{\gamma}\Delta^*\underline{\sigma}_2\underline{\gamma} - i\boldsymbol{M}\cdot\left(\underline{\boldsymbol{\sigma}}\underline{\gamma} - \underline{\gamma}\underline{\boldsymbol{\sigma}}^*\right) \\ &+ D\left[\underline{\boldsymbol{A}}^2\underline{\gamma} - \underline{\gamma}\left(\underline{\boldsymbol{A}}^*\right)^2 + 2\left(\underline{\boldsymbol{A}}\underline{\gamma} + \underline{\gamma}\underline{\boldsymbol{A}}^*\right)\underline{\tilde{N}}\left(\underline{\boldsymbol{A}}^* + \underline{\tilde{\gamma}}\underline{\boldsymbol{A}}\underline{\gamma}\right)\right] \\ &+ 2iD\left[\nabla\underline{\gamma}\underline{\tilde{N}}\left(\underline{\boldsymbol{A}}^* + \underline{\tilde{\gamma}}\underline{\boldsymbol{A}}\underline{\tilde{\gamma}}\right) + \left(\underline{\boldsymbol{A}} + \underline{\gamma}\underline{\boldsymbol{A}}^*\underline{\gamma}\right)\underline{N}\nabla\underline{\gamma}\right]. \end{aligned} \tag{3.31}$$

We get the other four differential equations by taking the tilde conjugation of the equation above. The KL boundary condition with this parameterization becomes

$$\boldsymbol{e}_i\cdot\nabla\underline{\gamma}_L = \frac{1}{L\zeta}\left(1-\underline{\gamma}_L\underline{\tilde{\gamma}}_R\right)\underline{N}_R\left(\underline{\gamma}_R - \underline{\gamma}_L\right) + i\boldsymbol{e}_i\cdot\left(\underline{\boldsymbol{A}}\underline{\gamma}_L + \underline{\gamma}_L\underline{\boldsymbol{A}}^*\right), \tag{3.32}$$

$$\boldsymbol{e}_i\cdot\nabla\underline{\gamma}_R = \frac{1}{L\zeta}\left(1-\underline{\gamma}_R\underline{\tilde{\gamma}}_L\right)\underline{N}_L\left(\underline{\gamma}_R - \underline{\gamma}_L\right) + i\boldsymbol{e}_i\cdot\left(\underline{\boldsymbol{A}}\underline{\gamma}_R + \underline{\gamma}_R\underline{\boldsymbol{A}}^*\right). \tag{3.33}$$

Here, $\boldsymbol{e}_i$ is the normal vector of the interface pointing from what we define as left to what we define as right. In a normal metal, the retarded Green's function is simply $\hat{g} = \hat{\tau}_3$ and thus

$$\underline{N}_N = \underline{\sigma}_3 \qquad \underline{\gamma}_N = 0. \tag{3.34}$$

And in a superconductor, we can from the theta-parameterization in equation (3.29) get

$$\underline{N}_{BCS} = \frac{1}{2}(\cosh(\theta(\epsilon)) + 1)\underline{\sigma}_0 \qquad \underline{\gamma}_{BCS} = \frac{\sinh(\theta(\epsilon))e^{i\phi}}{\cosh(\theta(\epsilon)) + 1} i\underline{\sigma}_2. \tag{3.35}$$

3.7 Spin-Orbit Coupling

We are also interested in how we can incorporate spin-orbit coupling into our equations. Later, we will look at both Rashba and Dresselhaus spin-orbit coupling [30, 31] which couples to the momenta of the quasiparticles. Thus, the spin-orbit coupling terms will be on the form

$$H_R + H_D = \frac{1}{\hbar m}(\boldsymbol{p} \cdot \boldsymbol{W})\boldsymbol{\sigma} = \frac{1}{\hbar m}\sum_{ij} p_i W_{ij} \underline{\sigma}_j \tag{3.36}$$

where $\boldsymbol{W}$ is the interaction matrix and m is the effective mass of the quasiparticles. The interaction matrix describes how the different spin-orbit coupling effects interact with the momentum $\boldsymbol{p}$. So for example, if we have a planar structure in the xy-plane with a very small width in the z-direction, we have the following interaction matrix:

$$\boldsymbol{W} = \begin{bmatrix} \beta & -\alpha & 0 \\ \alpha & -\beta & 0 \\ 0 & 0 & 0 \end{bmatrix}, \tag{3.37}$$

where α and β are the Rashba and Dresselhaus constants, respectively. With this $\boldsymbol{W}$ the spin-orbit coupling Hamiltonian becomes

$$H_{SOC} = H_R + H_D = \frac{\alpha}{\hbar m}(\underline{\sigma}_1 p_y - \underline{\sigma}_2 p_x) + \frac{\beta}{\hbar m}\left(\underline{\sigma}_1 p_x - \underline{\sigma}_2 p_y\right). \tag{3.38}$$

If we assume that both the Rashba and Dresselhaus constant is small, we can incorporate the Hamiltonian into the vector potential in the canonical momentum operator. This operator is normally defined as

$$\boldsymbol{p} = m\boldsymbol{v} - e\boldsymbol{A} = -i\hbar\nabla. \tag{3.39}$$

We then define a new vector potential as

$$\boldsymbol{A} \to \underline{\boldsymbol{A}} = e\boldsymbol{A} + \boldsymbol{W}\underline{\sigma}. \tag{3.40}$$

The vector potential normally exhibits a $U(1)$ gauge field, but now with the spin-orbit coupling present, the vector potential becomes a vector of Pauli matrices and thus becomes a $SU(2)$ gauge field. We will later assume that there is no ordinary vector potential present and only spin-orbit coupling and so we set the original vector potential to zero, i.e. $\boldsymbol{A} = 0$. To incorporate this into our equations later, we simply define [29]

$$\tilde{\nabla}(\cdot) = \nabla(\cdot) - i\left[\hat{\boldsymbol{A}}, (\cdot)\right]_-, \tag{3.41}$$

where $\hat{\boldsymbol{A}} = \text{diag}(\underline{\boldsymbol{A}}, -\underline{\boldsymbol{A}}^*)$, and we can combine the kinetic and spin-orbit coupled Hamiltonian as

$$H_0 + H_{SOC} = -\frac{\hbar^2}{2m}\tilde{\nabla}^2. \tag{3.42}$$

It is possible to show that this new $SU(2)$ gauge-invariant derivative, will substitute the normal derivatives $\nabla \to \tilde{\nabla}$ in both the Usadel equation and in the Kupriyanov-Lukichev boundary condition.

3.8 Precessing Magnetization

When a ferromagnet is placed in an external magnetic field, its magnetic field $\boldsymbol{M}(t)$ will start precessing around the axis of the external field if a torque is added. This precession is governed by the Landau-Lifshitz-Gilbert (LLG) equation [13, 53, 68]

$$\frac{d\boldsymbol{M}(t)}{dt} = -\gamma \boldsymbol{M}(t) \times \boldsymbol{H}_{\text{eff}}(t) + \alpha \boldsymbol{M}(t) \times \frac{d\boldsymbol{M}(t)}{dt}. \tag{3.43}$$

Here, $\boldsymbol{H}_{\text{eff}}$ is the effective magnetic field, γ is the gyromagnetic ration and α is the Gilbert damping constant. The two terms on the right hand side decide two different factors: The first term decides how fast the precession of the magnetic field is. The bigger γ, the faster the angular precession Ω. The second term is the damping term, and it is responsible for decreasing the angle θ between the magnetic field $\boldsymbol{M}(t)$ and the externally applied field. To combat this damping term we can apply a microwave field with a magnetic component $\boldsymbol{h}_t$ perpendicular to the applied field $\boldsymbol{H}_{\text{eff}} = H_0 \boldsymbol{e}_z$ [14, 15]. This method is called ferromagnetic resonance (FMR), and at resonance, we get that the magnetic field precesses as

$$\boldsymbol{M}(t) = M\Big(\sin(\theta)\cos(\Omega t), \sin(\theta)\sin(\Omega t), \cos(\theta) \Big). \tag{3.44}$$

Where the tilt angle θ and the angular frequency at resonance Ω, also called Larmor frequency, are independent of time. A more realistic precessional motion of the magnetic field is possible to find [53] which includes the Gilbert damping, but we will use the above magnetization for simplicity. To find the variables we have to solve the LLG equation with the material specific γ. We will not do so in this thesis, but merely assume that we can manipulate both variables, θ and Ω, as we see fit.

At resonance, one can estimate the tilt angle from the LLG equation to be $\theta \approx \mu|\boldsymbol{h}_t|/\alpha\hbar\Omega$ μ is the Bohr magneton [7]. A large tilt angle $\theta \approx 15^\circ$ can be obtained in soft ferromagnets. The resonance frequency Ω can be calculated from the LLG equation by using the magnetic field in equation (3.44) with $\boldsymbol{H}_{\text{eff}}(t) = H_0 \boldsymbol{e}_z$. This yields $\Omega = \gamma H_0$. And for moderate fields H_0, the resonance frequency can become on the order of $\hbar\Omega \approx k_B T$, which for $T = 1\text{K}$ is approximately $\Omega = 30\text{GHz}$. This yields energies on the order of $\hbar\Omega \approx 2 \cdot 10^{-2}$ meV, which is much less than the Fermi energies in metals of around $1 - 10$ eV. We will therefore neglect any spin-relaxation and therefore assume that spin-accumulation does not decay [13].

It was recently shown that the tilt angle θ in a ferromagnet in a SFS Josephson junction decreases at resonance when the temperature is decreased from above the transition temperature T_c to under it [76]. This tells us that the Gilbert damping term in the LLG equation has increased. The researchers only showed this to be true in a ferromagnet in a SFS Josephson junction, and not in a FS bilayer. The researchers argued that this is due to the supercurrent

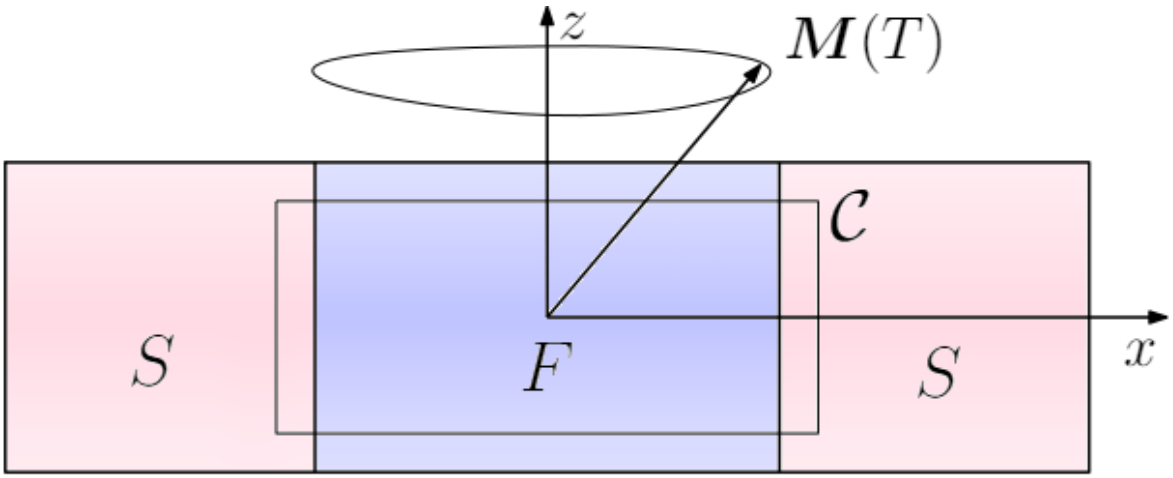

Figure 3.1: SFS Josephson junction with a precessing magnetic field. $\mathcal{C}$ is a contour in the xz-plane.

carried by equal spin up triplet pairs that are aligned with the applied magnetic field H_0, and thus, they add a torque to the exchange field of the ferromagnet which effectively decreases the tilt angle θ. Since no current can flow in an isolated FS bilayer, this effect is not seen in such a hybrid structure.

3.8.1 Gauge-Invariant Phase Difference

When calculating the properties of a Josephson junction within the quasiclassical framework, one usually use the macroscopic phases as an input variable which one sets to an arbitrary value. One thus do not calculate the gauge-invariant phase which in the case of a precessing magnetization will change the phase over time. The gauge-invariant phase difference γ will then become [3]

$$\gamma \equiv \Delta\phi - \frac{2\pi}{\Theta_0}\int_{\mathcal{C}} \boldsymbol{A}(T)\cdot d\boldsymbol{s}. \tag{3.45}$$

Here, Θ_0 is the magnetic quantum flux defined as $\Theta_0 = h/2e$, and the integration goes along a contour $\mathcal{C}$ going through both superconductors as seen in figure 3.1. The vector potential can be found from the equation $\boldsymbol{B}(T) = \nabla \times \boldsymbol{A}(T)$. Using Stokes' theorem, one can write the gauge-invariant phase difference as

$$\gamma = \Delta\phi - \frac{2\pi}{\Theta_0}\int \boldsymbol{B}(T)\cdot d\boldsymbol{a}. \tag{3.46}$$

Since the integration area has to connect both superconductors, the flux will have the y and z-component of the exchange field, $B_y(T)$ and B_z. Both components will depend linearly on position and if the flux area is large then the current may move in both directions for different transverse positions, (y, z), in the junction. For small junctions, one assumes the flux area is small and one can thus neglect the flux, but we are interested in seeing how the time-dependent flux through $B_y(T)$ changes the gauge-invariant phase difference, and so we only neglect the z-component of the flux. The gauge-invariant phase then becomes

$$\gamma = \Delta\phi - \frac{2\pi}{\Theta_0} A B_y(T) \tag{3.47}$$

Here, A is the cross section area, and can be written as $A = L_F z$ where L_F is the length of the ferromagnet. This shows that the gauge-invariant phase difference gets a term that is proportional to $\sin(\Omega T)$. This phase difference can be picked up by the Usadel equation if we consider the contribution from the vector potential, but we will later neglect this contribution when solving the Usadel equation for simplicity. The point is that there is in fact a time-dependent contribution to the gauge-invariant phase difference. One other way to get a time-contribution to the phase difference is to have an applied voltage difference between two superconductors in a Josephson junction. One can easily show that this gives the phase difference an additional term that is linear in time in the quasiclassical framework [59, 60], which yields the time-varying phase relation Josephson showed in his paper in equation (2.3).

The time-varying and gauge-invariant phase difference above will not be used in our calculations later since the time convolution operator will make the problem close to impossible to solve, and we will simply assume that it is small and can be neglected.

3.8.2 Green's Function Transformation

We will in this section see how we can transform the Green's function into a frame where the magnetization is constant in time. We therefore need to find a transformation $\hat{U}(t)$ such that we transform into a stationary frame where the magnetization in (3.44) becomes time-independent,

$$\hat{U}(t)\boldsymbol{M}(t)\cdot\hat{\boldsymbol{\sigma}}\hat{U}^\dagger(t) = \boldsymbol{M}(0)\cdot\hat{\boldsymbol{\sigma}}. \tag{3.48}$$

Such a transformation is known [7, 13] and is simply $\hat{U}(t) = \exp(i\Omega t\hat{\tau}_3\hat{\sigma}_3)$, and the equation above can easily be verified by the identity $\exp(ia\hat{\tau}_3\hat{\sigma}_3) = \cos(a)\hat{\tau}_0 + i\sin(a)\hat{\tau}_3\hat{\sigma}_3$. Note that we will in this section, and most of the thesis, neglect the time-dependence of the phase difference stemming from the time-dependent magnetic flux through the junction. If we had not neglected this contribution, the transformation $\hat{U}(t)$ would not leave the phase difference time-independent in the stationary frame. However, in a FS bilayer, we have no phase difference across the ferromagnet, and thus the transformation $\hat{U}(t)$ will always leave the new frame stationary.

Next, we are interesting in knowing how this transformation effects the Usadel equation in the new, stationary frame. We therefore go back to the roots of the Usadel equation, namely Gorkov's equation. From now on, we will start setting $\hbar = 1$. Gorkov's equation in a system with ferromagnetism and superconductive ordering is given as [6, 34]

$$\begin{gathered} i\frac{\partial}{\partial t_1}\hat{\tau}_3\check{G}(1,2) + i\frac{\partial}{\partial t_2}\check{G}(1,2)\hat{\tau}_3 = \\ \begin{bmatrix} \xi(1)+\underline{\lambda}(1) & -\underline{\Delta}(1) \\ -\underline{\Delta}^*(1) & \xi(1)+\underline{\lambda}^*(1) \end{bmatrix}\check{G}(1,2) - \check{G}(1,2)\begin{bmatrix} \xi(2)+\underline{\lambda}^\dagger(2) & -\underline{\Delta}(2) \\ -\underline{\Delta}^*(2) & \xi(2)+\underline{\lambda}^T(2) \end{bmatrix}. \end{gathered} \tag{3.49}$$

Here, we have defined the matrices

$$\underline{\Delta}(1) = i\sigma_2\Delta(1), \tag{3.50}$$

$$\xi(1) = e\phi(1) - \mu + V_{\text{imp}}(1), \tag{3.51}$$

$$\underline{\lambda}(1) = -\frac{1}{2m}\nabla^2 - \boldsymbol{M}(1)\cdot\underline{\boldsymbol{\sigma}}. \tag{3.52}$$

Here, Δ is the gap energy, V_{imp} is the potential due to non-magnetic impurities. μ is the chemical potential and ϕ is the electrical potential. Note, that we do not include any intrinsic spin-orbit coupling like Rashba and Dresselhaus type in this equation. We then apply the transformation to a new Green's function, $\check{G}(1,2) \to \check{G}(\boldsymbol{r}, \boldsymbol{R}, t, T) = \hat{U}^\dagger(t_1)\check{G}'(\boldsymbol{r}, \boldsymbol{R}, t)\hat{U}(t_2)$. Thus, the center-of-mass time T dependence lies in the transformation $\hat{U}$. And we are now interested in finding an equation of motion for the new Green's function $\check{G}'(\boldsymbol{r}, \boldsymbol{R}, T)$ in the stationary frame. Applying this Green's function to the part of Gorkov's equation that contains any exchange fields above gives us,

$$
\begin{aligned}
&- \boldsymbol{M}(t_1)\cdot\hat{\boldsymbol{\sigma}}\hat{U}^\dagger(t_1)\check{G}'(1,2)\hat{U}(t_2) + \hat{U}^\dagger(t_1)\check{G}'(1,2)\hat{U}(t_2)\boldsymbol{M}(t_2)\cdot\hat{\boldsymbol{\sigma}} \\
&= \hat{U}^\dagger(t_1)\left(-\hat{U}(t_1)\boldsymbol{M}(t_1)\cdot\hat{\boldsymbol{\sigma}}\hat{U}^\dagger(t_1)\right)\check{G}'(1,2)\hat{U}(t_2) \\
&- \hat{U}^\dagger(t_1)\check{G}'(1,2)\left(-\hat{U}(t_2)\boldsymbol{M}(t_2)\cdot\hat{\boldsymbol{\sigma}}\hat{U}(t_2)^\dagger\right)\hat{U}(t_2) \qquad (3.53) \\
&= \hat{U}^\dagger(t_1)\left[-\boldsymbol{M}(0)\cdot\hat{\boldsymbol{\sigma}}, \check{G}'(1,2)\right]_-\hat{U}(t_2). \qquad (3.54)
\end{aligned}
$$

In the last line, we used that $\hat{U}(t)\boldsymbol{M}(t)\cdot\hat{\boldsymbol{\sigma}}\hat{U}^\dagger(t) = \boldsymbol{M}(0)\cdot\hat{\boldsymbol{\sigma}}$, and we explicitly see that the transformation yields a stationary exchange field. Then we need to do the transformation on the left hand side of Gorkov's equation,

$$
\begin{aligned}
&i\frac{\partial}{\partial t_1}\check{\tau}_3\hat{U}^\dagger(t_1)\check{G}'(1,2)\hat{U}(t_2) + i\frac{\partial}{\partial t_2}\hat{U}^\dagger(t_1)\check{G}'(1,2)\hat{U}(t_2)\check{\tau}_3 \\
&= i\check{\tau}_3\hat{U}^\dagger(t_1)\left(-i\frac{\Omega}{2}\hat{\tau}_3\hat{\sigma}_3 + \frac{\partial}{\partial t_1}\right)\check{G}'(1,2)\hat{U}(t_2) \\
&+ i\hat{U}^\dagger(t_1)\left(i\frac{\Omega}{2}\check{G}'(1,2)\hat{\tau}_3\hat{\sigma}_3 + \frac{\partial}{\partial t_2}\check{G}'(1,2)\right)\hat{U}(t_2)\check{\tau}_3 \\
&= \hat{U}^\dagger(t_1)\left(\frac{\Omega}{2}\hat{\sigma}_3 + \frac{\partial}{\partial t_1}\right)\check{G}'(1,2)\hat{U}(t_2) \\
&+ \hat{U}^\dagger(t_1)\left(-\frac{\Omega}{2}\check{G}'(1,2)\hat{\sigma}_3 + \frac{\partial}{\partial t_2}\check{G}'(1,2)\right)\hat{U}(t_2) \\
&= \hat{U}^\dagger(t_1)\left(\left[\frac{\Omega}{2}\hat{\sigma}_3, \check{G}'(1,2)\right]_- + i\hat{\tau}_3\frac{\partial}{\partial t_1}\check{G}'(1,2) + i\frac{\partial}{\partial t_2}\check{G}'(1,2)\hat{\tau}_3\right)\hat{U}(t_2) \qquad (3.55)
\end{aligned}
$$

Here, we used the fact that $\hat{\tau}_3$, $\hat{\sigma}_3$, $\hat{U}^\dagger(t_1)$ and $\hat{U}(t_2)$ all commute with each other and that $\hat{\tau}_3^2 = \hat{\tau}_0$. By combining the left term above with the new, stationary exchange field, we get

$$
\begin{aligned}
&\hat{U}^\dagger(t_1)\left[-\boldsymbol{M}(0)\cdot\hat{\boldsymbol{\sigma}} - \frac{\Omega}{2}\hat{\sigma}_3, \check{G}'(1,2)\right]_-\hat{U}(t_2) \qquad (3.56) \\
&= \hat{U}^\dagger(t_1)\left[-\left(\boldsymbol{M}(0)\cdot\hat{\boldsymbol{\sigma}} + \frac{\Omega}{2}\hat{\sigma}_3\right), \check{G}'(1,2)\right]_-\hat{U}(t_2) \qquad (3.57) \\
&= \hat{U}^\dagger(t_1)\left[-\left(M\sin(\theta)\hat{\sigma}_1 + \left(M\cos(\theta) + \Omega/2\right)\hat{\sigma}_3\right), \check{G}'(1,2)\right]_-\hat{U}(t_2). \qquad (3.58)
\end{aligned}
$$

We get a new, effective exchange field $\boldsymbol{M}' = (M\sin(\theta), 0, M\cos(\theta) + \Omega/2)$ in this new, stationary frame. Note that the transformation leaves every other matrices in Gorkov's equation invariant, such as $\hat{\Delta}(1)$, i.e. $\hat{U}(t)\hat{\Delta}(1)\hat{U}^\dagger(t) = \hat{\Delta}(1)$. This is unlike a Josephson

junction with an applied voltage as shown in references [59, 60]. With an applied voltage the transformation is on the form $\hat{U}(t) = e^{ieVt\hat{\tau}_3}$. Applying this transformation to $\hat{\Delta}$ will give a time-varying phase, and in turn give an AC current. This does not happen with our spin-space rotation transformation.

By multiplying our new Gorkov's equation with $\hat{U}(t_1)$ on the left side, and $\hat{U}^\dagger(t_2)$ on the right side, we can get rid of the unwanted transformations, and we are left with the old Gorkov's equation, but with a new, stationary exchange field $\boldsymbol{M}'$. It should be noted that we will get an effective, non-zero exchange field even when $M = 0$. In that case, we get $\boldsymbol{M}' = \Omega/2\boldsymbol{e}_z$. Thus, the stationary frame causes a Zeeman split which energetically favors a spin-up direction if the rotation is counter-clockwise, $\Omega > 0$.

We have therefore shown that by making the transformation $\check{G}(1,2) \rightarrow \check{G}(\boldsymbol{r}, \boldsymbol{R}, t, T) = \hat{U}^\dagger(t_1)\check{G}'(\boldsymbol{r}, \boldsymbol{R}, t)\hat{U}(t_2)$, we get a stationary Gorkov's equation for the new Green's function $\check{G}'(\boldsymbol{r}, \boldsymbol{R}, t)$. With this new equation, one can derive the Usadel equation in the usual way, obtaining a stationary Usadel equation valid for the new, stationary Green's function, except that we have to use the new, effective exchange field $\boldsymbol{M}'$, and the ring products will be reduced to regular matrix multiplications in this frame. We will later show how we can go back go back to laboratory Green's function in energy space for the quasiclassical Green's function. It is important to note that we will use an apostrophe to denote variables and functions in the stationary frame such as $\check{G}'$ and $\boldsymbol{M}'$, while the corresponding variables and functions without an apostrophe will mean they are given in the laboratory frame. It will later prove effectively to find the Green's functions in the stationary frame and express observables in the laboratory frame with these stationary Green's functions.

Note that the transformation $\hat{U}(t)$ repeats itself along the diagonal in Keldysh space, and thus it acts equally on the three components of the Green's function in Keldysh space, namely the retarded, advanced and Keldysh Green's function.

4 | Observables

So far we have found a transport equation for the Green's functions and distribution function in the quasiclassical theory, but they themselves are not observables. We are therefore interested in using these functions to express currents and other observables that can be measured in a laboratory. The derivations in this chapter are mostly following the derivations found in references [6, 34, 81].

4.1 Gap Energy

We are now interested in how we can acquire the gap energy from the quasiclassical Green's functions. The superconducting order parameter is defined as [6, 12]

$$\Delta(1) = \lambda(1)\langle\psi_\downarrow(1)\psi_\uparrow(1)\rangle, \tag{4.1}$$

where λ is the coupling constant of the electron-lattice interaction. This can be expressed by either of the two off-diagonal Keldysh anomalous Green's functions

$$\underline{F}^K_{\uparrow\downarrow}(1,1) = -i\langle[\psi_\uparrow(1),\psi_\downarrow(1)]_-\rangle = -2i\langle\psi_\uparrow(1)\psi_\downarrow(1)\rangle, \tag{4.2}$$

$$\underline{F}^K_{\downarrow\uparrow}(1,1) = -i\langle[\psi_\downarrow(1),\psi_\uparrow(1)]_-\rangle = 2i\langle\psi_\uparrow(1)\psi_\downarrow(1)\rangle, \tag{4.3}$$

where we have used the anti-commutation relations for fermions. Thus the gap energy can be written in the two following ways:

$$\Delta(1) = \frac{\lambda i}{2}\underline{F}^K_{\uparrow\downarrow}(1,1), \tag{4.4}$$

$$\Delta(1) = -\frac{\lambda i}{2}\underline{F}^K_{\downarrow\uparrow}(1,1), \tag{4.5}$$

but later on it will be to our advantageous to combine both off-diagonal anomalous Keldysh Green's functions to express the gap energy. Doing so gives us

$$\Delta(1) = \frac{\lambda i}{4}\left(\underline{F}^K_{\uparrow\downarrow}(1,1) - \underline{F}^K_{\downarrow\uparrow}(1,1)\right). \tag{4.6}$$

So far this expression for the gap energy is exact as long as the superconductor is a conventional BCS superconductor. We are now interested in expressing this with our quasiclassical Green's function. In doing so, we also switch over to mixed coordinates

$$\begin{aligned}\underline{F}^K(1,1) &= \lim_{\boldsymbol{r}\to 0}\lim_{\boldsymbol{t}\to 0}\underline{F}^K(\boldsymbol{R}+\boldsymbol{r}/2, T+t/2; \boldsymbol{R}-\boldsymbol{r}/2, T-t/2)\\ &= \lim_{\boldsymbol{r}\to 0}\lim_{\boldsymbol{t}\to 0}\frac{1}{(2\pi)^4}\int d\boldsymbol{p}d\epsilon e^{i(\boldsymbol{p}\cdot\boldsymbol{r}-\epsilon t)}\underline{F}^K(\boldsymbol{R},T)\\ &= \frac{1}{(2\pi)^4}4\pi\int p^2 dp d\epsilon\frac{d\Omega}{4\pi}\underline{F}^K(\boldsymbol{R},T). \end{aligned} \tag{4.7}$$

We then express the angular average over momentum space as $\int \frac{d\Omega}{4\pi}\underline{F}^K(\boldsymbol{R},T) = \langle\underline{F}^K(\boldsymbol{R},T)\rangle$. We also convert the momentum integral into an integral over the kinetic energy $\xi = \frac{p^2}{2m} - \mu$. This gives $p^2dp = m^{3/2}\sqrt{2(\xi+\mu)}d\xi$. The quasiclassical approximation states that the kinetic energy $p^2/2m$ of quasiparticles lie close to the Fermi energy, so we can approximate $\xi = 0$. We then get

$$\underline{F}^K(1,1) = \frac{1}{4\pi^3}m^{3/2}\sqrt{2\mu}\int d\xi d\epsilon\langle\underline{F}^K(\boldsymbol{R},T)\rangle. \tag{4.8}$$

Expressing this with the quasiclassical Green's function yields

$$\underline{F}^K(1,1) = -\frac{i}{2}N_0\int d\epsilon\underline{f}^K(\boldsymbol{R},T), \tag{4.9}$$

where N_0 is the density of states at Fermi level. We can now express the gap energy as

$$\Delta(\boldsymbol{R},T) = \frac{N_0\lambda}{8}\int_{-\omega_c}^{\omega_c} d\epsilon f^K_{\uparrow\downarrow}(\boldsymbol{R},T) - f^K_{\downarrow\uparrow}(\boldsymbol{R},T). \tag{4.10}$$

Only electrons with energies less than the Debye frequency ω_c will experience the positive attraction from the electron-lattice interaction λ [8, 12], and thus the integration interval has been set accordingly. We can express the Debye frequency as a function of the coupling constant λ and density of states N_0 by solving the above equation in a bulk BCS superconductor at zero temperature $T = 0$. This bulk BCS gap will throughout the thesis be called Δ_0. Taking the limit $\lim_{\beta\to\infty} h_1 = \lim_{\beta\to\infty}\tanh(\beta\epsilon/2) = \mathrm{sgn}(\epsilon)$, and using the known bulk BCS Green's function with the identity $\hat{g}^A = -\hat{\tau}_3\left(\hat{g}^R\right)^\dagger\hat{\tau}_3$, we get

$$\Delta_0 = \frac{N_0\lambda}{4}\int_{-\omega_c}^{\omega_c}\mathrm{sgn}(\epsilon)\Delta_0\left[\frac{\mathrm{sgn}(\epsilon)}{\sqrt{\epsilon^2-|\Delta_0|^2}} + \left(\frac{\mathrm{sgn}(\epsilon)}{\sqrt{\epsilon^2-|\Delta_0|^2}}\right)^*\right]. \tag{4.11}$$

The integrand is obviously even in ϵ, and thus we only need to integrate over positive energies. We can also compact the right side of the integrand to a real number, and we can divide both sides by Δ_0. The equation now becomes

$$1 = N_0\lambda\int_0^{\omega_c}\Re\left(\frac{1}{\sqrt{\epsilon^2-|\Delta_0|^2}}\right) \tag{4.12}$$

$$= N_0\lambda\int_{|\Delta_0|}^{\omega_c}\frac{1}{\sqrt{\epsilon^2-|\Delta_0|^2}}. \tag{4.13}$$

This integral can be solved exactly [8], and by reordering we get that the Debye frequency is

$$\omega_c = |\Delta_0|\cosh(1/N_0\lambda). \tag{4.14}$$

Later, when we will calculate the gap energy self-consistently, we will use the value $N_0\lambda = 0.25$ which yields $\omega_c \approx 27.3|\Delta_0|$. This choice is on the lower end of what is true for most conventional superconductors. For example, for Beryllium $N_0\lambda = 0.23$ while for Niobium $N_0\lambda = 0.82$, and Tin $N_0\lambda = 0.6$ [35]. We choose a low $N_0\lambda$ to lower the amount of numerical calculations we have to make later when calculating the gap energy numerically in the inverse proximity effect.

4.2 Charge and Spin-Currents

We are in this section interested in how we can describe a flow of both charge and spin in the diffusive limit. The charge and spin densities are given as

$$\begin{aligned}\rho_e(1) &= e\sum_\sigma \langle \psi_\sigma^\dagger(1)\psi_\sigma(1)\rangle \\ &= e\sum_{\sigma\sigma'} \langle \psi_\sigma^\dagger(1)\sigma^0_{\sigma\sigma'}\psi_{\sigma'}(1)\rangle, \qquad (4.15)\\ \boldsymbol{\rho}_s(1) &= \frac{1}{2}\sum_{\sigma\sigma'} \langle \psi_\sigma^\dagger(1)\boldsymbol{\sigma}_{\sigma\sigma'}\psi_{\sigma'}(1)\rangle. \qquad (4.16)\end{aligned}$$

As we can see, both the charge density and spin density are similar, and we will thus only show the derivation for the charge-current. But the derivation will be similar for the spin-currents. All densities must satisfy the continuation equation which yields the following known charge current:

$$\boldsymbol{j}_Q(1) = \sum_\sigma \frac{e}{m}\Re\langle \psi_\sigma^\dagger(1)\left(\boldsymbol{p}(1) - e\boldsymbol{A}(1)\right)\psi_\sigma(1)\rangle, \qquad (4.17)$$

we introduce the momentum operator $\boldsymbol{p}(1) = -i\nabla_1$, and we get

$$\begin{aligned}\boldsymbol{j}_Q(1) &= \frac{e}{2m}\sum_\sigma \left(\langle \psi_\sigma^\dagger(1)(-i\nabla_1 - e\boldsymbol{A}(1))\psi_\sigma(1)\rangle + \langle \psi_\sigma^\dagger(1)(-i\nabla_1 - e\boldsymbol{A}(1))\psi_\sigma(1)\rangle^*\right) \qquad (4.18)\\ &= \frac{e}{2m}\sum_\sigma \left(\langle \psi_\sigma^\dagger(1)(-i\nabla_1 - e\boldsymbol{A}(1))\psi_\sigma(1)\rangle + \langle \psi_\sigma^\dagger(1)(i\nabla_1 - e\boldsymbol{A}(1))\psi_\sigma(1)\rangle\right). \qquad (4.19)\end{aligned}$$

We then make an infinitesimal difference in the coordinates of the right brackets so that we can make use of the anti-commutation relations, $\left[\psi_\sigma(1), \psi_\sigma^\dagger(2)\right]_+ = \delta(1-2)$. The charge current can now be written as

$$\boldsymbol{j}_Q(1) = \lim_{2\to 1}\frac{-ie}{2m}\sum_\sigma \left[(\nabla_1 - ie\boldsymbol{A}(1)) - (\nabla_2 + ie\boldsymbol{A}(2))\right]\langle \psi_\sigma^\dagger(2)\psi_\sigma(1)\rangle \qquad (4.20)$$

We have here removed the term with the Dirac delta function since we are not allowing the coordinates (1) and (2) to ever be equal, but only be close to each other. We now incorporate the normal Keldysh Green's function,

$$G^K_{\sigma\sigma'} = i\left(\langle \psi_\sigma^\dagger(2)\psi_\sigma(1)\rangle - \langle \psi_\sigma(1)\psi_\sigma^\dagger(2)\rangle\right), \qquad (4.21)$$

by using the anti-commutation relation and ignoring its Dirac delta function again. This gives us

$$\boldsymbol{j}_Q(1) = \lim_{2\to 1} -\frac{e}{4m}\mathrm{Tr}\left[(\nabla_1 - \nabla_2 - ie\boldsymbol{A}(1) - ie\boldsymbol{A}(2))\,\underline{G}^K(1,2)\right] \tag{4.22}$$

.

We then switch over to mixed coordinates by inserting the Fourier transformed Green's function in the equation above. In this case, the limit $2 \to 1$ is equal to $\boldsymbol{r} \to 0$ and $t \to 0$. This also gives us $\nabla_1 - \nabla_2 = 2\nabla_r$. We now have

$$\begin{aligned}\boldsymbol{j}_Q(\boldsymbol{R},T) &= \lim_{(r,t)\to(0,0)} -\frac{e}{4m}\mathrm{Tr}\left[(2\nabla_r - ie\boldsymbol{A}(1) - ie\boldsymbol{A}(2))\int d\epsilon \frac{1}{2\pi}e^{-i\epsilon t}\int d\boldsymbol{p}\frac{1}{(2\pi)^3}e^{i\boldsymbol{r}\cdot\boldsymbol{p}}\underline{G}^K(\boldsymbol{R},\boldsymbol{p};T,\epsilon)\right] \\ &= -\frac{e}{2m}\int d\boldsymbol{p}d\epsilon\frac{1}{(2\pi)^4}\mathrm{Tr}\left[(i\boldsymbol{p} - ie\boldsymbol{A}(\boldsymbol{R},T))\,\underline{G}^K(\boldsymbol{R},\boldsymbol{p};T,\epsilon)\right]. \end{aligned} \tag{4.23}$$

It can be shown that the term proportional to $\boldsymbol{A}(\boldsymbol{R},T)$ only gives an imaginary contribution [34] and is therefore un-physical. We will therefore remove it. We continue by making the quasiclassical approximation, that is, we force the momentum to be equal to the Fermi momentum. We also rewrite $d\boldsymbol{p} = d\Omega p^2 dp = d\Omega m^{3/2}\sqrt{2(\xi+\mu)}d\xi$ and by using the quasiclassical approximation in equation (3.10) we get

$$\boldsymbol{j}_Q = -\frac{eN_0}{4m}\int d\epsilon \mathrm{Tr}\left(\int \frac{d\Omega}{4\pi}\boldsymbol{p}_f \underline{g}^K(\boldsymbol{R},\boldsymbol{p}_f;T,\epsilon)\right). \tag{4.24}$$

In the diffusive limit, it is possible to show that

$$\boldsymbol{p}_f\check{g} = -p_f\tau v_f \check{g}_s \circ \nabla\check{g}_s, \tag{4.25}$$

where $\check{g}_s$ is the spherical harmonics Green's function, v_f is the Fermi velocity, τ is the lifetime of the particle. By then defining the diffusion constant to be $D = \frac{1}{3}v_f^2\tau$ and averaging over the angular space, we get

$$\boldsymbol{j}_Q = \frac{N_0 e}{4}\int d\epsilon \mathrm{Tr}\left(\left(\underline{g}\circ\nabla\underline{g}\right)^K\right). \tag{4.26}$$

So far we have only found the charge current for electrons. We must also add the current of holes which propagate in the opposite direction of electrons, and thus by expanding to Nambu space. By expressing this as a current rather than a current density we arrive at

$$I_Q = \frac{N_0 DeA}{4}\int d\epsilon \mathrm{Tr}\left(\hat{\tau}_3\left(\check{g}\circ\nabla\check{g}\right)^K\right), \tag{4.27}$$

where A is the cross section. As we mentioned, the calculations for finding the spin-currents are similar to derive, and they become

$$I_s^v = \frac{N_0 DA}{8}\int d\epsilon \mathrm{Tr}\left(\hat{\tau}_3\hat{\sigma}_v\left(\check{g}\circ\nabla\check{g}\right)^K\right), \tag{4.28}$$

for $v \in \{1,2,3\}$. Note that we have not incorporated intrinsic spin-orbit coupling into our equations, but it is possible to show [8] that making the transformation in equation (3.41) in

the expression for the charge-current above will preserve the supercurrent in a material with spin-orbit coupling, i.e. $\nabla I_Q = 0$.

We will later be curious about the decomposition of the currents since they are not necessarily supercurrents. As can be seen from the expressions for the currents, some terms will contain the position derivative of the distribution functions, while some other will contain the distribution functions themselves. We can expand as follows:

$$(\check{g} \circ \nabla \check{g})^K = \hat{g}^R \circ \nabla \hat{g}^R \circ \hat{h} - \hat{h} \circ \hat{g}^A \circ \nabla \hat{g}^A \tag{4.29}$$

$$+ \nabla \hat{h} - \hat{g}^R \circ \left(\nabla \hat{h} \right) \circ \hat{g}^A. \tag{4.30}$$

In equilibrium, $\hat{h}$ will be constant in space and thus the upper line gives the contribution from the dissipationless supercurrent. The lower line on the other hand requires a non-zero gradient of the distribution function and thus a non-constant chemical potential. This drives a flow of quasiparticles in the direction of the gradient of the distribution function. This current is not dissipationless, and thus we will call the lower line the resistive current. Note that in a normal state metal which is not in proximity to a superconductor, we have $\hat{g}^R = \hat{\tau}_3 = -\hat{g}^A$, and using that $\left[\hat{h}, \hat{\tau}_3\right]_- = 0$, the bottom line simply becomes $2\nabla\hat{h}$.

4.3 Charge and Spin-Accumulation

Starting from equation (4.15) and (4.16), we can derive the charge and spin densities, which we will call charge and spin-accumulations, using the same approach as when we derived the currents. By separating the coordinates of the creation and annihilation operator by an infinitesimal difference, and using the definition of the Keldysh component (4.21) with the anti-commutation relations for fermions, we get

$$\rho_Q = \lim_{2 \to 1} -i \frac{e}{2} \mathrm{Tr} \left(G^K(1,2) \right) \tag{4.31}$$

$$\boldsymbol{\rho}_s = \lim_{2 \to 1} -i \frac{1}{4} \mathrm{Tr} \left(\boldsymbol{\sigma} G^K(1,2) \right). \tag{4.32}$$

We then continue by doing pretty much the same thing when deriving the currents: We switch over to mixed coordinates, use the quasiclassical approximation and take the dirty limit. We also have to remember to add the negative charges and opposite spins of holes, and we end up with

$$\rho_Q = -\frac{N_0 e}{4} \int d\epsilon \mathrm{Tr} \left(\hat{g}^K \right), \tag{4.33}$$

$$\boldsymbol{\rho}_s = \frac{N_0}{8} \int d\epsilon \mathrm{Tr} \left(\hat{\boldsymbol{\sigma}} \hat{g}^K \right). \tag{4.34}$$

To understand how the distribution function affects these accumulations, we can look at the case of a normal state metal with no pair correlations. Then we have $\hat{g}^K = 2\hat{\tau}_3\hat{h}$, and thus

$$\begin{aligned} \rho_Q &= -2N_0 e \int d\epsilon \mathrm{Tr} \left(\hat{\tau}_3 \hat{h} \right) /4 \\ &= -2N_0 e \int d\epsilon h_5, \end{aligned} \tag{4.35}$$

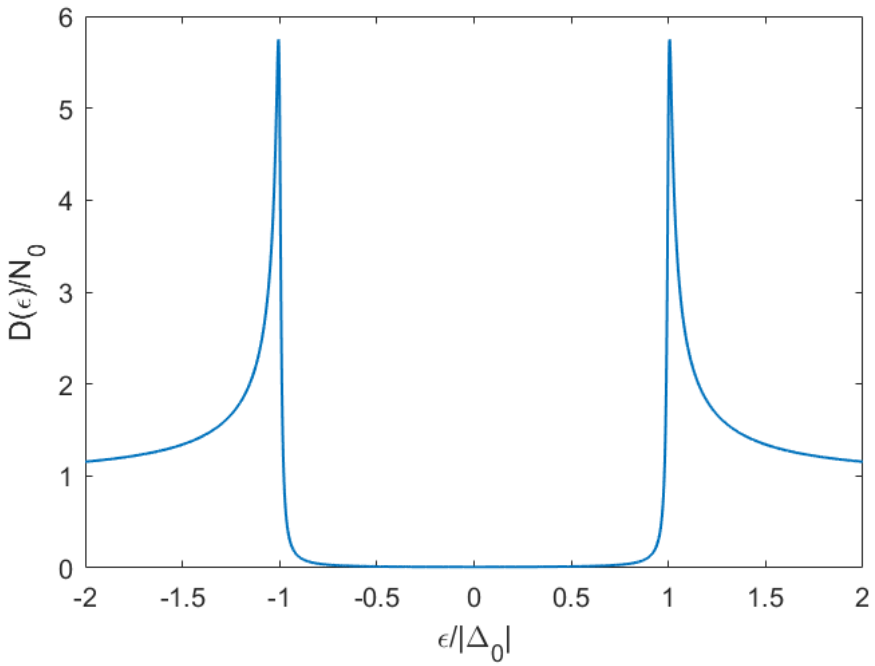

Figure 4.1: Density of states in a bulk BCS superconductor

and

$$\begin{aligned}\boldsymbol{\rho}_s &= N_0 \int d\epsilon \mathrm{Tr}\left(\hat{\boldsymbol{\sigma}}\hat{\tau}_3\hat{h}\right)/4 \\ &= N_0 \int d\epsilon \left(h_6, h_7, h_8\right), \end{aligned} \tag{4.36}$$

where we have used the identity $h_n = \mathrm{Tr}\left(\hat{\rho}_n\hat{h}\right)/4$ and $\hat{\rho}_n$ is defined in equation (3.20). We thus see that these distribution functions describe the accumulation of charge and spin. If we had calculated the currents above in a normal state metal without pair correlations, we would see that the currents are simply described by a gradient of their respective distribution functions.

4.4 Density of States

These spin-dependent density of states $D_\sigma(\boldsymbol{R}, T, \epsilon)$ can be found by taking the imaginary part of the Green's function [44],

$$D_\sigma(\boldsymbol{R}, \epsilon) = \lim_{\boldsymbol{r}\to 0} -\frac{1}{\pi}\Im\left(G^R_{\sigma\sigma}(\boldsymbol{R}, r; T, \epsilon)\right) \tag{4.37}$$

$$= \lim_{\boldsymbol{r}\to 0} -\frac{1}{\pi}\Im\left(\int \frac{d\boldsymbol{p}}{(2\pi)^3} e^{i\boldsymbol{p}\cdot\boldsymbol{r}} G^R_{\sigma\sigma}(\boldsymbol{R}, p; T, \epsilon)\right). \tag{4.38}$$

By then rewriting $d\boldsymbol{p} = p^2 dp d\Omega = m^{3/2}\sqrt{2(\xi+\mu)}d\xi d\Omega$, using the quasiclassical approximation and average over all spherical angles, we end up with

$$D_\sigma(\boldsymbol{R}, T, \epsilon) = N_0 \Re \left(g_{\sigma\sigma}(\boldsymbol{R}, T, \epsilon) \right). \tag{4.39}$$

If we are not interested in the spin, we can average both spin-directions and get a spin-independent density of states

$$D(\boldsymbol{R}, T, \epsilon) = \frac{N_0}{2} \mathrm{Tr} \left(\underline{g}(\boldsymbol{R}, T, \epsilon) \right). \tag{4.40}$$

In a conventional bulk BCS superconductor, the density of states can be seen in figure 4.1. We see that no quasiparticles can exist with energies less than the energy gap $|\epsilon| < |\Delta_0|$, and therefore, these quasiparticles are pushed outside this region and to energies close to, but larger than $|\Delta_0|$.

5 | Project 1: Precessing Exchange Field in Heterostructures

We are now going to look at the first of two research projects in this thesis which is FS bilayers and SFS Josephson junctions where the ferromagnet has a precessing magnetization on the form $\boldsymbol{M}(t) = M(\sin(\theta)\cos(\Omega t), \sin(\theta)\sin(\Omega t), \cos(\theta))$. In section 3.8.2 we showed how we can make the problem stationary by making the transformation $\check{G}(1,2) \to \check{G}(\boldsymbol{r}, \boldsymbol{R}, t, T) = \hat{U}^\dagger(t_1)\check{G}'(\boldsymbol{r}, \boldsymbol{R}, t)\hat{U}(t_2)$. In this stationary frame, the effective exchange field is $\boldsymbol{M'} = (M\sin(\theta), 0, M\cos(\theta) + \Omega/2)$, and we get the stationary Usadel equation for the transformed Green's function $\check{g}'(\epsilon)$ with this stationary exchange field. We still need to know what the laboratory Green's function is to be able to find observables like the gap energy and currents. The question is then, how do we go from the transformed Green's function to laboratory Green's function?

5.1 Going from the Transformed Frame to the Laboratory Frame

In the relative time space the quasiclassical retarded Green's function is given as $\hat{g}(t,T) = \hat{U}^\dagger(t_1)\hat{g}'(t)\hat{U}(t_2)$. Here, $t = t_1 - t_2$ is the relative time and the center-of-mass time is $T = \frac{t_1+t_2}{2}$. We are interested in finding $\hat{g}'$ in energy space. In this section, we will only do so for the retarded Green's function, but the same procedure is valid for the advanced and Keldysh components as well since the transformation $\hat{U}(t)$ acts in the same way on these components, as we showed in section 3.8.2. We have an equation of motion for the transformed Green's function in energy space $\hat{g}'$, and so we have to Fourier transform to relative time space, apply the transformation, and Fourier transform back to energy space. Thus

$$\hat{g}(\epsilon, T) = \int dt e^{i\epsilon t}\hat{g}(t,T) \tag{5.1}$$

$$= \int dt e^{i\epsilon t}\hat{U}^\dagger(t_1)\hat{g}'(t)\hat{U}(t_2) \tag{5.2}$$

$$= \int dt e^{i\epsilon t}\hat{U}^\dagger(t_1)\left(\frac{1}{2\pi}\int d\epsilon' e^{-i\epsilon' t}\hat{g}'(\epsilon)\right)\hat{U}(t_2) \tag{5.3}$$

$$= \frac{1}{2\pi}\int d\epsilon' dt e^{i(\epsilon-\epsilon')t}\hat{U}^\dagger(t_1)\hat{g}'(\epsilon)\hat{U}(t_2). \tag{5.4}$$

Applying the transformation to $\hat{g}'(\epsilon)$ will give some terms in the matrix a center-of-mass time dependent phase, i.e. $e^{\pm i\Omega T}$ while the other terms will get a relative time dependent phase, $e^{\pm i\Omega t/2}$. The center-of-mass time dependent elements will not be affected by the Fourier

transform, but the relative time dependent elements will undergo an energy shift. This can be shown by looking at a singe element in the product $\hat{U}^\dagger(t_1)\hat{g}'(\epsilon)\hat{U}(t_2)$ that becomes dependent on the relative time t,

$$g_{ij}(\epsilon) = \frac{1}{2\pi}\int d\epsilon' dt e^{i(\epsilon-\epsilon')t} g'_{ij}(\epsilon') e^{\pm i\Omega t/2} \tag{5.5}$$

$$= \frac{1}{2\pi}\int d\epsilon' dt e^{i(\epsilon-\epsilon'\pm\Omega/2)t} g'_{ij}(\epsilon') \tag{5.6}$$

$$= \int d\epsilon' \delta(\epsilon-\epsilon'\pm\Omega/2) g'_{ij}(\epsilon') \tag{5.7}$$

$$= g'_{ij}(\epsilon\pm\Omega/2). \tag{5.8}$$

To see which elements are affected by the relative and center-of-mass time phases, we calculate all elements

$$\hat{U}^\dagger(t_1)\hat{g}'(\epsilon)\hat{U}(t_2) = \begin{bmatrix} g'_{11}e^{-i\Omega t/2} & g'_{12}e^{-i\Omega T} & g'_{13}e^{-i\Omega T} & g'_{14}e^{-i\Omega t/2} \\ g'_{21}e^{i\Omega T} & g'_{22}e^{i\Omega t/2} & g'_{23}e^{i\Omega t/2} & g'_{24}e^{i\Omega T} \\ g'_{31}e^{i\Omega T} & g'_{32}e^{i\Omega t/2} & g'_{33}e^{i\Omega t/2} & g'_{34}e^{i\Omega T} \\ g'_{41}e^{-i\Omega t/2} & g'_{42}e^{-i\Omega T} & g'_{43}e^{-i\Omega T} & g'_{44}e^{-i\Omega t/2} \end{bmatrix}, \tag{5.9}$$

which after doing the Fourier transformation in equation (5.4) becomes

$$\hat{g}(\epsilon,T) = \begin{bmatrix} g'_{11}(\epsilon-\Omega/2) & g'_{12}(\epsilon)e^{-i\Omega T} & g'_{13}(\epsilon)e^{-i\Omega T} & g'_{14}(\epsilon-\Omega/2) \\ g'_{21}(\epsilon)e^{i\Omega T} & g'_{22}(\epsilon+\Omega/2) & g'_{23}(\epsilon+\Omega/2) & g'_{24}(\epsilon)e^{i\Omega T} \\ g'_{31}(\epsilon)e^{i\Omega T} & g'_{32}(\epsilon+\Omega/2) & g'_{33}(\epsilon+\Omega/2) & g'_{34}(\epsilon)e^{i\Omega T} \\ g'_{41}(\epsilon-\Omega/2) & g'_{42}(\epsilon)e^{-i\Omega T} & g'_{43}(\epsilon)e^{-i\Omega T} & g'_{44}(\epsilon-\Omega/2) \end{bmatrix}. \tag{5.10}$$

Thus, we see that every element of the laboratory Green's function either becomes center-of-mass time dependent or experiences an energy shift. Before going further, we will look at how the anomalous Green's function is affected by this transformation from the stationary frame to the laboratory frame. We choose to take use of the so-called d-vector [11]:

$$\underline{f} = (f_s + \boldsymbol{d}\cdot\underline{\boldsymbol{\sigma}})\, i\underline{\sigma}_2 = \begin{bmatrix} id_y - d_x & d_z + f_s \\ d_z - f_s & id_y + d_x \end{bmatrix}, \tag{5.11}$$

which expressed with the stationary Green's function $\hat{g}'$ in equation (5.10) becomes

$$\underline{f}(\epsilon) = \begin{bmatrix} (id'_y(\epsilon) - d'_x(\epsilon))e^{-i\Omega T} & d'_z(\epsilon-\Omega/2) + f'_s(\epsilon-\Omega/2) \\ d'_z(\epsilon+\Omega/2) - f'_s(\epsilon+\Omega/2) & (id'_y(\epsilon) + d'_x(\epsilon))e^{i\Omega T} \end{bmatrix}. \tag{5.12}$$

Solving d_x and d_y as a function of the transformed function d'_x and d'_y yields

$$d_x(\epsilon) = d'_x(\epsilon)\cos(\Omega T) - d'_y(\epsilon)\sin(\Omega T) \tag{5.13}$$

$$d_y(\epsilon) = d'_x(\epsilon)\sin(\Omega T) + d'_y(\epsilon)\cos(\Omega T). \tag{5.14}$$

If we write d_x and d_y as a vector $[d_x, d_y]$, the equation above can be written as

$$\begin{bmatrix} d_x(\epsilon,T) \\ d_y(\epsilon,T) \end{bmatrix} = \begin{bmatrix} \cos(\Omega T) & -\sin(\Omega T) \\ \sin(\Omega T) & \cos(\Omega T) \end{bmatrix} \begin{bmatrix} d'_x(\epsilon) \\ d'_y(\epsilon) \end{bmatrix}. \tag{5.15}$$

The matrix above is a well-known matrix in physics; it is simply the rotation matrix in Euclidean space in a given plane which in our case is the xy-plane. We will later show analytically in the weak proximity limit and numerically in the full proximity limit that if we choose the stationary exchange field to point along the x and z-axis and to be zero in the y-direction, then in the transformed frame we get $d'_y(\epsilon) = 0$. This shows that the triplet state vector $[d_x(\epsilon,T), d_y(\epsilon,T)] = d'_x(\epsilon)\,[\cos(\Omega T), \sin(\Omega T)]$ will always be parallel to the precessing exchange field in the xy-plane $(M_x, M_y) = M\,[\sin(\theta)\cos(\Omega T), \sin(\theta)\sin(\Omega T)] = M\sin(\theta)\,[\cos(\Omega T), \sin(\Omega T)]$.

5.2 Boundary Condition

Since the laboratory Green's function depends on center-of-mass time, the ring product in the KL boundary condition can not be ignored. At first glance, this seems like an impossible task to solve analytically since the ring product is an infinite series of time and energy derivatives, but fortunately we can use the following identity to help us: If $f(\epsilon,T) = e^{i\omega_1 T} f(\epsilon)$ and $g(\epsilon,T) = e^{i\omega_2 T} g(\epsilon)$, then

$$(f \circ g)(\epsilon,T) = e^{i(\omega_1+\omega_2)T} f(\epsilon - \omega_2/2) g(\epsilon + \omega_1/2). \tag{5.16}$$

The derivation of the identity can be found in Appendix C. This identity can be used on both the left and right hand side of the KL boundary condition. With this result we can derive a new useful identity. If we have two energy dependent matrices A'_{ij} and B'_{ij} in the stationary frame, then in the laboratory frame, the matrices become

$$\hat{A}(\epsilon,T) = \begin{bmatrix} A'_{11}(\epsilon-\Omega/2) & A'_{12}(\epsilon)e^{-i\Omega T} & A'_{13}(\epsilon)e^{-i\Omega T} & A'_{14}(\epsilon-\Omega/2) \\ A'_{21}(\epsilon)e^{i\Omega T} & A'_{22}(\epsilon+\Omega/2) & A'_{23}(\epsilon+\Omega/2) & A'_{24}(\epsilon)e^{i\Omega T} \\ A'_{31}(\epsilon)e^{i\Omega T} & A'_{32}(\epsilon+\Omega/2) & A'_{33}(\epsilon+\Omega/2) & A'_{34}(\epsilon)e^{i\Omega T} \\ A'_{41}(\epsilon-\Omega/2) & A'_{42}(\epsilon)e^{-i\Omega T} & A'_{43}(\epsilon)e^{-i\Omega T} & A'_{44}(\epsilon-\Omega/2) \end{bmatrix}, \tag{5.17}$$

$$\hat{B}(\epsilon,T) = \begin{bmatrix} B'_{11}(\epsilon-\Omega/2) & B'_{12}(\epsilon)e^{-i\Omega T} & B'_{13}(\epsilon)e^{-i\Omega T} & B'_{14}(\epsilon-\Omega/2) \\ B'_{21}(\epsilon)e^{i\Omega T} & B'_{22}(\epsilon+\Omega/2) & B'_{23}(\epsilon+\Omega/2) & B'_{24}(\epsilon)e^{i\Omega T} \\ B'_{31}(\epsilon)e^{i\Omega T} & B'_{32}(\epsilon+\Omega/2) & B'_{33}(\epsilon+\Omega/2) & B'_{34}(\epsilon)e^{i\Omega T} \\ B'_{41}(\epsilon-\Omega/2) & B'_{42}(\epsilon)e^{-i\Omega T} & B'_{43}(\epsilon)e^{-i\Omega T} & B'_{44}(\epsilon-\Omega/2) \end{bmatrix}. \tag{5.18}$$

With this in mind, we have the following identity: If we denote the matrix product of $(\hat{A}'\hat{B}')_{ij} = C'_{ij}$, then the ring product of the matrices in the laboratory frame is

$$\hat{C}(\epsilon,T) = \hat{A}(\epsilon,T) \circ \hat{B}(\epsilon,T) = \begin{bmatrix} C'_{11}(\epsilon-\Omega/2) & C'_{12}(\epsilon)e^{-i\Omega T} & C'_{13}(\epsilon)e^{-i\Omega T} & C'_{14}(\epsilon-\Omega/2) \\ C'_{21}(\epsilon)e^{i\Omega T} & C'_{22}(\epsilon+\Omega/2) & C'_{23}(\epsilon+\Omega/2) & C'_{24}(\epsilon)e^{i\Omega T} \\ C'_{31}(\epsilon)e^{i\Omega T} & C'_{32}(\epsilon+\Omega/2) & C'_{33}(\epsilon+\Omega/2) & C'_{34}(\epsilon)e^{i\Omega T} \\ C'_{41}(\epsilon-\Omega/2) & C'_{42}(\epsilon)e^{-i\Omega T} & C'_{43}(\epsilon)e^{-i\Omega T} & C'_{44}(\epsilon-\Omega/2) \end{bmatrix}. \tag{5.19}$$

This equation can easily be verified by using the identity in equation (5.16). We will now do this for the two matrix elements $(1,1)$ and $(1,2)$ in the matrix above.

$$\begin{aligned}\left(\hat{A}(\epsilon,T)\circ\hat{B}(\epsilon,T)\right)_{11} &= A'_{11}(\epsilon-\Omega/2)\circ B'_{11}(\epsilon-\Omega/2) + A'_{12}(\epsilon)e^{-i\Omega T}\circ B'_{21}(\epsilon)e^{i\Omega T}\\ &+ A'_{13}(\epsilon)e^{-i\Omega T}\circ B'_{31}(\epsilon)e^{i\Omega T} + A'_{14}(\epsilon-\Omega/2)\circ B'_{41}(\epsilon-\Omega/2)\\ &= A'_{11}(\epsilon-\Omega/2)B'_{11}(\epsilon-\Omega/2) + A'_{12}(\epsilon-\Omega/2)B'_{21}(\epsilon-\Omega/2)\\ &+ A'_{13}(\epsilon-\Omega/2)B'_{31}(\epsilon-\Omega/2) + A'_{14}(\epsilon-\Omega/2)B'_{41}(\epsilon-\Omega/2)\\ &= C'_{11}(\epsilon-\Omega/2). \end{aligned} \tag{5.20}$$

Here, we have only used the identity in equation (5.16). The next element is

$$\begin{aligned}\left(\hat{A}(\epsilon,T)\circ\hat{B}(\epsilon,T)\right)_{12} &= A'_{11}(\epsilon-\Omega/2)\circ B'_{12}(\epsilon)e^{-i\Omega T} + A'_{12}(\epsilon)e^{-i\Omega T}\circ B'_{22}(\epsilon+\Omega/2)\\ &+ A'_{13}(\epsilon)e^{-i\Omega T}\circ B'_{32}(\epsilon+\Omega/2) + A'_{14}(\epsilon-\Omega/2)\circ B'_{42}(\epsilon)e^{-i\Omega T}\\ &= A'_{11}(\epsilon)B'_{12}(\epsilon)e^{-i\Omega T} + A'_{12}(\epsilon)B'_{22}(\epsilon)e^{-i\Omega T}\\ &+ A'_{13}(\epsilon)B'_{32}(\epsilon)e^{-i\Omega T} + A'_{14}(\epsilon)B'_{42}(\epsilon)e^{-i\Omega T}\\ &= C'_{12}(\epsilon)e^{-i\Omega T}. \end{aligned} \tag{5.21}$$

All other elements can be calculated in similar ways. We see that the ring product of the two matrices $\hat{A}$ and $\hat{B}$ preserves the center-of-mass time dependencies and energy shifts that both the two matrices exhibit.

We now have everything we need to evaluate the KL boundary condition in the laboratory frame. We denote (i,j) component of $\hat{g}'(\epsilon)\nabla\hat{g}'(\epsilon)$ as $\Gamma'_{ij}(\epsilon)$ and thus, with the identity in equation (5.19) the left hand side of the KL boundary condition in the laboratory frame becomes

$$2\zeta L\hat{g}\circ\nabla\hat{g} = 2\zeta L\begin{bmatrix}\Gamma'_{11}(\epsilon-\Omega/2) & \Gamma'_{12}(\epsilon)e^{-i\Omega T} & \Gamma'_{13}(\epsilon)e^{-i\Omega T} & \Gamma'_{14}(\epsilon-\Omega/2)\\ \Gamma'_{21}(\epsilon)e^{i\Omega T} & \Gamma'_{22}(\epsilon+\Omega/2) & \Gamma'_{23}(\epsilon+\Omega/2) & \Gamma'_{24}(\epsilon)e^{i\Omega T}\\ \Gamma'_{31}(\epsilon)e^{i\Omega T} & \Gamma'_{32}(\epsilon+\Omega/2) & \Gamma'_{33}(\epsilon+\Omega/2) & \Gamma'_{34}(\epsilon)e^{i\Omega T}\\ \Gamma'_{41}(\epsilon-\Omega/2) & \Gamma'_{42}(\epsilon)e^{-i\Omega T} & \Gamma'_{43}(\epsilon)e^{-i\Omega T} & \Gamma'_{44}(\epsilon-\Omega/2)\end{bmatrix}. \tag{5.22}$$

We will now turn to the right hand side of the KL boundary condition. By denoting the (i,j) component of $[\hat{g}'_L(\epsilon),\hat{g}'_R(\epsilon)]_-$ as $\Pi'_{ij}(\epsilon)$, we get

$$[\hat{g}_L(\epsilon,T)\,\wr\,\hat{g}_R(\epsilon,T)]_- = \begin{bmatrix}\Pi'_{11}(\epsilon-\Omega/2) & \Pi'_{12}(\epsilon)e^{-i\Omega T} & \Pi'_{13}(\epsilon)e^{-i\Omega T} & \Pi'_{14}(\epsilon-\Omega/2)\\ \Pi'_{21}(\epsilon)e^{i\Omega T} & \Pi'_{22}(\epsilon+\Omega/2) & \Pi'_{23}(\epsilon+\Omega/2) & \Pi'_{24}(\epsilon)e^{i\Omega T}\\ \Pi'_{31}(\epsilon)e^{i\Omega T} & \Pi'_{32}(\epsilon+\Omega/2) & \Pi'_{33}(\epsilon+\Omega/2) & \Pi'_{34}(\epsilon)e^{i\Omega T}\\ \Pi'_{41}(\epsilon-\Omega/2) & \Pi'_{42}(\epsilon)e^{-i\Omega T} & \Pi'_{43}(\epsilon)e^{-i\Omega T} & \Pi'_{44}(\epsilon-\Omega/2)\end{bmatrix}. \tag{5.23}$$

We therefore see that the center-of-mass dependence can be removed, and we can make an energy substitution so that for every component we have $\Gamma'_{ij}(\epsilon)=\Pi'_{ij}(\epsilon)$, which is the same as the stationary KL boundary condition for the transformed Green's function $\hat{g}'$,

$$2\zeta L\hat{g}'(\epsilon)\nabla\hat{g}'(\epsilon) = [\hat{g}'_L(\epsilon), \hat{g}'_R(\epsilon)]_-. \tag{5.24}$$

Therefore, we can solve for the transformed Green's function with equations (3.13) and (5.24), and enter them into equation (5.10) to find the Green's function in the laboratory frame. We will use these stationary Green's functions to calculate any observables we need in the laboratory frame. Note that if we had spin-active interfaces, then the boundary condition would become time-dependent as noted in reference [70]. This time-dependence could potentially make the problem much more difficult, but has not been investigated in this thesis.

5.3 Observables

5.3.1 Gap Energy

By using the gap energy equation (4.10) and the laboratory Keldysh component which is on the form (5.10), we can express the order parameter with the Green's functions in the stationary frame. Thus, we get

$$\Delta(x) = \frac{N_0\lambda}{8}\int_{-\omega_c}^{\omega_c} d\epsilon f'^K_{\uparrow\downarrow}(\epsilon - \Omega/2) - f'^K_{\downarrow\uparrow}(\epsilon + \Omega/2). \tag{5.25}$$

In principle, all eight distribution functions can be non-zero, depending on the exact non-equilibrium conditions in our system. As we will show later, this is possible in an SFS junction with a non-zero macroscopic phase difference and a precessing exchange field. Thus, we will not try to express this gap equation with all the distribution functions and condensate functions. But to decrease the amount of calculations we have to make to evaluate this integral numerically, we can write the gap equation as

$$\Delta(x) = \frac{N_0\lambda}{8}\Bigg[\int_{-\omega_c+\Omega/2}^{\omega_c-\Omega/2} d\epsilon f'^K_{\uparrow\downarrow}(\epsilon) - f''^K_{\downarrow\uparrow}(\epsilon) \tag{5.26}$$

$$+ \int_{-\omega_c-\Omega/2}^{-\omega_c+\Omega/2} d\epsilon f'^K_{\uparrow\downarrow}(\epsilon) - \int_{\omega_c-\Omega/2}^{\omega_c+\Omega/2} d\epsilon f'^K_{\downarrow\uparrow}(\epsilon)\Bigg]. \tag{5.27}$$

Note that since the gap energy is time-independent, the phase of the gap energy will also not change over time. This is unlike a system where we force a voltage across the sandwiched material in a Josephson junction [59, 60]. As we argued in section 3.8.1, we will nevertheless see a time-varying phase in order for the phase difference to be gauge-invariant. We will however not take this effect into account due to the complexity of the ring product this brings, and so by assuming that the this time-dependent flux change is small, we can assume the gauge-invariant phase difference is constant in time and an input variable we can set as we see fit.

5.3.2 Charge and Spin-Currents

The spin-currents become

$$I_s^v = \frac{N_0 DA}{8} \int d\epsilon \mathrm{Tr}\left(\hat{\tau}_3 \hat{\sigma}_v \left(\check{g} \circ \nabla \check{g}\right)^K\right) \tag{5.28}$$

$$= \frac{N_0 DA}{8} \int d\epsilon \mathrm{Tr}\left(\hat{\tau}_3 \hat{\sigma}_v \left(\hat{g}^R \circ \nabla \hat{g}^K + \hat{g}^K \circ \nabla \hat{g}^A\right)\right). \tag{5.29}$$

And the charge-current is

$$I_Q = \frac{N_0 DAe}{4} \int d\epsilon \mathrm{Tr}\left(\hat{\tau}_3 \left(\check{g} \circ \nabla \check{g}\right)^K\right) \tag{5.30}$$

$$= \frac{N_0 DAe}{4} \int d\epsilon \mathrm{Tr}\left(\hat{\tau}_3 \left(\hat{g}^R \circ \nabla \hat{g}^K + \hat{g}^K \circ \nabla \hat{g}^A\right)\right). \tag{5.31}$$

The three matrices $\hat{g}^R$, $\hat{g}^K$ and $\hat{g}^A$ all exhibit the same time phase and energy shift symmetries, and thus by the identity in equation (5.19), we get by denoting the (i,j) component of $(\check{g}'(\epsilon)\nabla\check{g}'(\epsilon))^K$ as η'_{ij}

$$I_s^x = \frac{N_0 DA}{8} \int d\epsilon \left(\eta'_{21}(\epsilon)e^{i\Omega T} + \eta'_{12}(\epsilon)e^{-i\Omega T} - \eta'_{43}(\epsilon)e^{-i\Omega T} - \eta'_{34}(\epsilon)e^{i\Omega T}\right) \tag{5.32}$$

$$I_s^y = \frac{N_0 DA}{8} \int d\epsilon i \left(-\eta'_{21}(\epsilon)e^{i\Omega T} + \eta'_{12}(\epsilon)e^{-i\Omega T} - \eta'_{43}(\epsilon)e^{-i\Omega T} + \eta'_{34}(\epsilon)e^{i\Omega T}\right) \tag{5.33}$$

$$I_s^z = \frac{N_0 DA}{8} \int d\epsilon \left(\eta'_{11}(\epsilon - \Omega/2) - \eta'_{22}(\epsilon + \Omega/2) - \eta'_{33}(\epsilon + \Omega/2) + \eta'_{44}(\epsilon - \Omega/2)\right). \tag{5.34}$$

Thus, only the z-polarized spin-current is time-independent. The charge-current will also be time-independent and becomes

$$I_Q = \frac{N_0 DeA}{4} \int d\epsilon \left(\eta'_{11}(\epsilon - \Omega/2) + \eta'_{22}(\epsilon + \Omega/2) - \eta'_{33}(\epsilon + \Omega/2) - \eta'_{44}(\epsilon - \Omega/2)\right). \tag{5.35}$$

5.3.3 Charge and Spin-Accumulation

The charge and spin-accumulations are expressed as

$$\rho_Q = -\frac{N_0 e}{4} \int d\epsilon \mathrm{Tr}\left(\hat{g}^K\right), \tag{5.36}$$

$$\boldsymbol{\rho}_s = \frac{N_0}{8} \int d\epsilon \mathrm{Tr}\left(\hat{\boldsymbol{\sigma}} \hat{g}^K\right), \tag{5.37}$$

which with the stationary Green's functions become

$$\rho_Q = -\frac{N_0 e}{4} \int d\epsilon \left(g'^K_{11}(\epsilon - \Omega/2) + g'^K_{22}(\epsilon + \Omega/2) + g'^K_{33}(\epsilon + \Omega/2) + g'^K_{44}(\epsilon - \Omega/2)\right), \tag{5.38}$$

$$\rho_s^x = \frac{N_0}{8} \int d\epsilon \left(g'^K_{21}(\epsilon)e^{i\Omega T} + g'^K_{12}(\epsilon)e^{-i\Omega T} + g'^K_{43}(\epsilon)e^{-i\Omega T} + g'^K_{34}(\epsilon)e^{i\Omega T}\right), \tag{5.39}$$

$$\rho_s^y = \frac{N_0}{8} \int d\epsilon i \left(-g'^K_{21}(\epsilon)e^{i\Omega T} + g'^K_{12}(\epsilon)e^{-i\Omega T} + g'^K_{43}(\epsilon)e^{-i\Omega T} - g'^K_{34}(\epsilon)e^{i\Omega T}\right), \tag{5.40}$$

$$\rho_s^z = \frac{N_0}{8} \int d\epsilon \left(g'^K_{11}(\epsilon - \Omega/2) - g'^K_{22}(\epsilon + \Omega/2) + g'^K_{33}(\epsilon + \Omega/2) - g'^K_{44}(\epsilon - \Omega/2)\right). \tag{5.41}$$

Once again we see the observables directed in the x and y-direction precess with the magnetic field while the charge and z-polarized spin-accumulations stay constant in time.

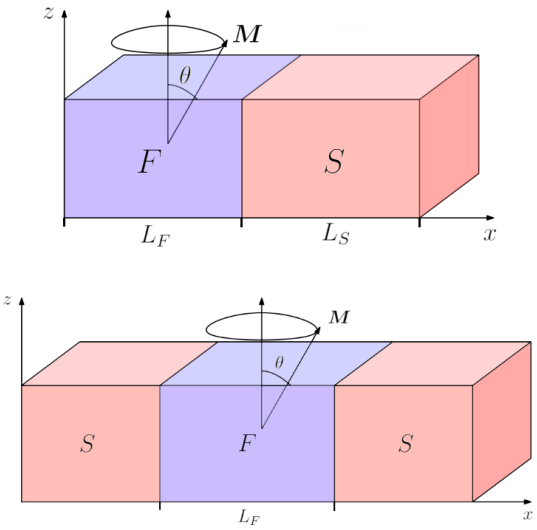

Figure 5.1: Top figure shows a FS bilayer, while the bottom shows a SFS Josephson junction. Both geometries have a ferromagnet with a precessing exchange field.

5.3.4 Density of States

The spin-dependent density of states will simply become

$$D_\sigma(\epsilon) = N_0 \Re\left(\underline{g}_{\sigma\sigma}(\epsilon)\right), \tag{5.42}$$

which with the stationary frame Green's function in (5.10) becomes

$$D_\uparrow(\epsilon) = N_0 \Re\left(\underline{g}'_{\uparrow\uparrow}(\epsilon - \Omega/2)\right), \tag{5.43}$$

$$D_\downarrow(\epsilon) = N_0 \Re\left(\underline{g}'_{\downarrow\downarrow}(\epsilon + \Omega/2)\right). \tag{5.44}$$

First, we see that the density of states become independent of time, but they both undergo an energy shift going from the stationary frame to the laboratory frame. This can be interpreted as effectively removing the Zeeman split we get in the stationary field $\boldsymbol{M}' = \Omega/2\boldsymbol{e}_z$. The spin-independent density of states is simply the average of the two,

$$D(\epsilon) = \frac{N_0}{2} \Re\left(\underline{g}'_{\uparrow\uparrow}(\epsilon - \Omega/2) + \underline{g}'_{\downarrow\downarrow}(\epsilon + \Omega/2)\right). \tag{5.45}$$

5.4 Weak Proximity Limit

In this section, we will show how we can calculate the anomalous Green's function $\underline{f}$ in the weak proximity limit. We will consider both a FS bilayer and a SFS Josephson junction found in figure 5.1. In this limit, we are only interested in the anomalous Green's function while setting $\underline{g} = \underline{\sigma}_0$. We can either Fourier transform the BCS bulk solution in the superconductor to the stationary frame and use the transformed KL boundary condition or we can use the laboratory frame KL boundary condition in equation (3.21). We will do the latter. The upper-right elements of the KL boundary condition at the FS interface is

$$2\zeta L \begin{bmatrix} 1 \circ \nabla f'_{\uparrow\uparrow}(\epsilon)e^{-i\Omega T} & 1 \circ \nabla f'_{\uparrow\downarrow}(\epsilon - \Omega/2) \\ 1 \circ \nabla f'_{\downarrow\uparrow}(\epsilon + \Omega/2) & 1 \circ \nabla f'_{\downarrow\downarrow}(\epsilon)e^{i\Omega T} \end{bmatrix}\Bigg|_{x=F/S} = \underline{\sigma}_0 \circ i\underline{\sigma}_2 \sinh(\theta(\epsilon))e^{i\phi} + i\underline{\sigma}_2 \sinh(\theta(\epsilon))e^{i\phi} \circ \underline{\sigma}_0. \tag{5.46}$$

The ring product has no impact since one side of the ring product is 1 which is independent of both time and energy. This is also true in a Josephson junction where we technically have a time-varying and gauge-invariant phase difference. Therefore, a time-varying phase difference will not be complicated by the ring product in the weak proximity limit. In the full proximity effect, the right hand side will couple the ring product to terms that are at least dependent of energy and possibly time. In that case, the ring product will be extremely difficult, if not impossible, to calculate analytically because ϕ has a term that is proportional to $\sin(\Omega T)$ which we saw in section 3.8. But on the other hand, in the weak proximity limit this is not a problem since the time convolution operator acts on the identity matrix. Nevertheless, we now get

$$\zeta L \begin{bmatrix} \nabla f'_{\uparrow\uparrow}(\epsilon)e^{-i\Omega T} & \nabla f'_{\uparrow\downarrow}(\epsilon - \Omega/2) \\ \nabla f'_{\downarrow\uparrow}(\epsilon + \Omega/2) & \nabla f'_{\downarrow\downarrow}(\epsilon)e^{i\Omega T} \end{bmatrix}\Bigg|_{x=F/S} = i\underline{\sigma}_2 \sinh(\theta(\epsilon))e^{i\phi}. \tag{5.47}$$

Now since the right hand side is anti-diagonal, the time dependence in the diagonal terms can be removed. The KL boundary condition at a vacuum interface is simply the left hand side of the equation above equals zero. We solve these equation using the d-vector formalism [11] which have already proved to be advantageous to our situation due to the precession of d_x and d_y component being similar to the precession of the magnetic field. The anomalous Green's function in a ferromagnet in a FS bilayer and SFS Josephson junction has been solved and can be found in Appendix D.

Looking at the solution for both a SF bilayer and a SFS Josephson junction in Appendix D, we clearly see that the system creates long-ranged components if the non-equilibrium conditions are satisfied, namely $\Omega \neq 0$ and $\theta \neq 0$. In the stationary frame, the superconductor does not only act as a source of singlet states, but also long-ranged d_z-components due to the effective Zeeman-split term $\boldsymbol{M'} = \Omega/2\boldsymbol{e}_z$ being present in the superconductor in the stationary frame. If the tilt-angle is non-zero, the real exchange field $\boldsymbol{M}$ will have a component that is perpendicular to induced Zeeman field, which cause long-ranged components according to the d-vector condition, $d_{LRC} \propto |\boldsymbol{d} \times \boldsymbol{M}| \neq 0$ [11].

From equation (5.10), the laboratory frame anomalous Green's function becomes

$$\underline{f} = \begin{bmatrix} f'_{\uparrow\uparrow}(\epsilon)e^{-i\Omega T} & f'_{\uparrow\downarrow}(\epsilon - \Omega/2) \\ f'_{\downarrow\uparrow}(\epsilon + \Omega/2) & f'_{\downarrow\downarrow}(\epsilon)e^{i\Omega T} \end{bmatrix}. \tag{5.48}$$

Using that $d'_y = 0$ for both the FS bilayer and SFS Josephson junction, and inserting $f_{\uparrow\uparrow} = -d_x$, $f_{\downarrow\downarrow} = d_x$, $f_{\uparrow\downarrow} = d_z + f_s$ and $f_{\downarrow\uparrow} = d_z - f_s$ gives us

$$\begin{aligned} \underline{f} &= \begin{bmatrix} -d'_x(\epsilon)e^{-i\Omega T} & d'_z(\epsilon - \Omega/2) + f_s(\epsilon - \Omega/2) \\ d'_z(\epsilon + \Omega/2) - f'_s(\epsilon + \Omega/2) & d'_x(\epsilon)e^{i\Omega T} \end{bmatrix} \\ &= \begin{bmatrix} -d'_x(\epsilon)\cos(\Omega T) + id'_x(\epsilon)\sin(\Omega T) & d'_z(\epsilon - \Omega/2) + f_s(\epsilon - \Omega/2) \\ d'_z(\epsilon + \Omega/2) - f'_s(\epsilon + \Omega/2) & d'_x(\epsilon)\cos(\Omega T) + id'_x(\epsilon)\sin(\Omega T) \end{bmatrix}. \end{aligned} \tag{5.49}$$

Using the fact that $f_{\uparrow\uparrow} = +id_y - d_x$ and $f_{\downarrow\downarrow} = id_y + d_x$, we get in the laboratory frame that

$$d_x(\epsilon) = d'_x(\epsilon)\cos(\Omega T) \tag{5.50}$$
$$d_y(\epsilon) = d'_x(\epsilon)\sin(\Omega T). \tag{5.51}$$

which shows that the two triplet components d_x and d_y processes with the x and y component of the exchange field as mentioned previously. The other two anomalous Green's functions are

$$f_s(\epsilon) = \frac{d'_z(\epsilon - \Omega/2) + f'_s(\epsilon - \Omega/2) - d'_z(\epsilon + \Omega/2) + f'_s(\epsilon + \Omega/2)}{2} \tag{5.52}$$
$$d_z(\epsilon) = \frac{d'_z(\epsilon + \Omega/2) - f'_s(\epsilon + \Omega/2) + d'_z(\epsilon - \Omega/2) + f'_s(\epsilon - \Omega/2)}{2}. \tag{5.53}$$

Here, we see something interesting. The long-ranged components of d_z actually gets a shorter decay length for larger frequencies Ω at energies close to the Fermi energy, $\epsilon = 0$. This is due to the long-ranged component experiencing an additional, effective Zeeman split $\Omega/2$, which causes the d_z component to decay as $\xi_F = \sqrt{D/(\epsilon \pm \Omega/2)}$ just like it would in a magnetic field where $\boldsymbol{M} = \Omega/2\boldsymbol{e}_z$. Note that the transverse long-ranged components d_x and d_y do not have these energy shifts because the additional Zeeman split only splits the spin up and spin down states in the z-direction. Thus only the transverse components d_x and d_y stay truly long-ranged, in that they decay as $\xi_N = \sqrt{D/\epsilon}$.

From equation (5.47), we also see something interesting at frequencies $\Omega = \pm 2|\Delta_0|$. By setting the energy to zero $\epsilon = 0$, the two derivatives formally diverge at these frequencies. In reality the divergence will be limited by inelastic scattering processes, but nevertheless, this tells us that both the triplet and the singlet states will for these frequencies give large zero-energy correlations.

With our weak proximity solutions in the ferromagnet, we can do as in reference [7] and show that we get a long-ranged supercurrent through a SFS junction with a precessing exchange field. This has not been done analytically in this thesis, but we will later focus on solving the system numerically where we will show that we in fact get a long-ranged supercurrent flowing through the junction.

5.5 Distribution Function

Even though our transformed system is stationary, it is still not in equilibrium. Thus the distribution function $\hat{h}$ will depend on position, and we can expect the other distribution functions to be non-zero $h_n \neq 0$ for $n \neq 1$. The distribution function is the solution to

$$\hat{g}^K(\epsilon, T) = \hat{g}^R(\epsilon, T) \circ \hat{h}(\epsilon, T) - \hat{h}(\epsilon, T) \circ \hat{g}^A(\epsilon, T). \tag{5.54}$$

We saw in equation (5.22) and (5.23) that the ring product of two matrices with the same center-of-mass time dependence and energy shift symmetries will also exhibit the same symmetries. Therefore, it would be advantageous to us if the three Green's functions above had these symmetries. But as we showed in section 3.8.2, the transformation is repeated along the diagonal of the Keldysh space, and thus it acts equally on the retarded, advanced and Keldysh component. We can also show explicitly that the advanced component will have these symmetries by using the identity $\hat{g}^A = -\hat{\rho}_3 \left(\hat{g}^R\right)^\dagger \hat{\rho}_3$ [6],

$$\hat{g}^A = \begin{bmatrix} -g'^*_{11}(\epsilon - \Omega/2) & -g'^*_{21}(\epsilon) e^{-i\Omega T} & g'^*_{31}(\epsilon) e^{-i\Omega T} & g'^*_{41}(\epsilon - \Omega/2) \\ -g'^*_{12}(\epsilon) e^{i\Omega T} & -g'^*_{22}(\epsilon + \Omega/2) & g'^*_{32}(\epsilon + \Omega/2) & g'^*_{42}(\epsilon) e^{i\Omega T} \\ g'^*_{13}(\epsilon) e^{i\Omega T} & g'^*_{23}(\epsilon + \Omega/2) & -g'^*_{33}(\epsilon + \Omega/2) & -g'^*_{43}(\epsilon) e^{i\Omega T} \\ g'^*_{14}(\epsilon - \Omega/2) & g'^*_{24}(\epsilon) e^{-i\Omega T} & -g'^*_{34}(\epsilon) e^{-i\Omega T} & -g'^*_{44}(\epsilon - \Omega/2) \end{bmatrix}, \tag{5.55}$$

where g'_{ij} are the components of the retarded Green's function in the stationary frame. This shows that $\hat{g}^A$ exhibit the same time dependencies and energy shifts as $\hat{g}^R$. This will also be the case for the Keldysh component as we argued, and therefore one way to satisfy equation (5.54) is that the distribution function $\hat{h}$ also has these symmetries. We already know that the distribution function is diagonal in Nambu space, and thus the distribution function will be on the form

$$\hat{h}(\epsilon, T) = \begin{bmatrix} h'_{11}(\epsilon - \Omega/2) & h'_{12}(\epsilon) e^{-i\Omega T} & 0 & 0 \\ h'_{21}(\epsilon) e^{i\Omega T} & h'_{22}(\epsilon + \Omega/2) & 0 & 0 \\ 0 & 0 & h'_{33}(\epsilon + \Omega/2) & h'_{34}(\epsilon) e^{i\Omega T} \\ 0 & 0 & h'_{43}(\epsilon) e^{-i\Omega T} & h'_{44}(\epsilon - \Omega/2) \end{bmatrix} \tag{5.56}$$

where the elements h'_{ij} are the element in the stationary frame distribution function $\hat{h}'$, i.e.

$$\hat{h}'(\epsilon) = \begin{bmatrix} h'_{11}(\epsilon) & h'_{12}(\epsilon) & 0 & 0 \\ h'_{21}(\epsilon) & h'_{22}(\epsilon) & 0 & 0 \\ 0 & 0 & h'_{33}(\epsilon) & h'_{34}(\epsilon) \\ 0 & 0 & h'_{43}(\epsilon) & h'_{44}(\epsilon) \end{bmatrix} \tag{5.57}$$

which satisfies the following relation in the stationary frame: $\hat{g}^K(\epsilon) = \hat{g}^R\hat{h} - \hat{h}\hat{g}^A$. We are later going to look at both systems were a ferromagnet with a precessing exchange field is coupled to a superconductor or a normal metal. Deep inside the superconductor or normal metal, far away from the precessing magnetic field, we can assume that the distribution function is unaffected by this time varying magnetic field, and thus in the laboratory frame $\hat{h}(\epsilon, T) = \hat{h}(\epsilon) = \tanh(\beta\epsilon/2)\hat{\tau}_0$, which in the transformed frame becomes

$$\hat{h}' = \begin{bmatrix} \tanh\left(\frac{\beta(\epsilon+\Omega/2)}{2}\right) & 0 & 0 & 0 \\ 0 & \tanh\left(\frac{\beta(\epsilon-\Omega/2)}{2}\right) & 0 & 0 \\ 0 & 0 & \tanh\left(\frac{\beta(\epsilon-\Omega/2)}{2}\right) & 0 \\ 0 & 0 & 0 & \tanh\left(\frac{\beta(\epsilon+\Omega/2)}{2}\right) \end{bmatrix}. \tag{5.58}$$

When solving the distribution function in a region, we will use this distribution function as a boundary condition both in a superconductor and a normal metal. Later, when calculating the distribution functions in several materials numerically, we will require metals or superconductors acting as equilibrium reservoirs to be coupled to our system on both sides of the one-dimensional setup. Otherwise, the distribution functions will only converge to zero which is nonphysical. These reservoirs will then have the stationary frame distribution function given above.

We will continue by writing the distribution function as a set of matrices that span the block-diagonal spin-Nambu space. These matrices are as mentioned in section 3.3

$$\hat{h} = \sum \hat{\rho}_n h_n \tag{5.59}$$

where the matrices $\hat{\rho}_n$ are

$$\hat{\rho}_1 = \hat{\tau}_0\hat{\sigma}_0 \qquad \hat{\rho}_2 = \hat{\tau}_0\hat{\sigma}_1 \qquad \hat{\rho}_3 = \hat{\tau}_0\hat{\sigma}_2 \qquad \hat{\rho}_4 = \hat{\tau}_0\hat{\sigma}_3,$$
$$\hat{\rho}_5 = \hat{\tau}_3\hat{\sigma}_0 \qquad \hat{\rho}_6 = \hat{\tau}_3\hat{\sigma}_1 \qquad \hat{\rho}_7 = \hat{\tau}_3\hat{\sigma}_2 \qquad \hat{\rho}_8 = \hat{\tau}_3\hat{\sigma}_3, \tag{5.60}$$

and $h_n = \mathrm{Tr}(\hat{\rho}_n\hat{h})/4$. The distribution function in the stationary frame becomes

$$\hat{h}' = \begin{bmatrix} h'_1 + h'_4 + h'_5 + h'_8 & h'_2 - ih'_3 + h'_6 - ih'_7 & 0 & 0 \\ h'_2 + ih'_3 + h'_6 + ih'_7 & h'_1 - h'_4 + h'_5 - h'_8 & 0 & 0 \\ 0 & 0 & h'_1 + h'_4 - h'_5 - h'_8 & h'_2 + ih'_3 - h'_6 - ih'_7 \\ 0 & 0 & -h'_2 - ih'_3 + h'_6 + ih'_7 & h'_1 - h'_4 - h'_5 + h'_8 \end{bmatrix}. \tag{5.61}$$

And thus in the laboratory frame the distribution function becomes

$$\begin{aligned} \hat{h}(\epsilon, T) &= \begin{bmatrix} h_1 + h_4 + h_5 + h_8 & h_2 - ih_3 + h_6 - ih_7 & 0 & 0 \\ h_2 + ih_3 + h_6 + ih_7 & h_1 - h_4 + h_5 - h_8 & 0 & 0 \\ 0 & 0 & h_1 + h_4 - h_5 - h_8 & h_2 + ih_3 - h_6 - ih_7 \\ 0 & 0 & -h_2 - ih_3 + h_6 + ih_7 & h_1 - h_4 - h_5 + h_8 \end{bmatrix} \\ &= \begin{bmatrix} (h'_1 + h'_4 + h'_5 + h'_8)(\epsilon - \Omega/2) & (h'_2 - ih'_3 + h'_6 - ih'_7)(\epsilon)e^{-i\Omega T} & 0 & 0 \\ (h'_2 + ih'_3 + h'_6 + ih'_7)(\epsilon)e^{i\Omega T} & (h'_1 - h'_4 + h'_5 - h'_8)(\epsilon + \Omega/2) & 0 & 0 \\ 0 & 0 & (h'_1 + h'_4 - h'_5 - h'_8)(\epsilon + \Omega/2) & (h'_2 + ih'_3 - h'_6 - ih'_7)(\epsilon)e^{i\Omega T} \\ 0 & 0 & (-h'_2 - ih'_3 + h'_6 + ih'_7)(\epsilon)^{-i\Omega T} & (h'_1 - h'_4 - h'_5 + h'_8)(\epsilon - \Omega/2) \end{bmatrix}, \end{aligned} \tag{5.62}$$

where $(h_a + h_b)(\epsilon)$ should be interpreted as $h_a(\epsilon) + h_b(\epsilon)$. Solving these equations for the laboratory frame yield

$$h_1(\epsilon) = \frac{h'_1(\epsilon - \Omega/2) + h'_1(\epsilon + \Omega/2) + h'_8(\epsilon - \Omega/2) - h'_8(\epsilon + \Omega/2)}{2} \tag{5.63}$$
$$h_2(\epsilon, T) = h'_2(\epsilon)\cos(\Omega T) - h'_3(\epsilon)\sin(\Omega T) \tag{5.64}$$
$$h_3(\epsilon, T) = h'_2(\epsilon)\sin(\Omega T) + h'_3(\epsilon)\cos(\Omega T) \tag{5.65}$$
$$h_4(\epsilon) = \frac{h'_4(\epsilon - \Omega/2) + h'_4(\epsilon + \Omega/2) + h'_5(\epsilon - \Omega/2) - h'_5(\epsilon + \Omega/2)}{2} \tag{5.66}$$
$$h_5(\epsilon) = \frac{h'_4(\epsilon - \Omega/2) - h'_4(\epsilon + \Omega/2) + h'_5(\epsilon - \Omega/2) + h'_5(\epsilon + \Omega/2)}{2} \tag{5.67}$$
$$h_6(\epsilon, T) = h'_6(\epsilon)\cos(\Omega T) - h'_7(\epsilon)\sin(\Omega T) \tag{5.68}$$
$$h_7(\epsilon, T) = h'_6(\epsilon)\sin(\Omega T) + h'_7(\epsilon)\cos(\Omega T) \tag{5.69}$$
$$h_8(\epsilon) = \frac{h'_1(\epsilon - \Omega/2) - h'_1(\epsilon + \Omega/2) + h'_8(\epsilon - \Omega/2) + h'_8(\epsilon + \Omega/2)}{2}, \tag{5.70}$$

We immediately note the symmetries for the x and y spin-energy modes h_2 and h_3, and for the x and y spin-modes h_6 and h_7. The two pairs of distribution functions can be written in the nice form

$$\begin{bmatrix} h_6(\epsilon, T) \\ h_7(\epsilon, T) \end{bmatrix} = \begin{bmatrix} \cos(\Omega T) & -\sin(\Omega T) \\ \sin(\Omega T) & \cos(\Omega T) \end{bmatrix} \begin{bmatrix} h'_6(\epsilon) \\ h'_7(\epsilon) \end{bmatrix}. \tag{5.71}$$

The same goes for the pair (h_2, h_3). We once again see the rotation matrix which we saw for the triplet components d_x and d_y in the laboratory frame. Thus the pairs (h_2, h_3) and (h_6, h_7) moves with the magnetic field in the xy-plane. This makes sense since h_6 and h_7 describe the spin-accumulation polarized in the x and y-direction, respectively, while h_2 and h_3 describes the spin-distribution of spins pointing along the x and y-axis, respectively. The amplitude of the vectors (h_2, h_3) and (h_6, h_7) also do not change over time i.e. $h_6(\epsilon, T)^2 + h_7(\epsilon, T)^2 = h_6'(\epsilon)^2 + h_7'(\epsilon)^2$. The distribution functions that describe z-polarized spin, like the spin-energy and spin mode h_4 and h_8, are time-independent and only requires energy shifts going from the stationary to the laboratory frame.

We will now find the stationary frame distribution function in a ferromagnet *not* coupled to a superconductor, but to a normal state metal. There are two reasons for this: First, it proved too difficult to find the solution analytically when coupled to a superconductor, and secondly, it will be useful later when doing numerical calculations in FS bilayer and SFS Josephson junctions to compare the differences between a ferromagnet that is coupled to a superconductor and one that is coupled to a normal state metal. In a ferromagnet which is not in proximity to a superconductor, the retarded and advanced Green's functions are $\hat{g}^R = \hat{\tau}_3$ and $\hat{g}^A = -\hat{\tau}_3$. Entering this into the Keldysh component of the Usadel equation, yields the following differential equation for $\hat{h}'$:

$$iD\nabla^2\hat{h}' = [\boldsymbol{M}' \cdot \hat{\boldsymbol{\sigma}}, \tau_3\hat{h}']_-. \tag{5.72}$$

The energy term drops out on the right hand side since it is proportional to $\hat{\tau}_3$ which commutes with $\hat{h}'$ since it is diagonal in Nambu space. The boundary conditions for $\hat{h}'$ become

$$2\zeta L\nabla\hat{h}' = [\check{g}_L', \check{g}_R']_-^K. \tag{5.73}$$

Here L and R denotes the Green's function on the left and right side of the interface, respectively. As we already argued, their retarded and advanced Green's function will be trivial, but their Keldysh component will not since it will be a function of the distribution function. With equation (3.18) the Keldysh component becomes $\hat{g}^K = 2\hat{\tau}_3\hat{h}$. We will not solve the equations here, but the solution for the distribution function in the ferromagnet in a junction between two normal state metals can be found in Appendix D. Note that this normal state solution for the distribution function makes use of no further approximations.

With this distribution function, we can calculate the spin-current in a ferromagnet in a NFN junction. From equation (5.34), the laboratory frame spin-current polarized in the z-direction becomes

$$I_s^z = \frac{N_0 D}{2}\int d\epsilon \left(\frac{dh_8'(\epsilon + \Omega/2)}{dx} + \frac{dh_8'(\epsilon - \Omega/2)}{dx}\right) \tag{5.74}$$

$$= \frac{N_0 D}{2}\int d\epsilon \left(\frac{M_x^2}{M'^2}\frac{t_{pp} - t_{mm}}{2}\left(C_1\kappa\sinh(\kappa x) + C_2\kappa\sin(\kappa x)\right)\right), \tag{5.75}$$

where $t_{pp(mm)} = \tanh\left(\frac{\beta}{2}(\epsilon \pm \Omega)\right)$, $\kappa = \sqrt{-2iM'/D}$, and C_1 and C_2 are given in Appendix D. Only t_{pp} and t_{mm} depend on energy, thus taking the limits to be $\pm\infty$, we get an exact result for the z-polarized spin-current

$$I_s^z = N_0 D\frac{M_x^2}{M'^2}\Omega\kappa\left(C_1\sinh(\kappa x) + C_2\sin(\kappa x)\right). \tag{5.76}$$

Here we have used the integral

$$\int_{-\infty}^{\infty} d\epsilon \tanh(\beta(\epsilon+\Omega)/2) - \tanh(\beta(\epsilon-\Omega)/2) = 4\Omega. \tag{5.77}$$

It might not look obvious, but the expression for the spin-current can mathematically be shown to always be a real number, but an expression that explicitly shows this will be much longer. In the two cases we get equilibrium, $M_x = 0$ or $\Omega = 0$, we get no spin-current. We also see that the spin-current is independent of temperature.

Similarly, we can calculate the x and y-polarized spin-currents:

$$I_s^x(T) = N_0 D \int d\epsilon \frac{d}{dx} h_6' \cos(\Omega T) - \frac{d}{dx} h_7' \sin(\Omega T), \tag{5.78}$$

$$I_s^y(T) = N_0 D \int d\epsilon \frac{d}{dx} h_6' \sin(\Omega T) + \frac{d}{dx} h_7' \cos(\Omega T). \tag{5.79}$$

Once again we see the entrance of the rotation matrix by writing the above equations as

$$\begin{bmatrix} I_s^x(T) \\ I_s^y(T) \end{bmatrix} = \begin{bmatrix} \cos(\Omega T) & -\sin(\Omega T) \\ \sin(\Omega T) & \cos(\Omega T) \end{bmatrix} \begin{bmatrix} N_0 D \int d\epsilon \frac{d}{dx} h_6' \\ N_0 D \int d\epsilon \frac{d}{dx} h_7' \end{bmatrix}. \tag{5.80}$$

Thus, the x and y-polarized spin-currents are merely a time rotation of the position derivative of its corresponding spin mode distribution function. This can be interpreted as change in spin accumulation over distance which is equivalent to a transport of spin. We can also easily write these spin-currents by using the distribution functions in the laboratory frame in equation (5.71).

$$I_s^x(T) = N_0 D \int d\epsilon \frac{d}{dx} h_6(\epsilon, T), \tag{5.81}$$

$$I_s^y(T) = N_0 D \int d\epsilon \frac{d}{dx} h_7(\epsilon, T), \tag{5.82}$$

so as the two distribution functions $h_6(T)$ and $h_7(T)$ rotate over time, so do the two spin-currents rotate with them. Taking the limits of the energy integral to $\pm\infty$, and using the solutions for the distribution functions in Appendix D, the two spin-currents become

$$\begin{aligned} I_s^x = \Omega N_0 D \kappa \Bigg[& - \frac{M_x M_z'}{M'^2} \left(C_1 \sinh(\kappa x) + C_2 \sin(\kappa x)\right) \cos(\Omega T) \\ & + i \frac{M_x}{M'} \left(C_1 \sinh(\kappa x) - C_2 \sin(\kappa x)\right) \sin(\Omega T) \Bigg], \end{aligned} \tag{5.83}$$

$$\begin{aligned} I_s^y = \Omega N_0 D \kappa \Bigg[& - \frac{M_x M_z'}{M'^2} \left(C_1 \sinh(\kappa x) + C_2 \sin(\kappa x)\right) \sin(\Omega T) \\ & - i \frac{M_x}{M'} \left(C_1 \sinh(\kappa x) - C_2 \sin(\kappa x)\right) \cos(\Omega T) \Bigg]. \end{aligned} \tag{5.84}$$

Here, the currents will also always be a real number. We will later use these resistive spin-currents to compare how superconductive ordering changes these currents.

5.6 Numerical Analysis

We will now try to numerically solve the Green's function and distribution function in both a FS bilayer and a SFS Josephson junction where the ferromagnet has a precessing magnetic field. The respective functions will be calculated in the stationary frame, and then the equations given in section 5.3 will be used to find the observables in the laboratory frame.

Heterostructures with a precessing magnetic field and superconductive ordering could be considered self-consistently which means that we calculate the Green's function and distribution function in the ferromagnet first and then use those functions as boundary conditions to calculate the same functions in any adjacent superconductors. We could do this for several energies, and with enough energy solutions we could then apply the gap energy equation (5.25) which is an integral over energy solutions, and we could then repeat calculating the three functions: Green's function, distribution function, and gap energy until these three functions converge to a satisfying limit in all regions. This requires a lot of computer power and has only been done to calculate the gap energy in a superconductor in a FS bilayer. If interested in doing everything self-consistently, one should try programming it in a compiled programming language like Fortran which would decrease the computational time by an order of 2 or 3 in magnitude. This has already been done by Ouassou, see reference [22].

Instead, for most calculations we have set the superconductors to be in equilibrium and have a BCS bulk Green's function. This might not give quantitative correct results, but will still give us all the qualitative details we need. Thus, we will mostly solve the Usadel equation in the ferromagnetic region, and calculate observables in this region. To solve the equations numerically we use the Riccati parameterization to find the Green's function and use the kinetic equation derived in reference [21]. Assuming no second-order self-energy terms, the kinetic equation becomes

$$M_{nm}\nabla^2 h_m = -\left(\nabla M_{nm} + \boldsymbol{Q}_{nm}\right)\cdot\nabla h_m \tag{5.85}$$
$$-\left(\nabla\cdot\boldsymbol{Q}_{nm} + V_{nm}\right)h_m. \tag{5.86}$$

Here, we have defined the quantities

$$\boldsymbol{Q}_{nm} = \frac{D}{4}\mathrm{Tr}\left(\hat{\rho}_m\hat{\rho}_n\hat{g}^R\nabla\hat{g}^R - \hat{\rho}_n\hat{\rho}_m\hat{g}^A\nabla\hat{g}^A\right), \tag{5.87}$$

$$M_{nm} = \frac{D}{4}\mathrm{Tr}\left(\hat{\rho}_n\hat{\rho}_m - \hat{\rho}_n\hat{g}^R\hat{\rho}_m\hat{g}^A\right), \tag{5.88}$$

$$V_{nm} = \frac{i}{4}\mathrm{Tr}\left(\left[\hat{\rho}_n,\Sigma\right]_-\left(\hat{g}^R\hat{\rho}_m - \hat{\rho}_m\hat{g}^A\right)\right). \tag{5.89}$$

The Keldysh component of the Kupriyanov-Lukichev boundary conditions can be written as

$$M_{nm}\nabla h_m + Q_{nm}h_m = C^L_{nm}h^L_m - C^R_{nm}h^R_m, \tag{5.90}$$

where the notation L and R means the left and right side of the interface, respectively, and the matrix C is

$$C_{nm} = \frac{D}{8\zeta L}\mathrm{Tr}\left(\left[\hat{g}^A_L\hat{\rho}_n - \hat{\rho}_n\hat{g}^R_L\right]\left[\hat{g}^R_R\hat{\rho}_m - \hat{\rho}_m\hat{g}^A_R\right]\right). \tag{5.91}$$

Here, we have assumed that the interfaces are non-magnetic with only spin-independent tunneling. We have also assumed no spin-dependent reflection. A detailed derivation of the equation and more general expressions including spin-active interfaces and second order self-energies can be found in reference [21]. These quantities and equations will be solved in the stationary frame, and we will enter them into the equations for observables in the laboratory frame. When solving these equations, we will assume that the regions we are solving the equations in are coupled to a reservoir in equilibrium. For example, when calculating a FS bilayer self-consistently in both regions, we have coupled both the ferromagnet and the superconductor to a normal metal which only acts as a reservoir for the distribution functions, namely we effectively get a NFSN quad-layer. We thus neglect the proximity effect at the interface to these normal state metals which means no singlet or triplet states can leak into the normal metals, and only the distribution functions are affected by the forced equilibrium in these metals. The equilibrium distribution functions in these reservoirs are in the stationary frame

$$\hat{h}' = \begin{bmatrix} \tanh(\beta(\epsilon+\Omega/2)/2) & 0 & 0 & 0 \\ 0 & \tanh(\beta(\epsilon-\Omega/2)/2) & 0 & 0 \\ 0 & 0 & \tanh(\beta(\epsilon-\Omega/2)/2) & 0 \\ 0 & 0 & 0 & \tanh(\beta(\epsilon+\Omega/2)/2) \end{bmatrix}. \tag{5.92}$$

This can be verified by inserting the matrix elements above into equation (5.56). This distribution equation yields

$$h_1' = \frac{\tanh(\beta(\epsilon+\Omega/2)/2) + \tanh(\beta(\epsilon-\Omega/2)/2)}{2} \tag{5.93}$$

$$h_8' = \frac{\tanh(\beta(\epsilon+\Omega/2)/2) - \tanh(\beta(\epsilon-\Omega/2)/2)}{2}, \tag{5.94}$$

while all other $h_n' = 0$. Thus, these two distribution functions will be used as boundary conditions in the reservoirs. Note that we will normalize all energies to the bulk gap energy $|\Delta_0|$, and thus we will use the well known BCS result [3]

$$\frac{|\Delta_0|}{k_B T_c} = \frac{1}{\pi e^{\gamma}}, \tag{5.95}$$

where $\gamma = 0.5772$ is Euler's constant, and T_c is the transition temperature. We can now write the distribution functions by knowing the ratios T/T_c and $\epsilon/|\Delta_0|$. This means, for example, that the equilibrium distribution function can be written as

$$h_1 = \tanh(\beta\epsilon/2) = \tanh\left(\frac{\epsilon/|\Delta_0|}{2\pi e^{\gamma} T/T_c}\right). \tag{5.96}$$

The superconductors have a bulk Green's function, and so we have to remember to shift the energies in order for them to be correct in the stationary frame. By inverting equation (5.10) for the bulk BCS Green's function, we get in the stationary frame

$$\hat{g}'_{BCS}(\epsilon) = \begin{bmatrix} \cosh(\theta(\epsilon+\Omega/2)) & 0 & 0 & \sinh(\theta(\epsilon+\Omega/2))e^{i\phi} \\ 0 & \cosh(\theta(\epsilon-\Omega/2)) & -\sinh(\theta(\epsilon-\Omega/2))e^{i\phi} & 0 \\ 0 & -\sinh(\theta(\epsilon-\Omega/2))e^{-i\phi} & -\cosh(\theta(\epsilon-\Omega/2)) & 0 \\ \sinh(\theta(\epsilon+\Omega/2))e^{-i\phi} & 0 & 0 & -\cosh(\theta(\epsilon+\Omega/2)) \end{bmatrix}. \tag{5.97}$$

Note that since only the diagonal and anti-diagonal components are non-zero, the BCS Green's function in the stationary frame is completely time-independent. Using the identities $\underline{g} = 2\underline{N} - \underline{\sigma}_0$ and $\underline{f} = 2\underline{N}\underline{\gamma}$, the Riccati parameterization becomes:

$$\underline{N}'_{BCS} = \frac{1}{2}\begin{bmatrix} \cosh(\theta(\epsilon+\Omega/2))+1 & 0 \\ 0 & \cosh(\theta(\epsilon-\Omega/2))+1 \end{bmatrix}, \tag{5.98}$$

$$\underline{\gamma}'_{BCS} = \frac{1}{2}\left(\underline{N}'_{BCS}\right)^{-1}\begin{bmatrix} 0 & \sinh(\theta(\epsilon+\Omega/2))e^{i\phi} \\ -\sinh(\theta(\epsilon-\Omega/2))e^{i\phi} & 0 \end{bmatrix}. \tag{5.99}$$

5.6.1 Parameters

To justify our assumption of fixing the two superconductors to a BCS bulk state, we set the temperature low and equal to $T/T_C = 0.1$. If otherwise not stated, we set the length of the ferromagnetic layer to $L/\xi = 1$ where ξ is the superconducting coherence length. The interface transparency will be set to $\zeta = 3$. We will also typically use $\theta = 15°$ since this is close to the experimentally highest possible polar angle of a precessing exchange field in resonance [7]. We give the energy a small imaginary contribution to simulate inelastic scattering $\epsilon \to \epsilon + i\delta$ where $\delta/|\Delta_0| = 0.01$, this contribution is also called the Dynes parameter [63]. A large Dynes parameter makes the energy integrals when calculating currents substantially easier by smoothing out larger peaks of the integrands. If we set the Dynes parameter to zero, which is absolutely unrealistic since it allows no inelastic scattering, the integrands of the integrals will diverge to infinity for some energies, like for example when $\epsilon = |\Delta_0|$.

5.6.2 Charge-Current

Firstly, we will calculate the Josephson current through such a junction. It was analytically showed in the weak proximity limit by Houzet in reference [7] that such a junction would be able to carry a long-ranged supercurrent which is proportional to $\sin(\theta)^2$ in long ferromagnets. We have thus chosen to plot the supercurrent as a function of the length of the ferromagnetic film L/ξ with the angle $\theta = 15°$ and a stronger magnetic field $M = 20|\Delta_0|$ in figure 5.2a, where the charge-current normalization constant is $I_0 = N_0 DeA/4$. We clearly see in the figure that the supercurrent decays much slower if the magnetic field is precessing, but on the other hand, we see that the majority of the current contribution comes from a resistive current, namely the contribution from equation (4.30). But as we can see in figure 5.2b there is possible to find an angular frequency Ω where the resistive current is zero, while the supercurrent is non-zero. We will come back to the resistive current later when looking at the accumulation of charge that manifests itself when the phase difference is non-zero.

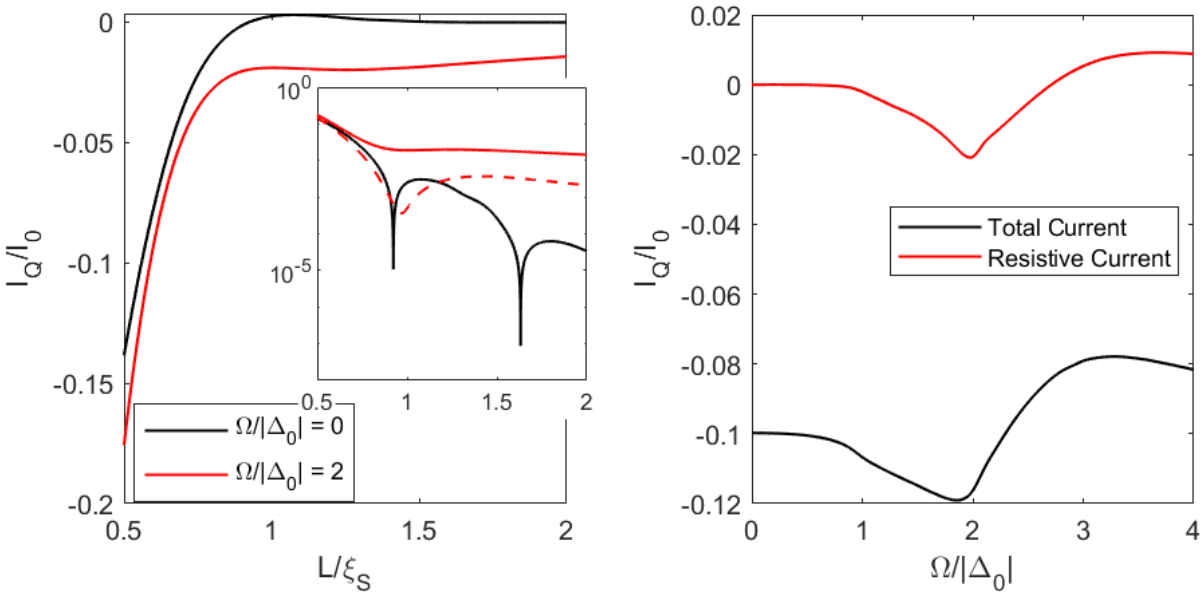

(a) $M = 20|\Delta_0|$ (b) $M = 5|\Delta_0|$

Figure 5.2: Charge-current is plotted as a function of the length of the ferromagnet in a). The inset plot is a logplot of the absolute value of the current, and the stippled line shows the dissipationless contribution to the current when $\Omega = 2|\Delta_0|$ which is clearly long-ranged. The right plot shows the resistive and total current as a function of angular frequency Ω. We see that the resistive current, given in equation (4.30), is zero around $\Omega/|\Delta_0| = 2.7$. All plots have the phase difference $\Delta\phi = \pi/2$.

5.6.3 Spin-Currents

To calculate the spin-currents, we use equations (5.32)-(5.34). As we can see from the equations, only the z-polarized spin-current is time independent and only involves energy shifts. The x and y-polarized currents on the other hand are time dependent, and by looking at the two equations (5.32) and (5.33), one would assume that the two currents are similar but out of phase. This has already been shown in the case of no-proximity limit in equations (5.83)-(5.84), and can also be shown to be true numerically.

A plot of the z-polarized spin-current in a NFS trilayer and a SFS junction can be found in figure 5.3, and the x and y-polarized spin-currents in a NFS trilayer can be found in figure 5.4. Note that the normal metal and the superconductor are as we mentioned forced to be in equilibrium and have their respective bulk Green's functions. Here, the normalization constant for spin-currents is $I_0 = N_0 DA/8$. Both plots show the equivalent spin-current without the ferromagnet being coupled to a superconductor, but instead only coupled to normal metals which we found an analytic solution to earlier in equations (5.76), (5.83) and (5.84). Starting with the z-polarized spin-current, we see that the superconductor suppresses the z-polarized spin-current, especially for frequencies $\Omega < |\Delta_0|$. Then as the Larmor frequency increases it will slowly converge to the normal state limit. Thus, for very large frequencies, superconductive order has no impact on the spin-currents. We see something similar when looking at the x and y-polarized spin-currents. The spin-current that is polarized parallel to the magnetic field in the xy-plane is seemingly suppressed by superconductive ordering. Remember that the magnetic field has a zero y-component when the center-of-mass time T is zero, $\Omega T = 0$, and a zero x-component when $\Omega T = \pi/2$. On the other hand, the spin-current polarized

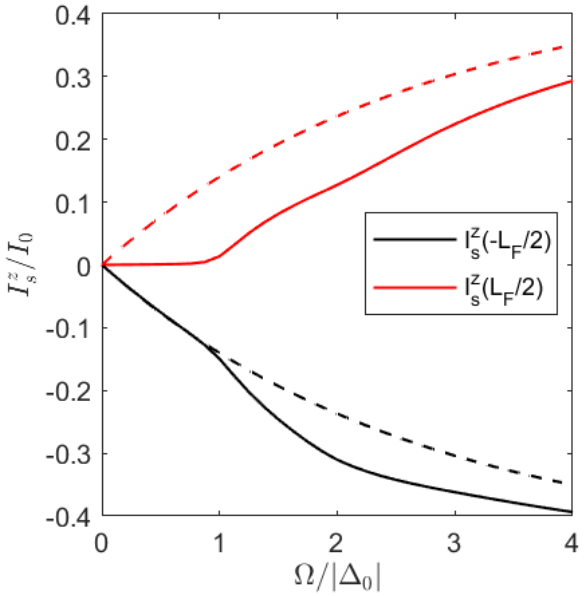

(a) NFS trilayer

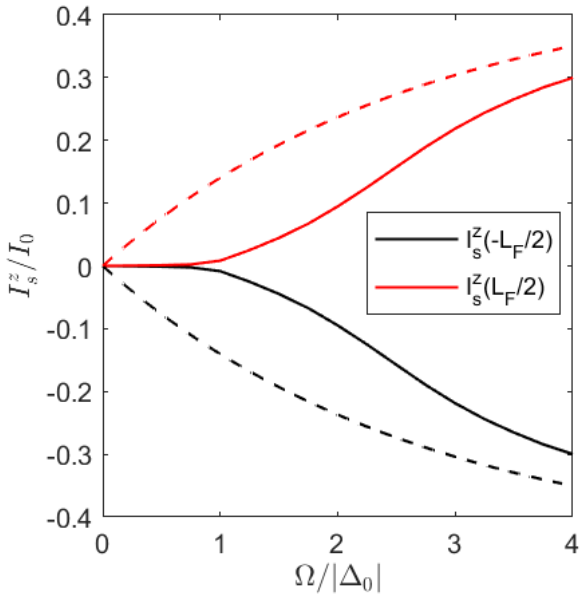

(b) SFS Josephson Junction with no macroscopic phase difference $\Delta\phi = 0$

Figure 5.3: z-polarized spin-current in the ferromagnet at the left and right interface $x = -L_F/2$. The stippled line shows the spin-currents in a NFN junction, namely without the ferromagnet being in proximity to a superconductor.

orthogonal to the magnetic field in the xy-plane seems to be enlarged by the superconductor. This is especially true at the right interface $x = L_F/2$ which is the interface that is coupled to the superconductor. While on the other side of the ferromagnet $x = -L_F/2$, the spin-current is close to the normal state case.

Numerically, we have verified that the majority of the spin-currents are resistive with superconductive ordering, and the resistive contribution to the current given in equation (4.30) can be expressed in the weak proximity limit as follows:

$$\nabla\hat{h}' - \hat{g}'^R\nabla\hat{h}'\hat{g}'^A = 2\nabla\hat{h}' - \begin{bmatrix} \underline{f}'\nabla\underline{h}'_\uparrow\underline{\tilde{f}}' & \underline{f}'\nabla\underline{h}'_\downarrow - \nabla\underline{h}'_\uparrow\underline{\tilde{f}}'^* \\ \underline{\tilde{f}}'\nabla\underline{h}'_\uparrow - \underline{h}'_\downarrow\underline{f}'^* & \underline{\tilde{f}}'\nabla\underline{h}'_\downarrow\underline{f}'^* \end{bmatrix}, \tag{5.100}$$

where we have used the notation

$$\hat{h}' = \begin{bmatrix} \underline{h}'_\uparrow & 0 \\ 0 & \underline{h}'_\downarrow \end{bmatrix}. \tag{5.101}$$

Entering this into the equation for an arbitrary resistive current yields

$$I^{\text{res}} \propto \int d\epsilon \text{Tr}\left[\hat{\tau}_3\hat{\sigma}_v\left(\nabla\hat{h}' - \hat{g}'^R\nabla\hat{h}'\hat{g}'^A\right)\right] \tag{5.102}$$

where $v \in \{0, 1, 2, 3\}$ and with the corresponding energy shifts and time dependence to make the expression valid in the laboratory frame. The point here is that only the diagonal terms in the matrix in (5.100) contributes to the integral because these terms are picked up by the trace, and thus this is equivalent to

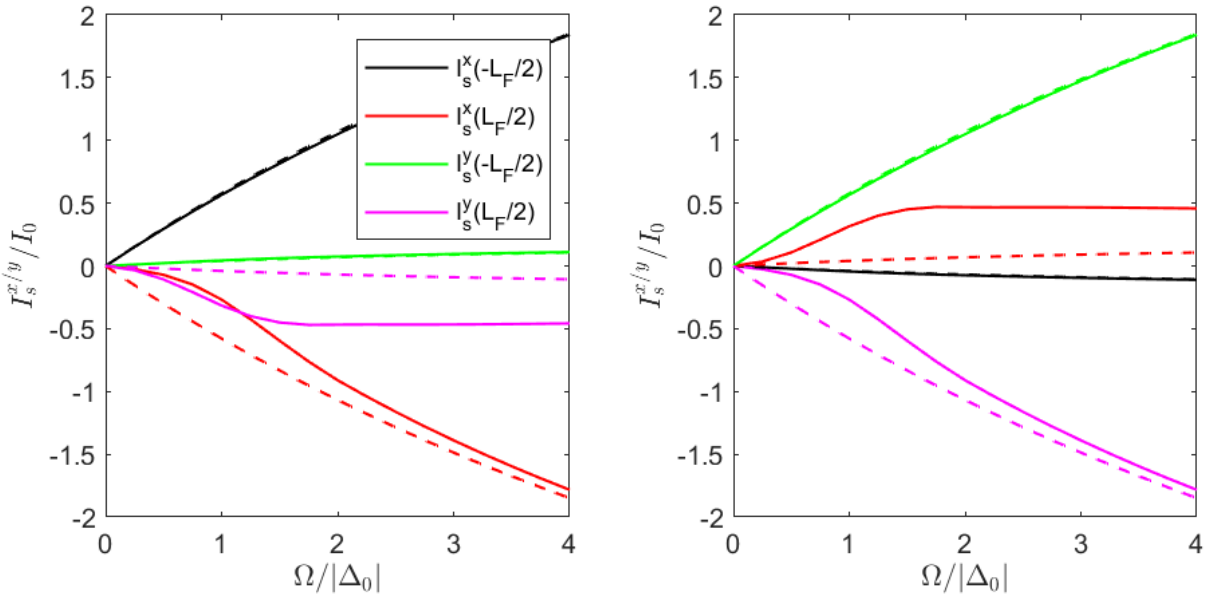

(a) $\Omega T = 0$ (b) $\Omega T = \pi/2$

Figure 5.4: x and y-polarized spin-currents in a ferromagnet in a NFS-bilayer where the superconductor interface is placed at $x = L_F/2$. The stippled lines are the corresponding spin-currents without being in proximity to a superconductor, namely a NFN junction.

$$I^{\text{res}} \propto \int d\epsilon \text{Tr}\left[\hat{\tau}_3\hat{\sigma}_v 2\nabla\hat{h}' - \left(\underline{\sigma}_v\underline{f}'\nabla\underline{h}'_\uparrow\underline{\tilde{f}}' - \underline{\sigma}_v^*\underline{\tilde{f}}'\nabla\underline{h}'_\downarrow\underline{f}'^*\right)\right]. \tag{5.103}$$

We see that the correction from the condensate functions are in second order, $O(\underline{f}^2)$, and thus has a small impact on the resistive current. We have also been able to find this to be true numerically. Thus, we conclude that the difference in resistive spin-currents come from the superconductors having a direct impact on the spin-accumulation distribution functions h_6, h_7 and h_8. Transforming back to laboratory frame will not change this conclusion since the condensate functions will still be small. In figure 5.5 and 5.6 we have plotted the gradient of h_6 and h_8, respectively, in the laboratory frame as a function of energy and position when $\Omega/|\Delta_0| = 2$. First, we note that in the normal state case, the energies that contribute to the z-polarized spin-currents have energies $|\epsilon| < 2|\Omega|$, while the x and y-polarized spin-current are mediated by quasiparticles with energies $|\epsilon| < |\Omega|$. This can be explained from the energy shifts in equation (5.70) which effectively removes the Zeeman splits caused by the precessing motion of the exchange field in the stationary frame. The two other distribution functions h_6 and h_7 do not undergo such energy shifts because there are no Zeeman splits from the precession itself in the stationary frame along the x or y-axis.

In figures 5.5 and 5.6 we see two completely different behaviors of the gradient of h_6 and h_8, respectively, in proximity to a superconductor. These gradients are, as we argued, the main cause of the spin-currents polarized in the x and z-direction. It can also be shown that the gradient of h_7 will be similar to that of h_6. When $\Omega/|\Delta_0| = 2$, they both have an increased magnitude of gradient at Fermi energy, $\epsilon = 0$, which is not true for $\frac{dh_8}{dx}$ for any parameters. Any values for Ω seem to give a zero gradient for h_8 at the superconductor interface for sub-gap energies. One could argue that the gradient of h_8 is zero at the superconductor interface for these energies $|\epsilon| < |\Delta|$ since no quasiparticle states exist in the superconductor for these

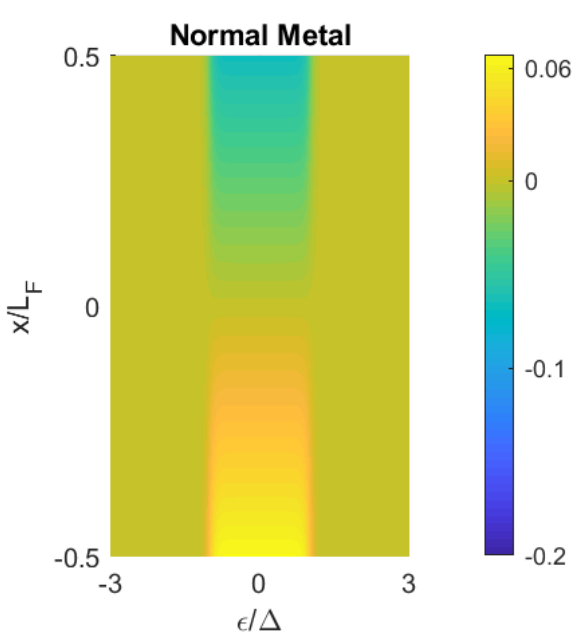

(a) NFN trilayer

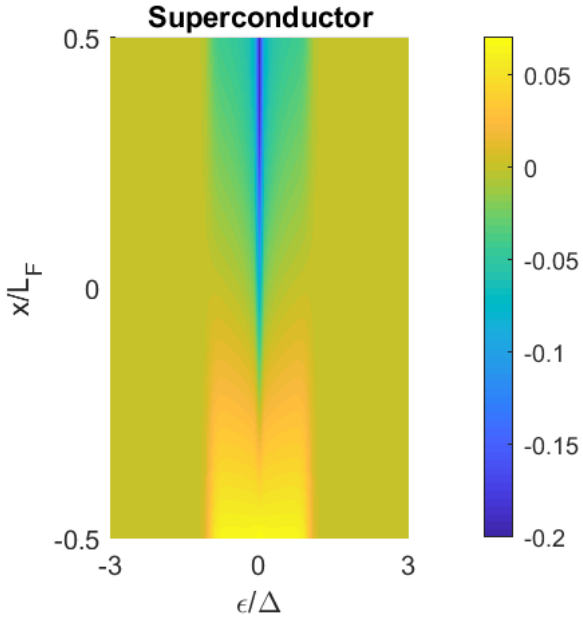

(b) NFS trilayer. Superconductor interface is placed at $x/L_F = 0.5$.

Figure 5.5: The gradient of h_6, $\frac{dh_6}{dx}$, is plotted as a function of energy and position both with and without superconductive ordering when $\Omega/|\Delta_0| = 2$, and $\Omega T = 0$.

sub-gap energies, but that explanation is not consistent with the behaviour of h_6 and h_7 at the interface. There is probably an easy explanation for this behaviour, which would most likely be more obvious if we were to solve the distribution functions in the weak proximity limit analytically.

5.6.4 Gap Energy

The relative gap energy is plotted in figure 5.7 and shows how much the precession of the exchange field changes the gap energy. Both the length of the ferromagnet and superconductor has been set to equal the superconductive coherence length ξ_S in a SF-bilayer, and the temperature has been set to $T/T_c = 0.5$. The distribution function, Green's function and gap energy have been solved in the ferromagnet and superconductor until they have converged. Both the superconductor and the ferromagnet is coupled to a normal metal that is in a forced equilibrium. As the angular frequency Ω is raised above zero, the gap energy is weakened as the generation of long-ranged triplets in the ferromagnet causes more singlet state Cooper pairs to leak into the ferromagnet and this weakens the gap energy. This assumption has been shown both experimentally and theoretically in reference [61]. There, the researchers placed two ferromagnets in a Josephson junction and showed that the angle between the exchange fields α gave a minimum in transition temperature of the superconductors when $\alpha = \pi/2$ which is the rotation that generates the most long-ranged triplet correlations. It is therefore safe to assume that an increase in the angular frequency Ω will lower the transition temperature of the superconductor which gives a clear experimental signature. We have not plotted the transition temperatures in this thesis due to time-limitations. The amount of time it requires to calculate the gap energy self-consistently is quite high, and other calculations have been prioritized.

For very large frequencies $\Omega \gg |\Delta_0|$, the gap energy slowly converges to the stationary limit

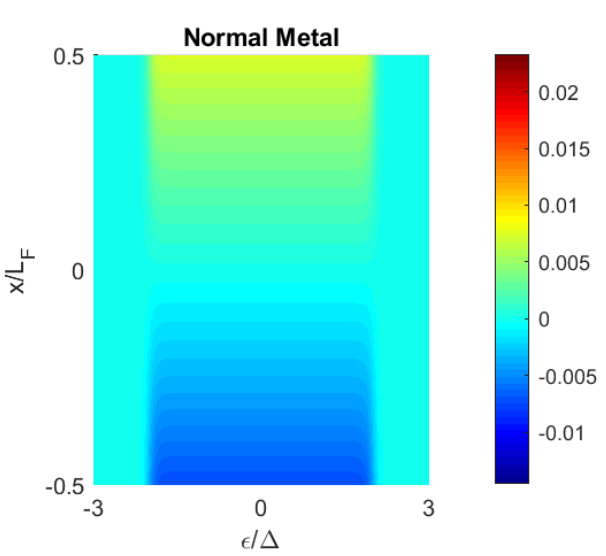

(a) NFN trilayer.

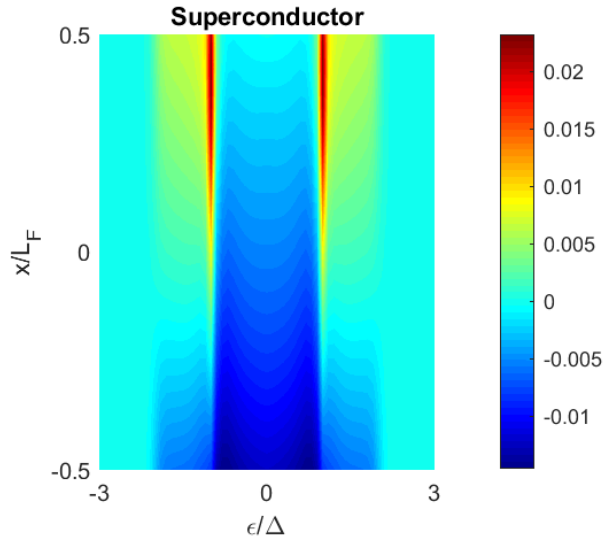

(b) NFS trilayer. The superconductor interface is placed at $x/L_F = 0.5$.

Figure 5.6: The gradient of h_8, $\frac{dh_8}{dx}$, is plotted as a function of energy and position both with and without superconductive ordering when $\Omega/|\Delta_0| = 2$.

where the effective magnitude of the exchange field is the same as the z-component of $\boldsymbol{M}$, $M \to M\cos(\theta)$. This has also been verified for a polar angle of $\theta = 90°$ when $\Omega = 10000|\Delta_0|$. In this case, the z-component of the exchange field is zero, and thus a high Larmor frequency will yield the same gap energy as it does in a NS bilayer, namely the effective exchange field is zero.

This can be explained as follows: When the angular frequency is large, the rotation of the exchange field rotates so fast that the radial component of the exchange field cancel itself out, and thus the quasiparticles will effectively only experience the z-component of the exchange field.

5.6.5 Zero Energy Density of States

In this section we will look at the zero energy density of states in a SFS Josephson junction. The spin-independent density of states is given as

$$D(\epsilon) = \frac{N_0}{2}\Re\left(\underline{g}'_{11}(\epsilon - \Omega/2) + \underline{g}'_{22}(\epsilon + \Omega/2)\right). \tag{5.104}$$

In the limit where the anomalous Green's functions are weak, the spin-independent density of states can with the d-vector formalism be written as

$$D(\epsilon = 0) = N_0\left(1 + \frac{|\boldsymbol{d}(0)|^2}{2} - \frac{|f_s(0)|^2}{2}\right). \tag{5.105}$$

This is a result of the normalization condition $\hat{g}^2 = \hat{\tau}_0$. The triplet and singlet states in the equation above are the laboratory frame triplet and singlet states, so we still have to make energy shifts for the stationary condensate functions, and we will therefore use equation (5.104) to find the zero energy density of states. The point is nevertheless, that the triplet states raise the density of states above the Fermi level while the singlet states lower it. The

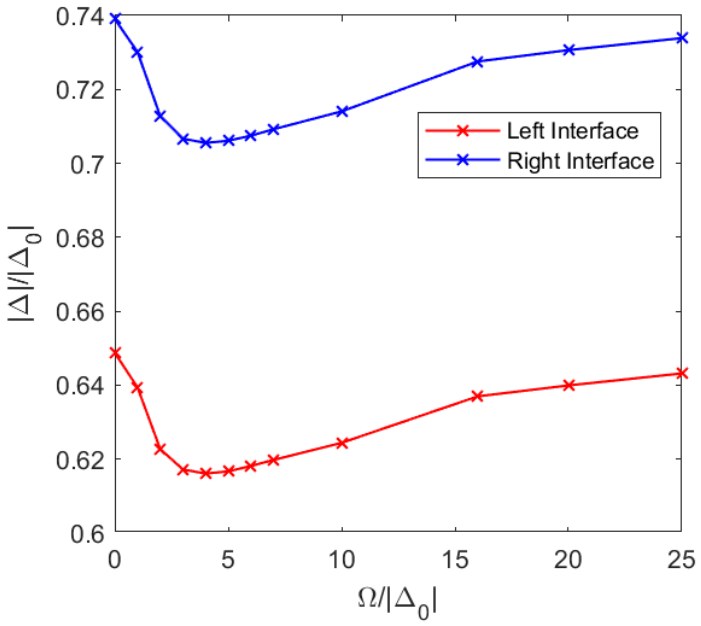

Figure 5.7: The relative gap energy at the left, ferromagnetic interface and the right vacuum interface is plotted as a function of Larmor frequency Ω at $T/T_c = 0.5$.

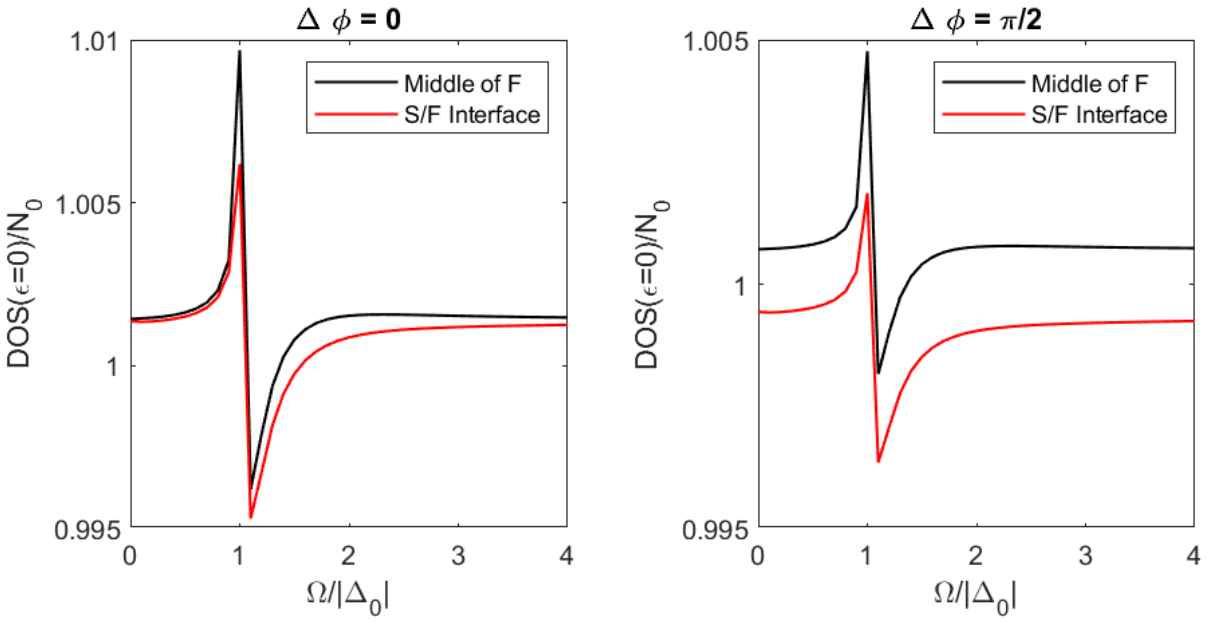

(a) (b)

Figure 5.8: Spin-independent density of states in a SFS Josephson junction is plotted as a function of Larmor frequency Ω.

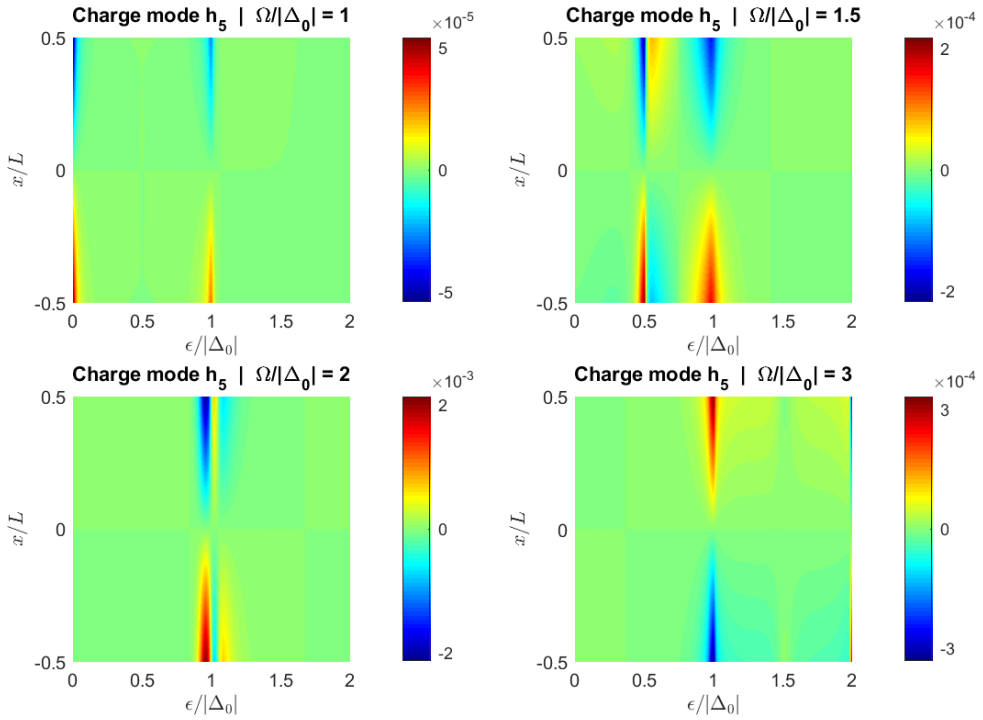

Figure 5.9: The charge mode h_5 is plotted as a function of energy and position in the ferromagnet. Note that the magnitude of the color scale is different in all the plots.

density of states in a SFS Josephson junction is plotted in figure 5.8. First, we see that the values of the density of states is close to the Fermi level, and thus the approximation above is valid. Secondly, we see that by tuning Ω close to $|\Delta|_0$ we can maximize or minimize the triplet components relative to the singlet states. This is interestingly not what researchers in reference [13] found in their setup. They considered a FNS trilayer where they found that the triplet components were most dominating in the normal metal when $\Omega = 2|\Delta_0|$. But we are on the other hand looking at a SFS junction where there is direct contact between the precessing exchange field in the ferromagnet and the superconductors. The researcher also considered very different parameters such as a very long normal metal and less transparent interfaces.

5.6.6 Charge Accumulation

In a FS bilayer, the energy spin-modes $h_2 - h_5$ stays zero for all frequencies Ω, but in a SFS Josephson junction with a non-zero phase difference, we see that all these four distribution functions suddenly become non-zero for a non-zero Larmor frequency $\Omega \neq 0$. In figure 5.9, we have plotted the charge mode h_5, which in the normal state case is solely responsible for charge accumulation as seen in equation (4.35). We have plotted it at different frequencies as a function of both position and energy when the phase difference is $\Delta\phi = \pi/2$. If we change the phase difference to be $\Delta\phi = -\pi/2$ the solution for h_5 switches sign. This suggests that the precession of the exchange field is able to induce a charge accumulation for some energies. Using the expression for charge accumulation (5.38) we end up with the result in figure 5.10 where we clearly see that we in fact get a charge accumulation on each interface in the ferromagnet with opposite sign. From what we understand, no one has before theoretically predicted a charge accumulation in a non-voltage biased SFS Josephson junction with a precessing exchange field. It is also interesting to see that there exists a frequency where this

charge accumulation becomes zero, at $\Omega \approx 2.7|\Delta_0|$. The charge accumulation as a function of angular frequency should be compared to the corresponding plot in figure 5.10b. These plots have same parameters, and we see that when $\Omega \approx 2.7|\Delta_0|$ both the resistive current and the charge accumulation are zero. This is as expected since the resistive current is driven by a gradient in charge accumulation.

This charge accumulation will in turn induce a potential difference across the junction. This can be seen from figure 5.11 where we have solved the charge accumulation in the superconductors as well when $\Omega/|\Delta_0| = 2$. In this plot, we have not solved the gap energy self-consistently and have simply set it equal to the bulk gap energy, $|\Delta| = |\Delta_0|$. The voltage difference across the junction can be calculated by using the standard equation for electric voltage

$$V(x) = \int dx' \frac{\rho(x')}{4\pi\epsilon_0|x - x'|}, \tag{5.106}$$

where ϵ_0 is the electric permittivity. Since the charge accumulation is anti-symmetric in position, the voltage difference will be non-zero from the equation above. By using Josephson's relation $\frac{d\Delta\phi}{dt} = 2eV/\hbar$ and approximating the charge accumulation in figure 5.10b to give a potential difference across the junction $V(T) = V_0 \sin(\Delta\phi)$, we get

$$\frac{d\Delta\phi(T)}{dT} = \frac{2eV_0}{\hbar} \sin(\Delta\phi(T)). \tag{5.107}$$

This differential equation has a solution which is

$$\Delta\phi(T) = 2 \arctan\left(C_0 e^{2eV_0T/\hbar}\right), \tag{5.108}$$

where C_0 is a constant of integration and sets the initial condition. For $C_0 = 1$, we get $\phi(T = 0) = \pi/2$. This function will also converge to $2\pi n$ for all C_0 where n is an integer number. If $C_0 = 0$ then the phase difference will for always stay zero, $\Delta\phi(T) = 0$. Nevertheless, this seems to suggest that the system will always converge to a state where the phase difference is zero. If we start the system with no precessing frequency and a non-zero phase difference we get a supercurrent. Then by suddenly making the magnetic field precess, the supercurrent will seemingly go to zero and self-destruct.

If we now assume that we in addition add a constant applied voltage V_1 to the junction, we get a potential on the form

$$V = V_0 \sin(\Delta\phi) + V_1 \tag{5.109}$$

which gives the differential equation

$$\frac{d\Delta\phi(T)}{dT} = \frac{2e}{\hbar} \left(V_0 \sin(\Delta\phi(T)) + V_1\right). \tag{5.110}$$

This differential equation can also be solved exactly and yields two different results depending on whether V_1 or V_0 is largest. If $|V_1| > |V_0|$ then the phase difference will always increase over time, but if the opposite is true, $|V_1| < |V_0|$, then the phase difference will converge to a non-zero constant. This can be found by setting equation (5.110) equal to zero, which is the same as setting the total potential equal to zero. This gives us the converged phase difference to be

$$\Delta\phi(T \to \infty) = -\arcsin(V_1/V_0), \tag{5.111}$$

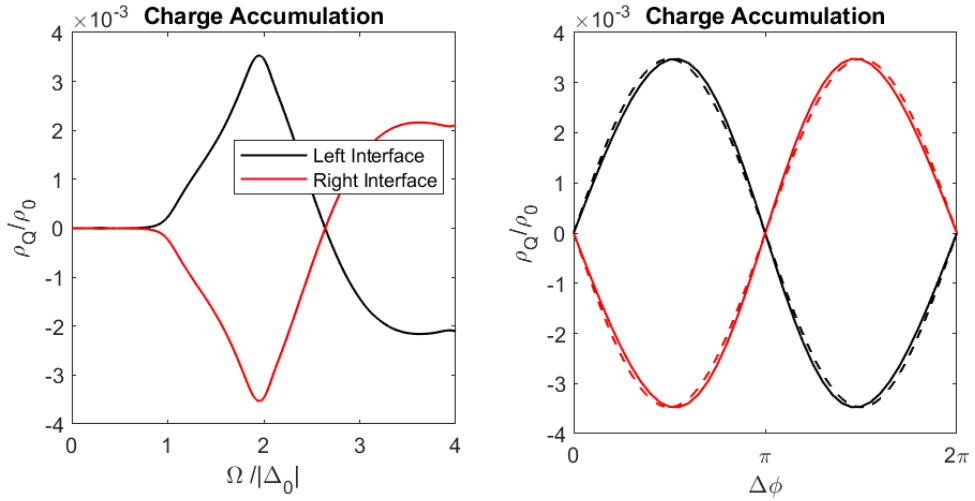

(a) $\Delta\phi = \pi/2$ (b) $\Omega/|\Delta_0| = 2$.

Figure 5.10: Charge accumulation in the ferromagnet at each interface in a SFS Josephson junction. The left plot is a function of frequency with $\Delta\phi = \pi/2$, and the right plot is a function of macroscopic phase difference $\Delta\phi$ with $\Omega/|\Delta_0| = 2$. The stippled line in the right plot is a sine curve with same amplitude. This is to highlight that the charge accumulation has a non-zero contribution from the second harmonics. The charge accumulation is normalized to the constant $\rho_0 = -N_0 e/4$. The Green's functions and distribution functions have only been solved in the ferromagnet and the corresponding functions in the superconductors have been assumed to be the BCS bulk solution in equilibrium.

which by tuning V_1 can give us any phase difference in the range $\Delta\phi(T \to \infty) \in \{-\pi/2, \pi/2\}$.

Before we get way ahead of ourselves we need to remember that we are violating one of our main assumptions: Only the magnetic field changes over time, and the phase difference is constant in time. Therefore, the result we just found is only accurate as a first order approximation. As we saw earlier, a time-varying phase does not alter the solution for the condensate functions in the weak proximity limit. The distribution functions on the other hand will most likely be affected in the weak proximity limit since they require the knowledge of the condensate functions which now will carry the time-varying phase. Since we now suddenly get a time-varying phase difference from the assumption of a constant phase difference suggests that the phase difference is something we have to solve self-consistently like we often have to do for the gap energy. The problem is that the ring product will become extremely complex and not something we can handle analytically. But the conclusion that we see a charge accumulation that depends on the phase difference should not change if we had calculated everything self-consistently with a time-varying phase. On the other hand, the time-dependent phase difference might differ a lot from the first order approximation we found in equation (5.108) if we were to calculate it self-consistently. Therefore, we can only conclude that it will change over time, and not how it will change over time or what it will converge to. More work needs to be done in order to conclude how the time-variation of the phase difference will be.

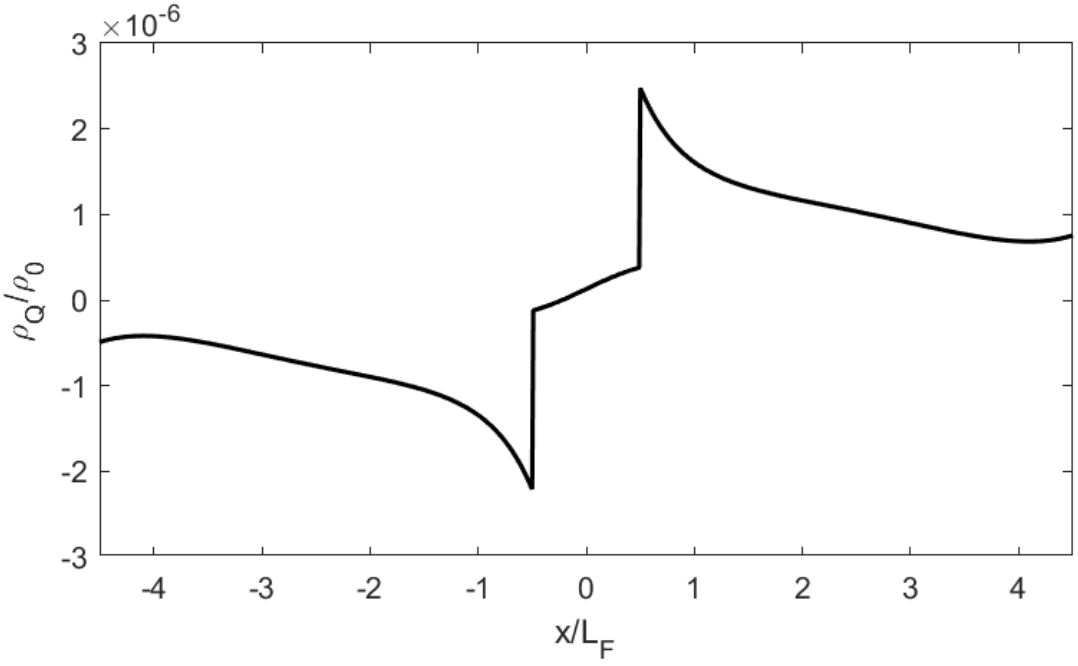

Figure 5.11: Charge accumulation in a SFS Josephson junction. The length of the ferromagnet is $L_F = \xi_S$ while the two superconductors have the length $L_S = 4\xi_S$. The angular frequency is set to $\Omega = 2|\Delta_0|$ and phase difference is $\Delta\phi = \pi/2$. The small congestion of charge at the end-points of the superconductors is due to the approximation that the adjacent normal metals are forced to be in the equilibrium state and can not receive the accumulation of charge.

5.7 Gauge-Invariant and Time Dependent Phase Difference

Before ending this chapter, we will in this section note how the gauge-invariant and time-dependent phase difference affects a SFS Josephson junction, and how we can try to solve the problem self-consistently. First, as we showed in section 3.8.2, the gauge-invariant phase difference will due to the precession of the magnetic field be on the form $\gamma(T) = \Delta\phi + b\sin(\Omega T)$, where $\Delta\phi$ is the phase difference which accounts for the magnetic flux along the z-axis, and the phase difference in the absence of magnetic fields, while b is the ratio between the flux in the y-direction and the quantum magnetic flux Θ_0. Our calculations so far have neglected this time-dependent phase difference, except when finding the condensate functions in the weak proximity effect since a time-varying phase does not complicate the ring product. We have therefore assumed that any flux contribution is small and can be neglected. If the flux contribution were to be large, and we had to incorporate this phase difference into our equations we would get into big problems with the ring product, but one could attempt to expand the time-varying phase by using Bessel function as done in reference [62]

$$e^{i\gamma} = e^{i\Delta\phi}e^{ib\sin(\Omega T)} \tag{5.112}$$

$$= e^{i\Delta\phi}\sum_n J_n(b)e^{in\Omega T}, \tag{5.113}$$

where $J_n(x)$ are the Bessel functions. With this phase difference, we can use the identity found in Appendix D to express observables by infinite series of Bessel functions.

As we saw in the last section, a SFS Josephson junction with a time-varying magnetic field will give rise to a charge accumulation if $\Delta\phi \neq 0$. If one wants to solve such a system self-consistently in time, one has to face many challenges. For one thing, the first order approximation of $\Delta\phi$ without the flux contribution in equation (5.108) is highly complex, and it will create problems when taking the ring product required by the Usadel equation and the KL boundary condition. One thing worth attempting is to assume the induced voltage difference is small and find the first order Taylor series of equation (5.108) in center-of-mass time T. One can then see if how this changes the voltage-difference and phase-difference.

In addition, one needs to remember to add the time varying electric potential to the self-energy in the Usadel equation. In a stationary system, the electric potential will commute with the Green's function and can be removed from the self-energy, but due to the electric potential being time-dependent, the ring product can not be turned into matrix multiplication and the electric potential has to be included in the Usadel equation.

6 | Project 2: Lateral SFS Josephson Junction with Spin-Orbit Coupling

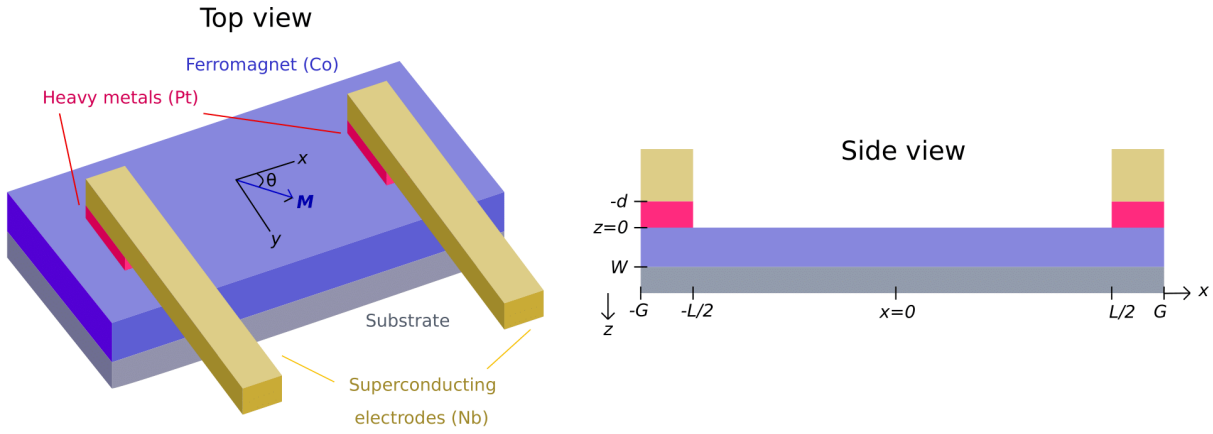

Figure 6.1: A lateral SFS structure with a thin ferromagnetic layer connected to two superconducting nodes with Rashba spin-orbit coupling in the heavy metals. The exchange field of the ferromagnetic film lies in the xy-plane and is tuned by the in-plane angle θ.

In this chapter we will be looking at the geometry depicted in figure 6.1: A lateral SFS Josephson junction with Rashba spin-orbit coupling at the contact points in the heavy metals. A similar system was first suggested by Bergeret and Tokatly [29] that would be able to create long-ranged triplets (LRTs), and also a long-ranged supercurrent. We will in this section go into much more details about such a system, and show that the long-ranged supercurrent is extremely sensitive to the in-plane rotation of the exchange field.

The motivation to consider a lateral Josephson junction rather than a typical, one-dimensional junction, is that the magnetization would be required to be out-of plane [8] in order to generate long-ranged triplets. This can be explained by the Rashba spin-orbit coupling at the contact region in the heavy metals. If we have a heavy metal that is thin in the z-direction, we will only have notable Rashba coupling perpendicular to the z-direction. Thus, if the quasiparticles are mainly flowing through the heavy metals in this direction, their momenta will be mainly z-directed, and their spin will not be notably affected by the Rashba coupling and electrons of the Cooper pair will not spin-rotated to be aligned with the exchange field. If we however force the quasiparticles to change momentum direction from a z-direction to a x-direction, then the momentum will couple to the Rashba coupling [29] and thus the spin of the particles will be affected and can be aligned with the exchange field. This is exactly what is happening in our geometry in figure 6.1 where the quasiparticles are forced to change their momentum direction in the heavy metals. Thus, in the case of Rashba coupling, a lateral geometry is required without the need of either an out-of-plane exchange field or an

inhomogenous exchange field to generate LRTs.

The problem with an out-of-plane exchange field is that it can create vortices in the superconductor, which makes it difficult to interpret measurements. It has experimentally been proved feasible [32], but it is still desirable to find a setup without these vortices. We will mostly focus on Rasha type spin-orbit coupling in the rest of this thesis. This is simply because this is experimentally more feasible. The Rashba coupling occurs at interfaces due to lack of inversion symmetry and can permeate through the material if it is sufficiently thin [8]. This can be realized by having a thin heavy metal sandwiched between a ferromagnet and a superconductor. We therefore suggest the materials in figure 6.1, where we have chosen the heavy metal platinum (Pt) to be coupled to a strong ferromagnet such as cobalt. We also suggest to use niobium as the superconducting material since it has a higher critical temperature of $T_c = 9$ K [54] which is higher than most low temperature superconductors. We will also derive our equations with Dresselhaus spin-orbit coupling for the sake of generality, but it will receive much less attention than Rashba type.

6.1 Weak Proximity Approximation

Most systems are too difficult to be solved analytically, so before resorting to a numerical analysis, we can draw several conclusions by taking use of the weak proximity approximation. The assumption is that in any non-superconducting materials, the Cooper pair correlations will be weak, and thus we make the approximation $\underline{f} \ll \underline{g}$ in such materials. The normalization conditions still has to be satisfied, $\hat{g}^2 = \hat{\tau}_0$, and thus we get $\underline{g} = \underline{\sigma}_0$. The Green's function then becomes

$$\hat{g} = \begin{bmatrix} \underline{\sigma}_0 & \underline{f} \\ -\underline{\tilde{f}} & -\underline{\sigma}_0 \end{bmatrix}. \tag{6.1}$$

We will apply this 4×4 Green's function matrix to the Usadel equation, and by looking exclusively at the top-right 2×2 element, we will get an equation that is completely independent of $\underline{\tilde{f}}$. Thus, we only need to solve for the four elements in $\underline{f}$ and to get $\underline{\tilde{f}}$ we do the tilde-conjugation, i.e. change sign of the energy and complex conjugate. The stationary Usadel equation with intrinsic spin-orbit coupling is

$$iD\tilde{\nabla} \cdot \left(\check{g} \tilde{\nabla} \check{g} \right) = \left[\epsilon \hat{\tau}_3 + \boldsymbol{M} \cdot \hat{\boldsymbol{\sigma}}, \check{g} \right]_- . \tag{6.2}$$

Where $\tilde{\nabla}(\cdot) = \nabla(\cdot) - i \left[\hat{\boldsymbol{A}}, (\cdot) \right]$, and $\hat{\boldsymbol{A}} = \mathrm{diag}(\underline{\boldsymbol{A}}, -\underline{\boldsymbol{A}}^*)$ as covered in section 3.7. Since the heavy metals exhibit intrinsic spin-orbit coupling, we first expand the left-hand side of the Usadel equation

$$\begin{aligned}\tilde{\nabla}\cdot\left(\hat{g}\tilde{\nabla}\hat{g}\right) &= \tilde{\nabla}\cdot\left(\hat{g}\nabla\hat{g} - i\hat{g}\left[\hat{\boldsymbol{A}},\hat{g}\right]_-\right)\\ &= \nabla\cdot(\hat{g}\nabla\hat{g}) - i\nabla\cdot\left(\hat{g}\left[\hat{\boldsymbol{A}},\hat{g}\right]_-\right)\\ &- i\left[\hat{\boldsymbol{A}},\hat{g}\nabla\hat{g} - i\hat{g}\left[\hat{\boldsymbol{A}},\hat{g}\right]_-\right]_-\\ &= \nabla\cdot(\hat{g}\nabla\hat{g}) - i\nabla\cdot\left(\hat{g}\left[\hat{\boldsymbol{A}},\hat{g}\right]_-\right)\\ &- i\left[\hat{\boldsymbol{A}},\hat{g}\nabla\hat{g}\right]_- - \left[\hat{\boldsymbol{A}},\hat{g}\left[\hat{\boldsymbol{A}},\hat{g}\right]_-\right]_-. \end{aligned} \tag{6.3}$$

We then apply the weak proximity Green's function matrix in (6.1) and insert $\hat{\boldsymbol{A}} = \mathrm{diag}(\underline{\boldsymbol{A}}, -\underline{\boldsymbol{A}}^*)$. To get an equation of motion for the anomalous Green's functions $\underline{f}$, we only need to worry about the top-right 2×2 spin-space element in the Usadel equation.

$$\left[\tilde{\nabla}\cdot\left(\hat{g}\tilde{\nabla}\hat{g}\right)\right]^{(1,2)} = \nabla^2\underline{f} - i\nabla\left(\underline{\boldsymbol{A}}\underline{f} + \underline{f}\underline{\boldsymbol{A}}^*\right) - i\left(\underline{\boldsymbol{A}}\nabla\underline{f} + \nabla\underline{f}\underline{\boldsymbol{A}}^*\right) \tag{6.4}$$

$$- \underline{\boldsymbol{A}}\left(\underline{\boldsymbol{A}}\underline{f} + \underline{f}\underline{\boldsymbol{A}}^*\right) - \left(\underline{\boldsymbol{A}}\underline{f} + \underline{f}\underline{\boldsymbol{A}}^*\right)\underline{\boldsymbol{A}}^* \tag{6.5}$$

$$= \nabla^2\underline{f} - 2i\left[\underline{\boldsymbol{A}},\nabla\underline{f}\right]_+^* - \left[\underline{\boldsymbol{A}},\left[\underline{\boldsymbol{A}},\underline{f}\right]_+^*\right]_+^*. \tag{6.6}$$

Here, we have defined the notation $[A,B]_\pm^* = AB \pm BA^*$. The self-energy part of the Usadel equation which exhibits an exchange field gives us the resulting linear Usadel equation,

$$\nabla^2\underline{f} - 2i\left[\underline{\boldsymbol{A}},\nabla\underline{f}\right]_+^* - \left[\underline{\boldsymbol{A}},\left[\underline{\boldsymbol{A}},\underline{f}\right]_+^*\right]_+^* + \frac{2\epsilon i}{D}\underline{f} + \frac{i}{D}\boldsymbol{M}\cdot\left[\underline{\boldsymbol{\sigma}},\underline{f}\right]_-^* = 0. \tag{6.7}$$

If we simply where to solve this equation with the KL boundary condition at the two ends $x=-G$ and $x=G$, see figure 6.1, we would simply get $\underline{f}=0$. This is because we haven't incorporated any singlet pair sources to our system. Our problem is fundamentally two dimensional, and the Cooper pair correlations are coming from the z-direction and into the heavy metals, so we have to incorporate the KL boundary condition into our Usadel equation by looking at the z-directional component of the Laplace operator ∇^2. By assuming that the width of the heavy metals and the ferromagnetic film much smaller than any characteristic length scales, we can average over the z-direction and use the KL boundary condition as an effective source of singlet state pairs in the linear Usadel equation. The KL boundary condition at the interface between one of the superconductors and its corresponding heavy metal in figure 6.1 becomes

$$\frac{\partial\underline{f}}{\partial z} - i\left[\underline{A}_z,\underline{f}\right]_+^*|_{S/F} = \frac{\cosh(\theta)}{\zeta L}\underline{f} - \frac{\sinh(\theta)}{\zeta L}e^{i\phi}i\underline{\sigma}_2. \tag{6.8}$$

As we have previously seen, due to the small width of the heavy metal, $\underline{A}_z$ will be assumed to be zero. We can also neglect the first term on the right-hand side since we are assuming that $||\underline{f}|| \ll 1$. We will now use this boundary condition by first expanding the Laplace operator $\nabla^2\underline{f} = \frac{\partial^2\underline{f}}{\partial x^2} + \frac{\partial^2\underline{f}}{\partial z^2}$, average over the z-direction and use the KL boundary conditions.

$$\frac{1}{W+d}\int_{-d}^{W}\frac{\partial^2\underline{f}}{\partial z^2}\mathrm{d}z = \frac{1}{W+d}\left(\frac{\partial\underline{f}}{\partial z}|_{z=W} - \frac{\underline{f}}{\partial z}|_{z=-d}\right) = \frac{\sinh(\theta)}{\zeta(W+d)^2}e^{i\phi}i\underline{\sigma}_y. \tag{6.9}$$

Here, we used that the length normal to the interface is simply $W + d$. By now averaging over all components in the linear Usadel equation, we get

$$\frac{d^2}{dx^2}\underline{f} - \frac{2id}{W+d}\left[\underline{A}_x, \frac{d}{dx}\underline{f}\right]_+^* - \frac{d}{W+d}\left[\underline{\boldsymbol{A}}, \left[\underline{\boldsymbol{A}}, \underline{f}\right]_+^*\right]_+^* + \frac{\sinh(\theta)}{\zeta(W+d)^2}e^{i\phi}i\underline{\sigma}_2 + \frac{2\epsilon i}{D}\underline{f} + \frac{i}{D}\boldsymbol{M}\cdot\left[\underline{\boldsymbol{\sigma}}, \underline{f}\right]_-^* = 0. \tag{6.10}$$

In the middle region where only the ferromagnetic film is, there will be no spin-orbit coupling and so we can set $\underline{\boldsymbol{A}} = 0$ in this region. There will also be no sources of singlet states from the z-direction in this ferromagnetic-only region. In the left and right region we have to use two different macroscopic phases such that the total difference in phase is $\Delta\phi = \phi_R - \phi_L$, where ϕ_R and ϕ_L are the macroscopic phases in the right and left superconductor, respectively. In the two superconducting nodes, the effective magnetic field will be reduced due to the heavy metals which exhibit no exchange fields. Thus the effective exchange field will be $\boldsymbol{M} \to \frac{W}{W+d}\boldsymbol{M}$ in these regions.

We have effectively three sets of differential equations corresponding to the three regions, and thus need a sufficient amount of boundary conditions. We require that the condensate functions $\underline{f}$ will be continuous and that the current will conserved between these regions. The latter is simply the KL boundary condition, and will in this case yield

$$\partial_x\underline{f}(-L/2^+) = \partial_x\underline{f}(-L/2^-) - \frac{d}{W+d}i\left[\underline{A}_x, \underline{f}(-L/2^-)\right]_+^* \tag{6.11}$$

$$\partial_x\underline{f}(L/2^-) = \partial_x\underline{f}(L/2^+) - \frac{d}{W+d}i\left[\underline{A}_x, \underline{f}(L/2^+)\right]_+^*. \tag{6.12}$$

We also require that the x-directed supercurrent will be zero at the ends $x = G$ and $x = -G$ which with the KL boundary condition is equivalent to $\frac{\partial f}{\partial x} - \frac{d}{W+d}i\left[\underline{A}_x, \underline{f}\right]_+^* = 0$. The width of the heavy metals will be thin in the z-direction, and thus, we model the spin-orbit coupling to be of the form

$$\underline{\boldsymbol{A}} = (\beta\underline{\sigma}_1 - \alpha\underline{\sigma}_2, \alpha\underline{\sigma}_1 - \beta\underline{\sigma}_2, 0). \tag{6.13}$$

Before moving on, we want to emphasize exactly why we choose a lateral structure. Note that the second term in equation (6.10) couples the spin-orbit coupling $\underline{\boldsymbol{A}}$ to the momentum direction of the quasiparticle. If we had chosen a one-directional setup, this term would be zero since the momentum of the quasiparticles would be perpendicular to $\underline{\boldsymbol{A}}$. On the other hand, the third term will become non-zero, but first of all, it is second order in $\underline{\boldsymbol{A}}$ and can be neglected for weak spin-orbit coupling. Secondly, as noted in reference [8], this term does not fulfill the requirement made by Bergeret and Tokatly for generation of LRTs in reference [29]. This requirement states that $[\underline{\boldsymbol{A}}, [\underline{\boldsymbol{A}}, \boldsymbol{M}\cdot\underline{\boldsymbol{\sigma}}]]$ can not be proportional to $\boldsymbol{M}\cdot\underline{\boldsymbol{\sigma}}$. But if there is only an in-plane magnetization, $M_z = 0$, it will always be proportional to $\boldsymbol{M}\cdot\underline{\boldsymbol{\sigma}}$, and no LRTs can be generated from this third term in equation (6.10). Therefore, only the second term in equation (6.10) gives rise to LRTs.

Moving on, we will in this chapter as well use the d-vector to represent our anomalous Green's functions

$$\underline{f} = (f_s + \boldsymbol{d}\cdot\underline{\boldsymbol{\sigma}})\, i\sigma_2 = \begin{bmatrix} id_y - d_x & d_z + f_s \\ d_z - f_s & id_y + d_x \end{bmatrix}. \tag{6.14}$$

This representation separates the short-ranged triplets from the long-ranged triplets. The long-ranged component will be the component that is perpendicular to the exchange field $d_{\mathrm{LRC}} \propto |\boldsymbol{d}\times\boldsymbol{M}|$ while the short-ranged component will be parallel to the exchange field $d_{\mathrm{SRC}} \propto \boldsymbol{d}\cdot\boldsymbol{M}$. The set of Pauli matrices with the addition of the identity matrices form a basis for the vector space of 2×2 matrices. Therefore, by using the identity $\underline{\sigma}_a\underline{\sigma}_b = \delta_{ab}\underline{\sigma}_0 + i\epsilon_{abc}\underline{\sigma}_c$, where δ_{ab} is the Kronecker delta and ϵ_{abc} is the Levi-Civita symbol, and we get four equations for each of the four matrix elements:

$$\frac{\partial^2 f_s}{\partial x^2} + \frac{\sinh(\theta)}{\zeta(W+d)^2}e^{i\phi} + \frac{2\epsilon i}{D}f_s + \frac{2i}{D}\left(M_x d_x + M_y d_y\right) = 0, \tag{6.15}$$

$$\frac{\partial^2 d_x}{\partial x^2} + \frac{d}{W+d}\left(-4\alpha\frac{\partial d_z}{\partial x} - 4(\alpha^2+\beta^2)d_x - 8\alpha\beta d_y\right) + \frac{2\epsilon i}{D}d_x + \frac{2iM_x}{D}f_s = 0, \tag{6.16}$$

$$\frac{\partial^2 d_y}{\partial x^2} + \frac{d}{W+d}\left(-4\beta\frac{\partial d_z}{\partial x} - 4(\alpha^2+\beta^2)d_y - 8\alpha\beta d_x\right) + \frac{2\epsilon i}{D}d_y + \frac{2iM_y}{D}f_s = 0, \tag{6.17}$$

$$\frac{\partial^2 d_z}{\partial x^2} + \frac{d}{W+d}\left(4\alpha\frac{\partial d_x}{\partial x} + 4\beta\frac{\partial d_y}{\partial x} - 8(\alpha^2+\beta^2)d_z\right) + \frac{2\epsilon i}{D}d_z = 0. \tag{6.18}$$

We can immediately draw several conclusions before attempting to solve the differential equations. First of all, we see that the transformation $d_x \leftrightarrow d_y, \alpha \leftrightarrow \beta, M_x \leftrightarrow M_y$ leaves the equations invariant. If we set $\beta = M_y = 0$, we decouple the third equation from the rest of the equations, and thus there is no way for the singlet state f_s to be transformed into a triplet d_y state. And thus the solution for $d_y = 0$. In this scenario, if we get a long-ranged triplet state, it should be proportional to d_z, i.e. $d_{\mathrm{LRC}} \propto |\boldsymbol{d}\times\boldsymbol{M}| = M_x d_z$. Due to the invariant transformation mentioned above, setting $\alpha = M_x = 0$ yields in the same way $d_x = 0$ and the long-ranged component, if it exists, will still be d_z.

If we now set $\beta = M_x = 0$ we are able to decouple the second and fourth differential equations from the other two. And thus $d_x = d_z = 0$. The Rashba coupling has in this case a very small impact on the system, and there will be no way to generate long-ranged triplet pair correlations since $d_{\mathrm{LRC}} = |\boldsymbol{d}\times\boldsymbol{M}| = 0$.

Note that in the case of Rashba coupling with the exchange field pointing along the x-axis, both the long-ranged component d_z and the short-ranged component d_x get an imaginary contribution to the energy,

$$\epsilon_{d_z} = \epsilon - i\frac{4dD}{W+d}\alpha^2, \tag{6.19}$$

$$\epsilon_{d_x} = \epsilon - i\frac{2dD}{W+d}\alpha^2. \tag{6.20}$$

Note that the imaginary contribution to the long-ranged component d_z is twice that of the short-ranged component d_x. Such imaginary energy contributions are associated with inelastic scattering which breaks the pair coherence apart. We can immediately see that a too large Rashba coefficient will break all triplets apart in the two superconducting nodes. Note that in the ferromagnetic-only region, there will still be induced a FFLO phase which

gives short-ranged triplets even with strong Rashba coupling in the heavy metals. But with a large Rashba type spin-orbit coupling, it is not possible to generate long-ranged triplet pairs in the heavy metals, and thus there will be no such LRTs traveling through the ferromagnetic bridge. On the other hand, with no Rashba coupling at all (and no Dresselhaus coupling), there is no way to generate d_z-components, and we get no long-ranged components. Therefore, there must exist a certain Rashba coefficient where the long-ranged components are largest when the exchange field is directed along the x-axis. This also means that if these long-ranged components can generate a long-ranged supercurrent, then there will be a certain Rashba coefficient where the supercurrent has the largest magnitude. Thus, an in-plane rotation of the exchange field from the x-direction to the y-direction will severely decrease the magnitude of the supercurrent as we soon will see is true analytically and numerically.

6.2 Pure Rashba Coupling and In-Plane Magnetization

In this section, we will show that we in fact do get a long-ranged supercurrent due to the long-ranged component generated in the heavy metals. Unfortunately, these equations have proved too difficult to solve even in the weak proximity limit, so we will only be looking at a pure Rashba spin-orbit coupling and set $\beta = 0$. The exchange field will be set along the x-axis, and so $M_y = 0$. We will let G and L be semi-infinite and much bigger than any characteristic lengths such as the coherence length. This means the superconducting nodes will be so far apart that the overlap between the condensate functions coming from the two regions will be small. Therefore, the condensate functions in the ferromagnetic region will be approximated to be a superposition of the condensate functions in two systems where only one effective superconducting node with spin-orbit coupling is present. We thus consider a system where we only have only one effective superconducting node with spin-orbit coupling in the region $x < 0$, and the region $x > 0$ will be a ferromagnetic-only region. The condensate function will converge to zero deep in the ferromagnet $x \gg 0$, and the KL boundary condition at $x = 0$ is enough to solve the system. We assume the Rashba coupling is weak, $\alpha^2 \ll |\boldsymbol{M}|/D$, and all second order α in the linear Usadel equation can be neglected. The Usadel equation then gives the general solution

$$f_s = -\frac{2\alpha k}{K_p^2 - k^2} C_4 e^{kx} + C_5 e^{K_p x} + C_6 e^{K_m x} + \frac{k^2}{K_p^2\left(2k^2 - K_p^2\right)} h e^{i\phi_1} \tag{6.21}$$

$$d_x = C_5 e^{K_p x} - C_6 e^{K_m x} - \frac{K_p^2 - k^2}{K_p^2\left(2k^2 - K_p^2\right)} h e^{i\phi_1} \tag{6.22}$$

$$d_z = C_4 e^{kx} - \frac{2\alpha K_p}{K_p^2 - k^2} C_5 e^{K_p x} - \frac{2\alpha K_m}{K_p^2 - k^2} C_6 e^{K_m x} \tag{6.23}$$

when $x < 0$. Here, $k = \sqrt{-2i\epsilon/D}$, $K_{p(m)} = \sqrt{-2i(\epsilon + (-)M_x)/D}$ and $h = \sinh(\theta(\epsilon))/\zeta(W+d)^2$. $\theta(\epsilon) = \operatorname{atanh}(|\Delta_0|/\epsilon)$ and in the region where we only have the ferromagnetic film, the general solution is

$$f_s = -C_1 e^{-K_m x} + C_2 e^{-K_p x} \tag{6.24}$$

$$d_x = C_1 e^{-K_m x} + C_2 e^{-K_p x} \tag{6.25}$$

$$d_z = C_3 e^{-kx}. \tag{6.26}$$

We thus see that the only long-ranged component is d_z as expected. Therefore, we are mostly interested in finding C_3. The boundary conditions at $x = 0$ gives us

$$C_3 = -\frac{3K_p^4 - kK_p^3 + (kK_m - 6k^2)K_p^2 + 2k^3K_p + k^4}{\left(4kK_p^6 - 12k^3K_p^4 + 8k^5K_p^2\right)} \frac{d}{W+d} \alpha h e^{i\phi_1}. \tag{6.27}$$

We immediately see that C_3 is proportional to the Rashba coefficient, and thus without spin-orbit coupling we would get no long-ranged component. By setting $|M_x| \gg \epsilon$, we get $|K_{(m/p)}| \gg |k|$ and C_3 is simplified to

$$C_3 = -\frac{3d\alpha h e^{i\phi_1}}{4(W+d)kK_p^2}. \tag{6.28}$$

We will now assume that the condensate function in the system in figure 6.1 is given as a superposition between two superconducting nodes that have semi-infinite lengths L and G. By placing a second superconducting node at $x = L/2$ and setting the superconducting node we considered above to $x = -L/2$, we let $\underline{f}$ be a superposition of two systems where only one of these superconducting nodes are present. This gives us the solution

$$\begin{aligned}
f_s &= -C_1^- e^{-K_m(x+L/2)} - C_1^+ e^{K_m(x-L/2)} + C_2^- e^{-K_p(x+L/2)} + C_2^+ e^{K_p(x-L/2)}, \\
d_x &= C_1^- e^{-K_m-(x+L/2)} + C_1^+ e^{K_m(x-L/2)} + C_2^- e^{-K_p(x+L/2)} + C_2^+ e^{K_m(x-L/2)}, \\
d_z &= C_3^- e^{-k(x+L/2)} + C_3^+ e^{k(x-L/2)}.
\end{aligned} \tag{6.29}$$

Here, C_n^- and C_n^+ are the coefficient for the left and right superconducting node, respectively. Thus, C_3^- will be the coefficient in equation (6.27), and C_3^+ can be found by changing the sign of k, K_p and K_m since the condensate functions are propagating in the opposite direction. We also have to use the macroscopic phase for the right superconductor ϕ_R in C_3^+. Entering this into the formula for the supercurrent in (4.27), we get

$$I_Q = 4N_0De \int_0^\infty d\epsilon \tanh(\beta\epsilon/2) \Re\Big(2K_m \left(C_1^+ \tilde{C}_2^- - C_1^- \tilde{C}_2^+ \right) e^{-K_m L} \tag{6.30}$$

$$+ 2K_p \left(C_2^+ \tilde{C}_1^- - C_2^- \tilde{C}_1^+ \right) e^{-K_p L} + k \left(C_3^+ \tilde{C}_3^- - C_3^- \tilde{C}_3^+ \right) e^{-kL} \Big). \tag{6.31}$$

Here, we have used the equilibrium distribution function $\hat{h} = \tanh(\beta\epsilon/2)\hat{\tau}_0$. The long-ranged supercurrent will come from the last term, and so entering the simplified C_3-coefficients, the long-ranged supercurrent becomes

$$\begin{aligned}
I_Q = 8N_0De \sin(\Delta\phi) \int_0^\infty d\epsilon \tanh(\beta\epsilon/2) \left(\frac{3d\alpha}{4(W+d)} \right)^2 \\
\times \Re\Big(-i \frac{h\tilde{h}}{kK_m^2 K_p^2} e^{-kL} \Big),
\end{aligned} \tag{6.32}$$

where $\Delta\phi = \phi_R - \phi_L$. And thus, this long-ranged triplet component also gives a long-ranged supercurrent that is proportional to α^2 for small α. We have here used the simplified solution for C_3 in (6.28) which assumes that the main contribution from the energy integral comes from the energies close to the gap energy which we have shown to be true numerically. We

could have used the whole solution for C_3 in equation (6.27), and we get a much longer and accurate expression for I_Q. But the point is nevertheless that we get a long-ranged supercurrent when $\alpha \neq 0$.

As argued before, the system is invariant under the transformation $d_x \leftrightarrow d_y, \alpha \leftrightarrow \beta, M_x \leftrightarrow M_y$ and hence we get the same expression for the long-ranged supercurrent with β instead of α if we set $\alpha = M_x = 0$ and keep β and M_y non-zero. Thus, we require either Rashba or Dresselhaus spin-orbit coupling to get a long-ranged supercurrent. As we previously argued, there will be no long-ranged triplet states if $\beta = M_x = 0$. *Thus rotating the exchange field from $\boldsymbol{M} = M\boldsymbol{e}_x$ to $\boldsymbol{M} = M\boldsymbol{e}_y$ with Rashba coupling, we should see a significant drop in the supercurrent.*

6.3 Numerical Solutions

The weak proximity approximation is only valid if $||\underline{f}|| \ll 1$ which might not always be the case. We will instead of solving the differential equations in the last chapter numerically, we will solve the non-linear Usadel equation numerically by using the Riccati parameterization with spin-orbit coupling which we presented in equation (3.31). We will still be making some approximations when solving the equations. The inverse-proximity effect will be neglected meaning that the gap energy will assumed to be unchanged close to the heavy metals and equal to the bulk gap energy, $|\Delta| = |\Delta_0|$. This is due to the thin width of the heavy metal and ferromagnetic film, and this approximation can be argued to be close to true by the numerical calculations in reference [8]. We will also make the problem effectively one-dimensional by averaging over the z-direction in the two superconducting nodes as we did in the weak proximity limit. The problem could be solved in two dimensions, but that would deem much more time and computational demanding. Even if it would give more accurate predictions, the conclusions we draw by making the problem one dimensional will hold true.

We continue by using the KL boundary condition as an effective source of singlet states in the heavy metal and ferromagnetic region. The KL boundary condition at the superconductor-heavy metal interface is

$$\frac{\partial}{\partial z}\underline{\gamma} = \frac{1}{L\zeta}\left(1 - \underline{\gamma}\underline{\tilde{\gamma}}_S\right)\underline{N}_S\left(\underline{\gamma} - \underline{\gamma}_S\right) + i\underline{A}_z\underline{\gamma} + i\underline{\gamma}\underline{A}_z^* \tag{6.33}$$

where ζ is the ratio between the barrier resistance and the bulk resistance of the heavy metal, and $\underline{\gamma}_S$ and $\underline{N}_S$ are the gamma matrix and normalization matrix in the superconductor, respectively. And as we previously have argued, $\underline{A}_z = 0$. By now averaging over the z-direction, we can use the above boundary condition as an effective source of singlet state pairs. Therefore, we expand the Laplace operator ∇^2 to include both the x and z-component, average over the z-direction, and thus we get the effective Usadel equation

$$\begin{aligned}
&D\left(\frac{\partial^2}{\partial x^2}\underline{\gamma} + \frac{1}{(W+d)\zeta}\left(1 - \underline{\gamma}\underline{\tilde{\gamma}}_S\right)\underline{N}_S\left(\underline{\gamma} - \underline{\gamma}_S\right) + 2\left(\frac{\partial}{\partial x}\underline{\gamma}\right)\underline{\tilde{N}}\underline{\tilde{\gamma}}\left(\frac{\partial}{\partial x}\underline{\gamma}\right)\right) \\
&= -2i\epsilon\underline{\gamma} - i\boldsymbol{M}\cdot\left(\underline{\boldsymbol{\sigma}}\underline{\gamma} - \underline{\gamma}\underline{\boldsymbol{\sigma}}^*\right) \\
&+D\frac{d}{W+d}\left(\underline{\boldsymbol{A}}^2\underline{\gamma} - \underline{\gamma}\left(\underline{\boldsymbol{A}}^*\right)^2 + 2\left(\underline{\boldsymbol{A}}\underline{\gamma} + \underline{\gamma}\underline{\boldsymbol{A}}^*\right)\underline{\tilde{N}}\left(\underline{\boldsymbol{A}}^* + \underline{\tilde{\gamma}}\underline{\boldsymbol{A}}\underline{\gamma}\right)\right) \\
&+2iD\frac{d}{W+d}\left(\left(\frac{\partial}{\partial x}\underline{\gamma}\right)\underline{\tilde{N}}\left(\underline{A}_x^* + \underline{\tilde{\gamma}}\underline{A}_x\underline{\gamma}\right) + \left(\underline{A}_x + \underline{\gamma}\underline{A}_x^*\underline{\tilde{\gamma}}\right)\underline{N}\left(\frac{\partial}{\partial x}\underline{\gamma}\right)\right).
\end{aligned} \tag{6.34}$$

The corresponding equation for $\underline{\tilde{\gamma}}$ can be found by tilde conjugating the equation above. Unlike the previous project where we had a precessing exchange field, our current system is in equilibrium. Thus, we do not need to solve the distribution function numerically since we already know that the only non-zero distribution function is $h_1 = \tanh(\beta\epsilon/2) = \tanh\left(\frac{\pi}{2e^\gamma}\frac{\epsilon/|\Delta_0|}{T/T_c}\right)$.

6.4 Parameters

We consider the system depicted in figure 6.1. Niobium has a gap energy of around $|\Delta_0| \approx 3$ meV [71], and we will normalize all energies to this quantity. The correlation length is set to $\xi_S = \sqrt{D/|\Delta_0|} = 25$ nm. We will assume that the diffusion constant is equal in all materials. We will have the lengths $W = d = 2$ nm and if otherwise not stated, $L = 25$ nm, and the width of the heavy metal region is 5 nm, which gives the ratio $G/L = 0.7$. We also get the ratio $\xi_S/L = 1$. The interface transparency is set to $\zeta = 5$, and the exchange field is placed in the xy-plane, $\boldsymbol{M} = M(\cos(\theta), \sin(\theta), 0)$. Thus, if the in-plane angle of the exchange field is $\theta = 0$, the exchange field points in the x-direction. Only the ferromagnet has an exchange field, and thus if the exchange field is $M_F = 50|\Delta_0|$ and $W = d$, the effective exchange field will be $M = 25|\Delta_0|$ in the two superconducting nodes and $M = 50|\Delta_0|$ in the ferromagnetic-only region. The macroscopic phase difference has been set to $\Delta\phi = \phi_R - \phi_L = \pi/2$, while the temperature is $T = 0.5T_c$, and in addition, we will now only assume a pure Rashba coupling which we will normalize to the length of the ferromagnetic bridge L and thus αL will be a dimensionless quantity. Note that, as we stated above, our results will be the same for pure Dresselhaus coupling by making an in-plane rotation of the exchange field by $\pi/2$. With only Rashba coupling, the spin-orbit coupling term is

$$\underline{\boldsymbol{A}} = (-\alpha\underline{\sigma}_2, \alpha\underline{\sigma}_1, 0). \tag{6.35}$$

The supercurrent is plotted 6.2a and 6.2b as a function of the in-plane exchange field angle θ and Rashba spin-orbit coupling, respectively. We see in the latter plot that the supercurrent is greatly enhanced by a non-zero Rashba coupling when the exchange field lies along the x-axis, $\theta = 0$. This is namely due to the generation of long-ranged triplets that is able to carry the current with less decay than the short-ranged triplets found without any spin-orbit coupling. We also confirm our theory that a too large Rashba coupling suppresses the long-ranged components due to an imaginary contribution to the energy of the long-ranged triplets which are associated with pair-breaking processes. Thus, an in-plane rotation from $\theta = 0$ to $\theta = \pi/2$ has a much smaller impact on the current with large spin-orbit coupling. With no spin-orbit coupling, the in-plane rotation makes no impact as expected. With our parameters, the optimal Rashba constant that creates the largest difference in current when rotating the exchange field from the x-axis to the y-axis is with SI units $\alpha L/\hbar^2 = 5$. This corresponds to the experimental value $\alpha/m \approx 1.310^{-11}$eV m if one assume that the effective mass of the quasiparticles is equal to rest mass of an electron. This is well within the interval of experimentally measured Rashba coefficients of many materials [72], and thus a suitable heavy metal with the right Rashba coefficient should be possible to find.

One other important finding is that an in-plane rotation of the exchange field with a non-zero Rashba constant can create $0-\pi$ transitions close to $\theta = \pi/2$. Thus, it is possible to go from high current at $\theta = 0$ to a low/no current close to $\theta = \pi/2$. This is something that can easily been done *in situ* and thus such a setup can act as a simple transistor where the in-plane

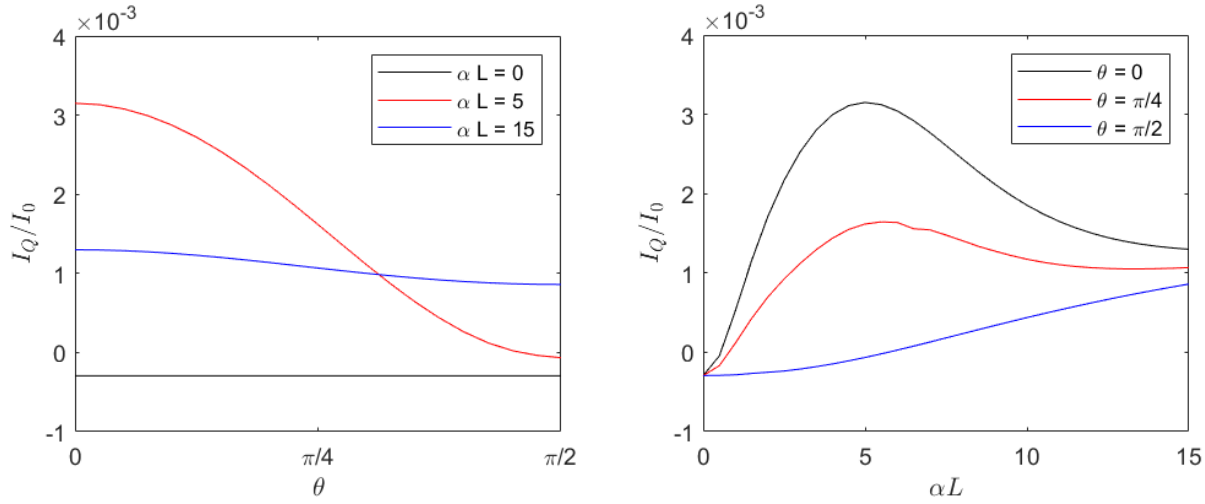

(a) (b)

Figure 6.2: The supercurrent is plotted as a function of exchange field θ and Rashba coupling αL. When $\theta = 0$ the exchange field only has a pure x-direction, while $\theta = \pi/2$ points the exchange field in the y-direction. Here, I_0 is a constant that is not of importance in this discussion. Note that the length L is fixed while the Rashba constant α is varying in the plots.

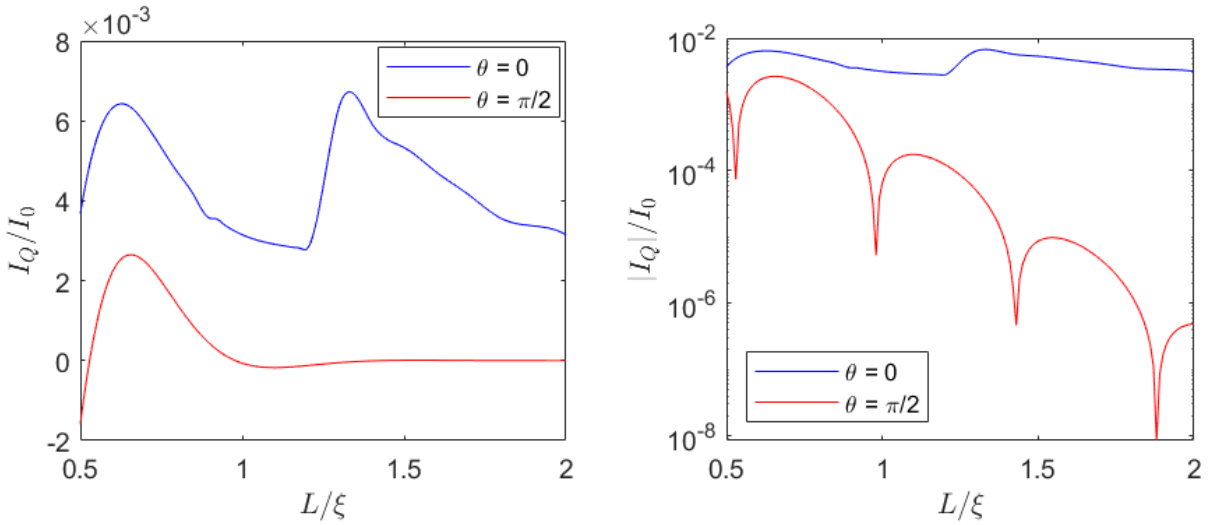

Figure 6.3: The supercurrent is plotted as a function of the length of the ferromagnetic-only region. The right figure shows a log plot of the absolute values of the current in the left figure. The sharp dips in the log plot shows where the current changes sign and are thus $0 - \pi$ transitions.

rotation of the exchange field decides whether the system is in a 1 state (high current) or a 0 state (low current).

Lastly, we show in figure 6.3 that the supercurrent is in fact long-ranged when $\theta = 0$. We see that the short-ranged current at $\theta = \pi/2$ undergoes several $0 - \pi$ transitions while the long-ranged currents undergo no such transitions. This is due to the FFLO phase where the short-ranged triplets and singlet states oscillate over space. Such oscillations allow for π-states to have a lower free energy than the 0-states. The long-ranged current in long junctions is dominated by long-ranged triplets which is not in a FFLO phase, and can thus not create $0 - \pi$ transitions.

Before finishing this section, we would like to make some comments about the approximation of making the problem effectively one-dimensional. If we had a typical, one-dimensional SNFNS Josephson junction with spin-orbit coupling in the N layers, we would only be able to get long-ranged component with an out-of plane magnetization. To generate long-ranged components with an in-plane magnetization, we need to make the momenta of the quasiparticles couple with the $SU(2)$ gauge-invariant vector potential $\underline{\boldsymbol{A}}$. With Rashba coupling in a thin heavy metal layer, this requires the quasiparticle to change momentum from the z-direction to the x-direction which is exactly what is happening in the region where we averaged over the heavy metal and ferromagnetic layer. But in reality, it is uncertain exactly how much momentum change the quasiparticles undergo in the heavy metal regions since they lie on top of the ferromagnetic layer, see figure 6.1. In reality, one would therefore most likely see weaker long-ranged components and thus a weaker long-ranged supercurrent, and one would need to solve the problem in two dimensions to get more accurate results. The optimal setup would be to have two heavy metals with Rashba coupling on each side of the ferromagnetic bride where the quasiparticles are allowed to propagate along the x-axis into the other superconducting node, but this is perhaps experimentally an unrealistic setup.

We also want to point out that if one had modeled the heavy metal as a two-dimensional interface with spin-orbit coupling by using the very recently discovered boundary conditions in reference [80], one would see no long-ranged components at all. This is because the quasiparticles need to be allowed to change their momenta so that they have a non-zero momenta in the x-direction and can thus couple with the x-component of the spin-orbit coupling vector $\underline{\boldsymbol{A}}$.

7 | Conclusion

We have in this thesis been looking at two different research projects where we studied the symbiosis between superconductive and ferromagnetic ordering. The first project looked at heterostructures with a ferromagnet that exhibits a precessing exchange field. With and without being in proximity to a superconductor, such a system is driven out of equilibrium which meant we had to also solve the distribution function which could make all eight distribution functions non-zero. We only scratched the surface of such a complex systems, and a lot more can be done to unravel the physics in these systems. For a starter, we did not incorporate the fully gauge-invariant phase difference into our numerical calculations, and we showed that a non-zero phase difference in a SFS Josephson junction with a precessing exchange field will yield a charge accumulation which gives rise to a potential difference across the junction. By using the Josephson's relation, we concluded that this potential difference will make the phase difference time-dependent. In the weak proximity limit, we showed that this time-varying phase does not complicate the calculations of the condensate functions, but in the full proximity limit we will turn into problems due to the time-convolution operator (ring product). But as we mentioned, there may be ways to overcome this problem. In addition, we did not self-consistently solve the gap energy, Green's function and distribution function in all the materials we considered in all systems. We only did so in a FS bilayer to show how the gap energy is affected by the precession of the exchange field. We did not solve everything self-consistently due to time limitations and lack of enough computational resources. Solving the problems numerically in a compiled language is more suitable since it can be several order of magnitude faster, and such implementations has already been created in Fortran [22].

In addition, it would also be interesting to see how superconductive ordering affects the Gilbert damping of the exchange field. In reference [76] it was shown experimentally that a SFS Josephson junction with a precessing exchange field has a much higher Gilbert damping than a FS bilayer, which the researchers argued was due to the equal-spin triplets that is allowed to flow as a supercurrent through a SFS junction. In our model, the Gilbert damping can be found by fixing the angular resonance precession Ω and find the tilt angle θ by self-consistently calculating the magnetization of the system. We made some calculations to test this out and our findings seem to suggest that this is true in our model as well, but it has not been pursued in this thesis due to time limitations.

In the second project we showed the possibility of a long-ranged supercurrent flowing through a lateral SFS Josephson junction with intrinsic spin-orbit coupling. With Rashba type spin-orbit coupling, the current only becomes long-ranged if the exchange field points in the direction of the ferromagnetic bridge, but if we make an in-plane rotation of 90° of the exchange field, the current becomes short-ranged. It can also undergo $0 - \pi$ transitions by an in-plane rotation of the exchange field. This means the supercurrent can in long junctions effectively be turned on and off by rotating the exchange field which can easily be done *in situ*. This opens up the possibility of using the setup as a transistor where an in-plane

rotation of 90° gives the difference between high current (1 bit) or low/no current (0 bit).

We mainly focused on Rashba type spin-orbit interaction, but we also showed that Dresselhaus type is equivalent by making a 90° in-plane rotation of the exchange field. Nevertheless, it would be interesting to see what would happen in a system where we would have both types present. One could also try to solve the problem in two dimensions and self-consistently find the gap energy close to the heavy metals. This would most likely not reveal any new details, but would nevertheless give quantitatively more accurate results. Solving the equations in two dimensions could require more computational resources, but an implementation using the finite element method has been created and proved to be successfully in terms of accuracy and time consumption [69].

A | Supercurrent in a SNS Josephson Junction

We will in this appendix show that in a superconductor/normal-metal/superconductor Josephson junction the supercurrent is proportional to $I_Q = I_c \sin(\Delta\phi)$ where I_c is the maximal supercurrent possible. We will also show that the supercurrent decays exponentially as $\xi_n = \sqrt{D/2\pi k_B T}$ in long junctions where D is the diffusion constant, k_B is the Boltzmann constant, and T is the temperature. We will in this section set $\hbar = 1$.

We will assume that the Cooper pair correlations in the normal state metal are weak, and we can therefore take use of the linear Usadel equation. The superconductors on either side will be conventional so only single state pairs leak through the interface and into the normal state metal. Since there are no exchange fields, these single state will not be able to transform into any triple states. The linear Usadel equation then simple becomes

$$\frac{\partial^2 f_s}{\partial x^2} + \frac{2\epsilon i}{D} f_s = 0 \tag{A.1}$$

which gives the solution $f_s(x) = Ae^{kx} + Be^{-kx}$ where $k = \sqrt{-2\epsilon i/D}$. The two interfaces are placed at $x = -L/2$ and $x = L/2$ so that the length of the normal state metal is L. The weak proximity Kupriyanov-Lukichev boundary conditions in equation (3.21) on each side become

$$\zeta L \frac{\partial f_s}{\partial x}(x = -L/2) = \sinh(\theta) e^{i\phi} \tag{A.2}$$

$$\zeta L \frac{\partial f_s}{\partial x}(x = L/2) = -\sinh(\theta) e^{-i\phi}, \tag{A.3}$$

where ζ is the ratio between the barrier and bulk resistance. Note that the phase difference in the two superconductors are $\Delta\phi = 2\phi$. We also have $\theta = \operatorname{atanh}(|\Delta_0|/\epsilon)$. We have taken use of the BCS bulk Green's function in equation (3.29). The solution for the coefficients A and B now become

$$A = -\frac{\sinh(\theta)\cosh(kL/2 - i\phi)}{\zeta L k \sinh(kL)} \tag{A.4}$$

$$B = -\frac{\sinh(\theta)\cosh(kL/2 + i\phi)}{\zeta L k \sinh(kL)}. \tag{A.5}$$

Note that $\tilde{A} = -B$ and $\tilde{B} = -A$, where the tilde conjugation is given as changing sign of ϵ and complex conjugating. Now applying the the solution for $f_s(x)$ into the formula for charge-current, we get

$$
\begin{aligned}
I_Q &= N_0 DeA \int_0^\infty d\epsilon \tanh\left(\frac{\beta\epsilon}{2}\right) \Re\left[\left(2f_s\frac{\partial \tilde{f}_s}{\partial x} - 2f_t\frac{\partial \tilde{f}_t}{\partial x} - f_\uparrow\frac{\partial \tilde{f}_\uparrow}{\partial x} - f_\downarrow\frac{\partial \tilde{f}_\downarrow}{\partial x}\right) - \tilde{[...]}\right] \\
&= N_0 DeA \int_0^\infty d\epsilon \tanh\left(\frac{\beta\epsilon}{2}\right) \Re\left(-k\left(A\tilde{B} - B\tilde{A}\right)\right) \\
&= N_0 DeA \int_0^\infty d\epsilon \tanh\left(\frac{\beta\epsilon}{2}\right) \Re\left(k\left(A^2 - B^2\right)\right) \\
&= N_0 DeA \int_0^\infty d\epsilon \tanh\left(\frac{\beta\epsilon}{2}\right) \Re\left(\frac{\sinh(\theta)^2\left(\cosh(kL/2 - i\phi)^2 - \cosh(kL/2 + i\phi)^2\right)}{\zeta^2 L^2 k \sinh(kL)^2}\right) \\
&= N_0 DeA \sin(\Delta\phi) \int_0^\infty d\epsilon \tanh\left(\frac{\beta\epsilon}{2}\right) \Re\left(\frac{-i\Delta^2}{\zeta^2 L^2\left(\epsilon^2 - \Delta^2\right) k \sinh(kL)}\right).
\end{aligned} \tag{A.6}
$$

Here, $\beta = 1/k_B T$, and in the last line we used the identity $\cosh(a - ib)^2 - \cosh(a + ib)^2 = -i\sinh(2a)\sin(2b)$, $\sinh(\theta)^2 = \Delta^2/(\epsilon^2 - \Delta^2)$ and that $\Delta\phi = 2\phi$. We have therefore shown that the supercurrent is proportional to $\sin(\Delta\phi)$. Using $\Re(-iz) = \Im(z)$ and noting that the imaginary part of $1/k\sinh(kL)$ is odd in ϵ which means the whole integrand is even in ϵ, we can extend the lower limit of the integration to minus infinity. We thus get

$$
I_Q = I_0 \Im\left(\int_{-\infty}^{\infty} d\epsilon \frac{\tanh(\beta\epsilon/2)}{(\epsilon^2 - \Delta^2) k \sinh(kL)}\right), \tag{A.7}
$$

where $I_0 = \frac{N_0 DeA\Delta^2 \sin(\Delta\phi)}{2\zeta^2 L^2}$. We will next add a small imaginary part to the energy $\epsilon \to \epsilon + i\delta$, $\delta > 0$ and solve the integral by the use of the Cauchy's residue theorem. The poles in the denominator in equation (A.7) are all in the lower half-plane, therefore, by choosing our contour to be the upper half-plane, the only poles we need to consider would be $\tanh(i(n+1/2)\pi) \to \infty$ when $\epsilon = i(2n+1)\pi k_B T = i\omega_n$ where ω_n is the Matsubara frequency and n is a positive integer or zero. By first making the substitution $u = \beta\epsilon/2$ and then using Cauchy's residue theorem, we get

$$
\begin{aligned}
I_Q &= I_0 \Im\left(4\pi i k_B T \sum_n \frac{1}{(\Delta^2 + \omega_n^2) k(i\omega_n)\sinh(k(i\omega_n)L)}\right) \\
&= I_0 4\pi k_B T \sum_n \frac{1}{(\Delta^2 + \omega_n^2) k(i\omega_n)\sinh(k(i\omega_n)L)},
\end{aligned} \tag{A.8}
$$

where we used that the sum is a real number in the last line. Because of the sinh-term in the denominator, the first term in the summation makes the biggest impact, and only considering this term, we get

$$
I_Q = I_0 4\pi k_B T \frac{1}{(\Delta^2 + (\pi k_B T)^2)\sqrt{2\pi k_B T/D}\sinh(\sqrt{2\pi k_B T/D}L)}. \tag{A.9}
$$

Since $1/\sinh(\sqrt{2\pi k_B T/D}L) \to 2e^{-\sqrt{2\pi k_B T/D}L}$ when L is large, we clearly see that the coherence length of a SNS-junction is $\xi_N = \sqrt{D/2\pi k_B T}$.

B | Ring Product

We will in this appendix introduce the ring operator $\circ$. This operator has two different definitions depending on what representations you have for the two functions A and B. If the functions are known in absolute times, $A(t_1, t_2)$ and $B(t_1, t_2)$, the definition is

$$(A \circ B)(t_1, t_2) = \int dt_3 A(t_1, t_3) B(t_3, t_2), \tag{B.1}$$

which after Fourier transforming to energy and momentum space becomes

$$(A \circ B)(T, \epsilon) = \int dt e^{i\epsilon t} \int dt_3 A(t_1, t_3) B(t_3, t_2), \tag{B.2}$$

where $t = t_1 - t_2$. If the functions are known in its mixed coordinate form $A(T, \epsilon)$ and $B(T, \epsilon)$, then it can be shown [6] that

$$(A \circ B)(T, \epsilon) = \exp\left(-i\left(\partial_T^A \partial_\epsilon^B - \partial_\epsilon^A \partial_T^B\right)\right) A(T, \epsilon) B(T, \epsilon). \tag{B.3}$$

Here, the notation ∂_T^A means the derivative of A with respect to T.

C | Convolution Identity

We will in this appendix prove the following identity: If $f(T,\epsilon) = e^{-i\omega_1 T} f(\epsilon)$ and $g(T,\epsilon) = e^{-i\omega_2 T} g(\epsilon)$, then

$$(f \circ g)(T,\epsilon) = e^{-i(\omega_1+\omega_2)T} f(\epsilon + \omega_2/2) g(\epsilon - \omega_1/2). \tag{C.1}$$

We are using mixed coordinates, so $t = t_1 - t_2$ and $T = (t_1 + t_2)/2$. The definition of the convolution operator $\circ$ is

$$(f \circ g)(t_1, t_2) = \int dt_3 f(t_1, t_3) g(t_3, t_2), \tag{C.2}$$

and thus, with mixed coordinates we get

$$(f \circ g)(T,t) = \int dt_3 f\left(\frac{t_1+t_3}{2}, t_1 - t_3\right) g\left(\frac{t_3+t_2}{2}, t_3 - t_2\right). \tag{C.3}$$

Expanding f and g yields

$$f\left(\frac{t_1+t_3}{2}, t_1 - t_3\right) = \int f\left(\epsilon, \frac{t_1+t_3}{2}\right) e^{-i\epsilon(t_1-t_3)} d\epsilon \tag{C.4}$$

$$= \int f(\epsilon) e^{-it_1(\epsilon+\omega_1/2) + it_3(\epsilon-\omega_1/2)} d\epsilon, \tag{C.5}$$

$$g\left(\frac{t_3+t_2}{2}, t_3 - t_2\right) = \int g(\epsilon) e^{-it_3(\epsilon+\omega_2/2) + it_2(\epsilon-\omega_2/2)} d\epsilon. \tag{C.6}$$

Entering these f and g into equation (C.3) thus becomes

$$(f \circ g)(T,t) = \int dt_3 d\epsilon d\epsilon' f(\epsilon) e^{-it_1(\epsilon+\omega_1/2) + it_3(\epsilon-\omega_1/2)} g(\epsilon') e^{-it_3(\epsilon'+\omega_2/2) + it_2(\epsilon'-\omega_2/2)} \tag{C.7}$$

$$= \int dt_3 d\epsilon d\epsilon' f(\epsilon) g(\epsilon') e^{it_3\left(\epsilon - \epsilon' - \frac{\omega_1+\omega_2}{2}\right) + it_2(\epsilon'-\omega_2/2) - it_1(\epsilon+\omega_1/2)}. \tag{C.8}$$

Integration over t_3 returns a Dirac's delta $\delta(\epsilon - \epsilon' - (\omega_1+\omega_2)/2)$ which after integration over ϵ' returns

$$(f \circ g)(T,t) = \int d\epsilon f(\epsilon) g(\epsilon - (\omega_1+\omega_2)/2) e^{it_2(\epsilon-\omega_1/2-\omega_2) - it_1(\epsilon+\omega_1/2)}. \tag{C.9}$$

Next, we Fourier transform the equation from relative time $t = t_1 - t_2$ to energy ϵ. We also substitute $t_1 = T + t/2$ and $t_2 = T - t/2$.

$$
\begin{aligned}
(f \circ g)(T, \epsilon) &= \int dt (f \circ g)(T, t) e^{i\epsilon t} && \text{(C.10)} \\
&= \int dt d\epsilon'' f(\epsilon'') g(\epsilon'' - (\omega_1 + \omega_2)/2) && \text{(C.11)} \\
&\times e^{i(T-t/2)(\epsilon'' - \omega_1/2 - \omega_2) - i(T+t/2)(\epsilon'' + \omega_1/2)} e^{i\epsilon t} && \text{(C.12)} \\
&= \int dt d\epsilon'' f(\epsilon'') g(\epsilon'' - (\omega_1 + \omega_2)/2) && \text{(C.13)} \\
&\times e^{-i(\omega_1+\omega_2)T} e^{-it(\epsilon'' - \epsilon - \omega_2/2)} && \text{(C.14)} \\
&= e^{-i(\omega_1+\omega_2)T} \int d\epsilon'' f(\epsilon'') g(\epsilon'' - (\omega_1 + \omega_2)/2) && \text{(C.15)} \\
&\times \delta\left(\epsilon'' - \epsilon - \omega_2/2\right) && \text{(C.16)} \\
&= e^{-i(\omega_1+\omega_2)T} f(\epsilon + \omega_2/2) g(\epsilon - \omega_1/2). && \text{(C.17)}
\end{aligned}
$$

D | Analytical Solutions to Condensate Functions and Distribution Functions

D.1 FS Bilayer with a Precessing Exchange Field

In this section we will give the solution of the condensate functions in the stationary frame in a ferromagnet with a precessing magnetic field. This ferromagnet is placed in proximity to a superconductor to make a FS bilayer. The vacuum interface is placed at $x = 0$ and the superconductor interface is placed at $x = L$ which makes the length of the ferromagnet equal to L. The solutions for the anomalous Green's functions when the gap energy in the superconductor is real are

$$f_s'(x) = -\frac{M'}{M_z'}A_{sm}\cosh(k_m x) + \frac{M'}{M'}A_{sp}\cosh(k_p x) \tag{D.1}$$

$$d_x'(x) = -\frac{M'}{M_x}A_l\cosh(kx) + \frac{M_x}{M_z'}A_{sm}\cosh(k_m x) + \frac{M_x}{M_z'}A_{sp}\cosh(k_p x) \tag{D.2}$$

$$d_y'(x) = 0, \tag{D.3}$$

$$d_z'(x) = A_l\cosh(kx) + A_{sm}\cosh(k_m x) + A_{sp}\cosh(k_p x), \tag{D.4}$$

where $k = \sqrt{-2i\epsilon/D}$, $k_{m(p)} = \sqrt{-2i\left(\epsilon - (+)M'\right)/D}$, $M' = \sqrt{M_x^2 + (M_z + \Omega/2)^2}$ is the effective exchange field amplitude, and $M_z' = M_z + \Omega/2$ is the effective exchange field in the z-direction. Note that the effective exchange field in the x-direction is the same in both the laboratory and stationary frame. The coefficients are

$$A_l = \frac{M_x^2 S_M}{\gamma L M'^2 k\sinh(kL)} \tag{D.5}$$

$$A_{sp} = \frac{-M_z'\left(M'S_P - M_z'S_M\right)}{2\gamma L M'^2 k_p\sinh(k_p L)} \tag{D.6}$$

$$A_{sm} = \frac{M_z'\left(M_z'S_M + M'S_P\right)}{2\gamma L M'^2 k_m\sinh(k_m L)}, \tag{D.7}$$

where $S_{P(m)} = \frac{s_p + (-)s_m}{2}$, and $s_{p(m)} = \sinh(\theta(\epsilon + (-)\Omega/2))$ and $\theta(\epsilon) = \text{atanh}(|\Delta_0|/\epsilon)$. Note that in equilibrium, when $\Omega = 0$ or $M_x = 0$, then $S_M = 0$ and there will be no long-ranged components.

D.2 SFS Josephson Junction with a Precessing Exchange Field

The anomalous Green's functions in the stationary frame in the ferromagnetic layer in a SFS Josephson junction are

$$f_s'(x) = -\frac{M'}{M_z'}\left(A_{sp}e^{k_p x} + B_{sp}e^{-k_p x}\right) + \frac{M'}{M_z'}\left(A_{sm}e^{k_m x} + B_{sm}e^{-k_m x}\right) \tag{D.8}$$

$$d_x'(x) = -\frac{M_z'}{M_x}\left(A_l e^{kx} + B_l e^{-kx}\right) + \frac{M_x}{M_z'}\left(A_{sp}e^{k_p x} + B_{sp}e^{-k_p x}\right) + \frac{M_x}{M_z'}\left(A_{sm}e^{k_m x} + B_{sm}e^{-k_m x}\right) \tag{D.9}$$

$$d_y'(x) = 0 \tag{D.10}$$

$$d_z'(x) = A_l e^{kx} + B_l e^{-kx} + A_{sp}e^{k_p x} + B_{sp}e^{-k_p x} + A_{sm}e^{k_m x} + B_{sm}e^{-k_m x} \tag{D.11}$$

where

$$A_l = \frac{M_x^2 S_M\left(e^{-kL/2} + e^{i\Delta\phi}\right)e^{-i\Delta\phi/2}}{2\gamma L M'^2 k\sinh(kL/2)} \tag{D.12}$$

$$B_l = \frac{M_x^2 S_M\left(e^{kL/2} + e^{i\Delta\phi}\right)e^{-i\Delta\phi/2}}{2\gamma L M'^2 k\sinh(kL/2)} \tag{D.13}$$

$$A_{sp} = \frac{(M_z'^2 S_M - M' M_z' S_P)\left(e^{-k_p L/2} + e^{i\Delta\phi}\right)e^{-i\Delta\phi/2}}{4\gamma L M'^2 k_p\sinh(k_p L/2)} \tag{D.14}$$

$$B_{sp} = \frac{(M_z'^2 S_M - M' M_z' S_P)\left(e^{k_p L/2} + e^{i\Delta\phi}\right)e^{-i\Delta\phi/2}}{4\gamma L M'^2 k_p\sinh(k_p L/2)} \tag{D.15}$$

$$A_{sm} = \frac{(M_z'^2 S_M + M' M_z' S_P)\left(e^{-k_m L/2} + e^{i\Delta\phi}\right)e^{-i\Delta\phi/2}}{4\gamma L M'^2 k_m\sinh(k_m L/2)} \tag{D.16}$$

$$B_{sm} = \frac{(M_z'^2 S_M + M' M_z' S_P)\left(e^{k_m L/2} + e^{i\Delta\phi}\right)e^{-i\Delta\phi/2}}{4\gamma L M'^2 k_m\sinh(k_m L/2)} \tag{D.17}$$

where $S_{P(M)} = \frac{\sinh(\theta(\epsilon+\Omega/2)+(-)\sinh(\theta(\epsilon-\Omega/2))}{2}$, and $M_z' = M_z + \Omega/2$ and $M' = \sqrt{M_x^2 + (M_z+\Omega/2)^2}$ is the effective exchange field in the z-direction and magnitude, respectively. $\Delta\phi = \phi_2 - \phi_1$ is the macroscopic phase difference. The two interfaces are placed at $x = -L/2$ and $x = L/2$ which makes the length of the ferromagnet equal to L. We see that in the equilibrium case, when $\Omega = 0$ or $M_x = 0$, the long range components are zero, i.e. $A_l = B_l = 0$.

D.3 Distribution Functions in a Precessing Exchange Field

The distribution function in the stationary frame in a ferromagnet with a processing magnetic field without any superconductive ordering are given by the differential equations

$$\nabla^2 h_1' = 0 \tag{D.18}$$
$$D\nabla^2 h_6' = -2\left(M_z + \Omega/2\right) h_7' \tag{D.19}$$
$$D\nabla^2 h_7' = -2M_x h_8' + 2\left(M_z + \Omega/2\right) h_6' \tag{D.20}$$
$$D\nabla^2 h_8' = 2M_x h_7' \tag{D.21}$$

and the boundary conditions at $x = +(-)L/2$ become

$$\gamma L \nabla h_1' = +(-)\left(\frac{t_p + t_m}{2} - h_1'\right) \tag{D.22}$$
$$\gamma L \nabla h_6' = +(-)(-h_6'), \tag{D.23}$$
$$\gamma L \nabla h_7' = +(-)(-h_7'), \tag{D.24}$$
$$\gamma L \nabla h_8' = +(-)\left(\frac{t_p - t_m}{2} - h_8'\right) \tag{D.25}$$

where $t_{p(m)} = \tanh(\frac{\beta}{2}(\epsilon + (-)\Omega/2))$. We have here assumed the ferromagnet is coupled to normal state metals which act as reservoirs in equilibrium. The solution to these equations are

$$h_1'(x) = T_P, \tag{D.26}$$
$$h_6'(x) = \frac{M_x M_z'}{M'^2} T_M \left(1 - C_1 \cosh(\kappa x) + C_2 \cos(\kappa x)\right), \tag{D.27}$$
$$h_7'(x) = -i\frac{M_x}{M'} T_M \left(C_1 \cosh(\kappa x) + C_2 \cos(\kappa x)\right), \tag{D.28}$$
$$h_8'(x) = \frac{1}{M'^2} T_M \left(M_z'^2 + M_x^2 \left(C_1 \cosh(\kappa x) - C_2 \cos(\kappa x)\right)\right), \tag{D.29}$$

where $\kappa = \sqrt{-2iM'/D}$ and $T_{P(M)} = (t_p + (-)t_m)/2$. $M' = \sqrt{M_x^2 + (M_z + \Omega/2)^2}$ and $M_z' = M_z + \Omega/2$ are the effective exchange field magnitude and the effective exchange field in the z-direction, respectively. Note that all other distribution functions $h_n' = 0$. The coefficients are

$$C_1 = \frac{1/2}{\kappa L\gamma \sinh(\kappa L/2) + \cosh(\kappa L/2)}, \tag{D.30}$$
$$C_2 = \frac{1/2}{\kappa L\gamma \sin(\kappa L/2) - \cos(\kappa L/2)}. \tag{D.31}$$

We explicitly see that if $\Omega = 0$ or $M_x = 0$ then the solution is $h_1'(x) = \tanh(\beta\epsilon/2)$ both in the stationary and laboratory frame while every other $h_n' = 0$. The other equilibrium case is when $M_x = 0$, then $h_1'(x) = (t_p + t_m)/2$ and $h_8'(x) = (t_p - t_m)/2$ which is the same solutions as equation (5.58) which in the laboratory frame simply becomes $\hat{h} = \tanh(\beta\epsilon/2)\hat{\tau}_0$. Thus, these two cases give us the equilibrium solution as they should do. In other cases we will not be in equilibrium and then to find the distribution function in laboratory frame, we insert our answer into equations (5.63)-(5.70).

E | Research Article

The following is a draft of an article that will be sent to review at Physics Review B when completed.

Long-ranged triplet supercurrent in a single in-plane ferromagnet with spin-orbit coupled contacts to superconductors

Johannes R. Eskilt
Center for Quantum Spintronics, Department of Physics, Norwegian University of Science and Technology, NO-7491 Trondheim , Norway

Niladri Banerjee
Department of Physics, Loughborough University, Loughborough, LE11 3TU, United Kingdom

Jacob Linder
Center for Quantum Spintronics, Department of Physics, Norwegian University of Science and Technology, NO-7491 Trondheim, Norway

(Dated: June 4, 2019)

By converting conventional spin-singlet Cooper pairs to polarized spin-triplet pairs, it is possible to sustain long-ranged spin-polarized supercurrents flowing through strongly polarized ferromagnets. Obtaining such a conversion via spin-orbit interactions, rather than magnetic inhomogeneities, has recently been explored in the literature. A challenging aspect with regard to experimental detection has been that in order for Rashba spin-orbit interactions, present e.g. at interfaces due to inversion symmetry breaking, to generate such long-ranged supercurrents, an out-of-plane component of the magnetization is required. This limits the choice of materials and can induce vortices in the superconducting region complicating the interpretation of measurements. Therefore, it would be desirable to identify a way in which Rashba spin-orbit interactions can induce long-ranged supercurrents for purely in-plane rotations of the magnetization. Here, we show that this is possible in a lateral Josephson junction where two superconducting electrodes are placed in contact with a ferromagnetic film via two thin, heavy normal metals. The magnitude of the supercurrent in such a setup becomes tunable by the in-plane magnetization angle when using only a single magnetic layer. These results could provide a new and simpler way to generate controllable spin-polarized supercurrents than previous experiments which utilized complicated magnetically textured Josephson junctions.

I. INTRODUCTION

When a conventional superconductor is placed in proximity to a normal state metal, the Cooper pairs will start leaking across the interface from the superconductor and into the metal. These singlet state order parameter will, in the metal, start decaying over a length scale of $\xi_N = \sqrt{D/T}$ where D is the diffusion constant of the metal and T is the temperature [1]. If the metal is a ferromagnet, then the anti-parallel electrons of the singlet Cooper pair will be injected into two different sub-bands (majority and minority) in the ferromagnet, making their Fermi momenta different. This makes the pair decay even faster, namely on a length scale of order $\xi_F = \sqrt{D/M}$ where M is the amplitude of the exchange field. This pair breaking effect can be avoided if the singlet pair can be converted into a triplet pair with a non-zero spin projection along the exchange field. With these so-called long-ranged triplets (LRTs), the pairs will decay slower and be comparable to correlation lengths of normal metal ξ_N. Physical quantities like supercurrents will be on the same order, and it is thus of great interest to be able to manipulate and create such LRTs. This topic is currently under intense focus [2, 3] because of the potential to develop not only cryogenic spintronics devices, but also radically novel theoretical and experimental aspects of how such pairs can be generated and tuned in a controllable manner.

It is well known theoretically and experimentally that LRT components can be created in an inhomogenous exchange field [4–9]. It can also be generated in ferromagnets that have a precessing exchange field [10]. More recently, it was shown [11] that spin-orbit coupling could act as a source of such triplets in diffusive superconductor/ferromagnet structures. It was proposed that lateral geometries would provide less stringent requirements to generate LRTs compared to a stacked geometry which was utilized to demonstrate the appearance of long-ranged supercurrents in Refs. [4, 5, 9]. It was shown in Ref. [12] that in S/F bilayers with Rashba spin-orbit coupling, the magnetization requires an out-of-plane component to generate the LRT. Although such a scenario is possible to obtain experimentally [13–15], it complicates the unambiguous identification of spin-polarized Cooper pairs due to the additional flux injection from domain walls from the ferromagnet and also severely restricts the choice of materials showing a tailored out-of-plane anisotropy. Very recently, Ref. [14] did not find any clear signature of a long-ranged triplet supercurrent in a Josephson junction including heavy metals and multilayers of ferromagnets with an effective canted magnetization direction. Therefore, it would be desirable to identify a setup where the LRTs can be tuned with a sole in-plane variation of the magnetization to minimize the stray field effect on the superconductor itself. This would be a different result than previous works [13, 14, 16–20] that have considered how to control the supercurrent via magnetization in Josephson contacts with spin-orbit coupling.

In this paper, we consider a lateral Josephson junction where two superconducting electrodes are placed in contact with a ferromagnetic layer through a heavy metal (see Fig. 1). Due to the inversion symmetry breaking and the large atomic

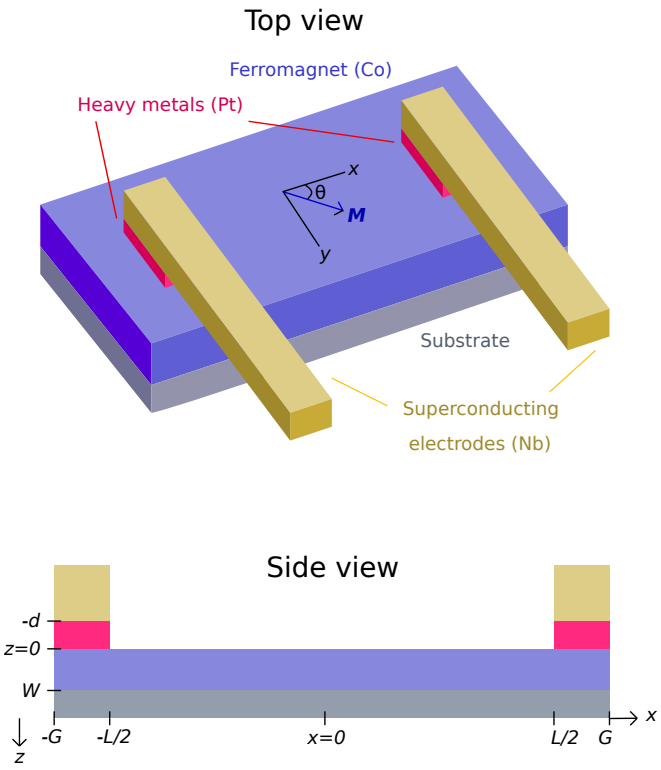

Figure 1. A lateral SFS Josephson junction with Rashba spin-orbit coupling in the heavy metals. The exchange field lies in the plane of the ferromagnet. A supercurrent is sent through the magnetic layer via the superconducting electrodes and is tuned via the in-plane angle θ of the ferromagnet.

number of such metals, Rashba spin-orbit coupling is assumed to be present at these interfaces. As we will show, such a setup will not only host long-ranged triplet Cooper pairs but also give a long-ranged supercurrent for certain in-plane rotations of the exchange field. Thus, the supercurrent in the ferromagnet is extremely sensitive to this in-plane rotation as long as there is a non-zero spin-orbit coupling present in the heavy metals. We will also show that for some parameters, the in-plane rotation is be able to create $0-\pi$ transitions, which means that for a certain in-plane rotation of the exchange field, the supercurrent is zero. Therefore, such a geometry can work as a transistor for supercurrents by simply rotating the in-plane magnetization. We emphasize that the main novelty and benefit of the present result and setup compared to previous works is that the supercurrent is tuned with a single ferromagnetic layer *and* the magnetization only needs to rotate in the plane of the magnet. Experimental observation of this effect would represent a significant advance with regard to simplifying control over long-ranged spin-polarized supercurrents, which has proved challenging before [9].

II. THEORY

In this paper we will use the quasiclassical theory of superconductivity [21, 22] and consider the dirty limit so that the quasiclassical Green's function $\check{g}$ in the ferromagnet can be described by the Usadel diffusion equation [23]

$$iD\tilde{\nabla}\cdot\left(\check{g}\tilde{\nabla}\check{g}\right)=[\epsilon\hat{\rho}_3+\boldsymbol{M}\cdot\hat{\boldsymbol{\sigma}},\check{g}]_-, \tag{1}$$

where D is the diffusion constant for the ferromagnet, ϵ is the energy of the quasiparticles, $\hat{\rho}_3=\mathrm{diag}(1,1,-1,-1)$, and $\boldsymbol{M}$ is the exchange field. The Pauli matrix vector is $\hat{\boldsymbol{\sigma}}=\mathrm{diag}(\underline{\boldsymbol{\sigma}},\underline{\boldsymbol{\sigma}}^*)$. The Green's function $\check{g}$ is the 8×8 Green's function in Keldysh space

$$\check{g}=\begin{bmatrix}\hat{g}^R & \hat{g}^K\\ 0 & \hat{g}^A\end{bmatrix}. \tag{2}$$

Due to the triangular structure of $\check{g}$, the Usadel equation becomes the same for the retaraded Green's function $\hat{g}^R$.

To incorporate spin-orbit coupling into our theory, we have defined [11] $\tilde{\nabla}(\cdot)=\nabla(\cdot)-i[\hat{\boldsymbol{A}},(\cdot)]_-$. Here, $\hat{\boldsymbol{A}}=\mathrm{diag}(\underline{\boldsymbol{A}},-\underline{\boldsymbol{A}}^*)$, where $\underline{\boldsymbol{A}}$ is a 2×2 matrix in spin space which couples to the momentum $\boldsymbol{k}$. In effect, the spin-orbit coupling is included as an effective SU(2) gauge-like field, which is possible if it is linear in momentum. We will include both Rashba and Dresselhaus effects in this paper denoted by their respective constants α and β, both being precisely linear in momentum. However, we emphasize that the main merit of the present setup is that *only* Rashba spin-orbit coupling and an in-plane rotation of the magnetization is required to get a tunable long-ranged spin-polarized supercurrent. The Dresselhaus term is thus simply included to make the results more general. Rashba spin-orbit coupling can arise from the lack of inversion symmetry at the interface between two materials. We will later consider two heavy metals where the width in the z-direction is small, and thus the Rashba Hamiltonian is of the form

$$H_R=\frac{\alpha}{m}(\boldsymbol{k}\times\underline{\boldsymbol{\sigma}})\cdot\boldsymbol{e}_z, \tag{3}$$

where $\boldsymbol{k}$ is the momentum of the quasiparticles. The Dresselhaus SOC, on the other hand, can be caused by lack of inversion center in the crystal structure. For two dimensional structures in the xy-plane this Hamiltonian becomes

$$H_D=\frac{\beta}{m}\left(k_y\underline{\sigma}_y-k_x\underline{\sigma}_x\right). \tag{4}$$

These are the two Hamiltonian we will consider in this paper, and will give the following $\underline{\boldsymbol{A}}$:

$$\underline{\boldsymbol{A}}=\left(\beta\underline{\sigma}_x-\alpha\underline{\sigma}_y\right)\boldsymbol{e}_x+\left(\alpha\underline{\sigma}_x-\beta\underline{\sigma}_y\right)\boldsymbol{e}_y. \tag{5}$$

We will complement the Usadel diffusion equation with Kupriyanov-Lukichev (KL) boundary conditions [24]

$$2\gamma L\check{g}\tilde{\nabla}\check{g}=[\check{g}_L,\check{g}_R]_-, \tag{6}$$

where L and R denotes the left and right side of the interface, respectively. Here, we have also added the gauge covariant derivative $\tilde{\nabla}$ to include spin-orbit coupling.

To calculate the supercurrent going through the ferromagnetic bridge, we will use quasiclassical expression for the electric current, following the notation of [25] and [12]

$$I_Q = \frac{N_0 DAe}{4}\int_{-\infty}^{\infty} d\epsilon \mathrm{Tr}\left(\hat{\rho}_3\left(\check{g}\tilde{\nabla}\check{g}\right)^K\right). \tag{7}$$

Here, A is the cross section, N_0 is the density of states at Fermi level, e is the electric charge. The superscript K denotes the Keldysh component of the 8×8 matrix. The system in consideration will be in equilibrium, and thus we can use the relation $\hat{g}^K = \tanh(\beta\epsilon/2)\left(\hat{g}^R - \hat{g}^A\right)$ where β in the inverse temperature $1/k_BT$. The expression for the charge supercurrent then takes the form

$$I_Q = I_0\int_{-\infty}^{\infty} d\epsilon \tanh(\beta\epsilon/2)\mathrm{Tr}\left(\hat{\rho}_3\left(\hat{g}^R\tilde{\nabla}\hat{g}^R - \hat{g}^A\tilde{\nabla}\hat{g}^A\right)\right), \tag{8}$$

where $I_0 = \frac{N_0 DAe}{4}$. We can find $\hat{g}^R$ with the Usadel equation, and with the relation $\hat{g}^A = -\hat{\rho}_3\left(\hat{g}^R\right)^\dagger\hat{\rho}_3$, we have everything we need to find the supercurrent. Later, we will compare our result with the supercurrent through a ferromagnetic film when no interfacial spin-orbit coupling is present. In this case, the derivatives become normal derivatives i.e., $\tilde{\nabla}\to\nabla$. It can easily be shown that this current is conserved in regions that are governed by the Usadel equation, both with and without spin-orbit coupling i.e., $\nabla\cdot I_Q = 0$ [12]. Thus the supercurrent in ferromagnetic region in Fig. 1 will be conserved.

Our problem is inherently two-dimensional, but we will make it effectively one-dimensional by assuming that the total width of the heavy metals and ferromagnetic film $W+d$ is much smaller than length scale over which the Green function varies. Thus, we can assume the Green's function stays roughly constant along the z-axis, and by averaging the condensate function along the z-axis we can apply the KL boundary condition at the superconductor/heavy-metal interfaces. This effectively gives the differential equations a source of singlet Cooper pairs in the two regions $-G < x < -L/2$ and $L/2 < x < G$.

III. RESULTS AND DISCUSSION

A. Analytical results

Before resorting to a numerical analysis, we can draw several conclusions by making use of the weak proximity effect approximation. The assumption is that in any non-superconducting materials, the Cooper pair correlations will be weak, and thus the retarded Green's function only slightly deviates from its normal-state value:

$$\hat{g} = \begin{bmatrix} \underline{1} & \underline{f} \\ -\underline{\tilde{f}} & -\underline{1}\end{bmatrix}, \tag{9}$$

where the tilde conjugation $\tilde{(\cdot)}$ changes the sign of the energy and complex conjugates. We insert this 4×4 Green's function matrix to the Usadel equation, and by looking exclusively at the top-right 2×2 element, we will get an equation that is completely independent of $\underline{\tilde{f}}$. Thus, we only need to solve for the four elements in $\underline{f}$ and to get $\underline{\tilde{f}}$ we perform the tilde-conjugation, i.e. change sign of the energy and complex conjugate.

By applying the weak proximity approximation to the Usadel equation, we can linearize it in the anomalous Green function $\underline{f}$ to obtain

$$\nabla^2\underline{f} - 2i\left[\underline{\boldsymbol{A}}, \nabla\underline{f}\right]_+^* - \left[\underline{\boldsymbol{A}}, \left[\underline{\boldsymbol{A}}, \underline{f}\right]_+^*\right]_+^* + \frac{2\epsilon i}{D}\underline{f} + \frac{i}{D}\boldsymbol{M}\cdot\left[\underline{\boldsymbol{\sigma}}, \underline{f}\right]_-^* = 0. \tag{10}$$

where we have used the notation $[A,B]_+^* = AB + BA^*$. We now proceed to show that the KL boundary condition provide an effective source of singlet pairs in our linearized Usadel equation. We will make the standard simplifying assumption that the inverse proximity effect can be neglected and the Green's function in the superconductor is the BCS bulk solution given as

$$\hat{g} = \begin{bmatrix} \cosh(\theta) & i\sigma^y\sinh(\theta)e^{i\phi} \\ -i\sigma^y\sinh(\theta)e^{-i\phi} & -\cosh(\theta)\end{bmatrix}, \tag{11}$$

where $\theta = \theta(\epsilon) = \mathrm{atanh}(\Delta/\epsilon)$. We then average over the z-direction, which causes the KL boundary condition to act as a source of singlet state pairs in the linear Usadel equation. Inserting the weak proximity Green's function for the ferromagnetic region and the BCS bulk Green's function, we get

$$\frac{\partial\underline{f}}{\partial z} - i\left[\underline{A}_z, \underline{f}\right]_+^*|_{S/F} = \frac{\cosh(\theta)}{\zeta L}\underline{f} - \frac{\sinh(\theta)}{\zeta L}e^{i\phi}i\underline{\sigma}^y. \tag{12}$$

As we already have seen, $\underline{A}_z = 0$. Since we are assuming that the elements of $\underline{f}$ are much smaller in magnitude than unity, the first term on the right-hand side can be neglected. We will now use this boundary condition by first expanding the Laplace operator $\nabla^2\underline{f} = \frac{\partial^2\underline{f}}{\partial x^2} + \frac{\partial^2\underline{f}}{\partial z^2}$, integrate over the z-direction and use the KL boundary conditions,

$$\int_{-d}^{W}\frac{\partial^2\underline{f}}{\partial z^2}\mathrm{d}z = \frac{\partial\underline{f}}{\partial z}|_{z=W} - \frac{\partial\underline{f}}{\partial z}|_{z=-d} = \frac{\sinh(\theta)}{\zeta(W+d)}e^{i\phi}i\underline{\sigma}^y. \tag{13}$$

Here, we used that the length normal to the interface is simply $W+d$. By now averaging over all components in the linear Usadel equation, we get

$$\frac{\partial^2}{\partial x^2}\underline{f} - \frac{2id}{W+d}\left[\underline{\boldsymbol{A}}, \frac{\partial}{\partial x}\underline{f}\right]_+^* - \frac{d}{W+d}\left[\underline{\boldsymbol{A}}, \left[\underline{\boldsymbol{A}}, \underline{f}\right]_+^*\right]_+^* + \frac{\sinh(\theta)}{\zeta(W+d)^2}e^{i\phi}i\underline{\sigma}^y + \frac{2\epsilon i}{D}\underline{f} + \frac{i}{D}\boldsymbol{M}\cdot\left[\underline{\boldsymbol{\sigma}}, \underline{f}\right]_-^* = 0. \tag{14}$$

This equation has to be solved in three regions, the two superconducting nodes i.e., $L/2 < x < G$ and $-G < x < -L/2$, and in the ferromagnetic bridge i.e., $-L/2 < x < L/2$. In the ferromagnetic bridge, we have no spin-orbit coupling and we can simply set $\underline{\boldsymbol{A}} = 0$ in this region. In the superconducting nodes, the effective magnetization $\boldsymbol{M}$ will be smaller than in the ferromagnetic film since there is no exchange field present in the heavy metals, so the effective exchange field is thus $\boldsymbol{M} \to \frac{W}{d+W}\boldsymbol{M}$. We also allow for different macroscopic phases for the nodes such that the phase difference is $\Delta\phi = \phi_R - \phi_L$.

Before solving equations, we have to know our boundary conditions. This two-dimensional problem is solved by making the problem effectively one-dimensional, and thus we apply the KL boundary conditions at the vacuum interfaces $x = -G$ and $x = G$ which effectively sets the current moving in the x-direction to zero at these edges. At the two interfaces between the three regions, $x = -L/2$ and $x = L/2$, we require that both the Green function and the current are continuous. The last condition gives us the following boundary conditions:

$$\partial_x \underline{f}(-L/2^+) = \partial_x \underline{f}(-L/2^-) - \frac{d}{W+d} i \left[\underline{A}_x, \underline{f}(-L/2^-)\right]_+^* \tag{15}$$

$$\partial_x \underline{f}(L/2^-) = \partial_x \underline{f}(L/2^+) - \frac{d}{W+d} i \left[\underline{A}_x, \underline{f}(L/2^+)\right]_+^* . \tag{16}$$

For the anomalous Green's function $\underline{f}$, we will make use of the so-called d-vector formalism [26] where all triplet correlations are compactly expressed through a vector $\boldsymbol{d}$. The total superconducting anomalous Green function matrix may then be written as:

$$\underline{f} = (f_s + \boldsymbol{d}\cdot\underline{\boldsymbol{\sigma}})\, i\sigma^y = \begin{bmatrix} id_y - d_x & d_z + f_s \\ d_z - f_s & id_y + d_x \end{bmatrix}. \tag{17}$$

The d-vector representation has the advantage of clearly separating the long-ranged and short-ranged triplet component of $\underline{f}$ [12]. The long-ranged component will be component that is perpendicular to the exchange field $d_{LRC} = |\boldsymbol{d}\times\boldsymbol{M}|$ while the short-ranged component is parallel to the exchange field $d_{SRC} = \boldsymbol{d}\cdot\boldsymbol{M}$. We can now enter our d-vector into equation (14). The set of Pauli matrices with the addition of the identity matrices form a basis for a general 2×2 matrix. Therefore, by using the identity $\sigma^a\sigma^b = \delta_{ab}\underline{I} + i\epsilon_{abc}\sigma^c$, we get four equations for each of the four matrices:

$$\frac{\partial^2 f_s}{\partial x^2} + \frac{\sinh(\theta)}{\zeta(W+d)^2}e^{i\phi} + \frac{2\epsilon i}{D}f_s + \frac{2i}{D}\left(M_x d_x + M_y d_y\right) = 0, \tag{18}$$

$$\frac{\partial^2 d_x}{\partial x^2} + \frac{d}{W+d}\Big(-4\alpha\frac{\partial d_z}{\partial x} - 4(\alpha^2+\beta^2)d_x - 8\alpha\beta d_y\Big) + \frac{2\epsilon i}{D}d_x + \frac{2iM_x}{D}f_s = 0, \tag{19}$$

$$\frac{\partial^2 d_y}{\partial x^2} + \frac{d}{W+d}\Big(-4\beta\frac{\partial d_z}{\partial x} - 4(\alpha^2+\beta^2)d_y - 8\alpha\beta d_x\Big) + \frac{2\epsilon i}{D}d_y + \frac{2iM_y}{D}f_s = 0, \tag{20}$$

$$\frac{\partial^2 d_z}{\partial x^2} + \frac{d}{W+d}\Big(4\alpha\frac{\partial d_x}{\partial x} + 4\beta\frac{\partial d_y}{\partial x} - 8(\alpha^2+\beta^2)d_z\Big) + \frac{2\epsilon i}{D}d_z = 0. \tag{21}$$

We can immediately draw several conclusions before attempting to solve the differential equations. First of all, the transformation $d_x \leftrightarrow d_y, \alpha \leftrightarrow \beta, M_x \leftrightarrow M_y$ leaves the equations invariant. We will mostly look at the case where we only have Rashba spin-orbit coupling present since this case is experimentally more feasible, but due to this invariance, our conclusions of the supercurrent and triplets will also be invariant to this transformation.

We continue by looking at the case $\beta = M_y = 0$. This decouples the third equation from the rest of the equations, and thus there is no way for the singlet state f_s to be transformed into a triplet d_y state. In this scenario, it is in principle possible to obtain a long-ranged triplet state $d_{LRC} = |\boldsymbol{d}\times\boldsymbol{M}| \propto d_z$.

If we now set $\beta = M_x = 0$ we are able to decouple the second and fourth differential equations from the other two. And thus $d_x = d_z = 0$. The Rashba coupling has in this case a very small impact on the system and will only impact singlet pairs and the short range triplets (SRTs) with no LRTs present. Thus, in the case of Rashba coupling, an in-plane rotation of the exchange field from $M_x\boldsymbol{e}_x$ to $M_y\boldsymbol{e}_y$ will make all LRTs vanish and only SRTs will remain.

In the case $\beta = M_y = 0$, we see that the energy of the long-ranged component d_z acquires an imaginary term,

$$\epsilon_{LRT} = \epsilon - i\frac{4dD}{W+d}\alpha^2. \tag{22}$$

Imaginary contributions to the energy are normally associated with pair-breaking processes, and therefore, these LRT components will decay faster if the Rashba coefficient is large. On the other hand, if the Rashba coefficient is zero, then there will be no LRTs at all. We therefore expect to see a certain α where the triplets and supercurrent are both at their largest and will decay after we keep increasing or decreasing α. We will later show numerically that this reasoning is correct, resulting in a non-monotonic behavior of the supercurrent as a function of α, and that an in-plane rotation of the exchange field will drastically change the magnitude of the supercurrent.

B. Pure Rashba Coupling and In-Plane Magnetization

We will now show explicitly that we get a long-ranged triplet pair correlation with spin-orbit coupling which in turn gives a long-ranged charge-supercurrent. We will only be looking at a pure Rashba spin-orbit coupling and set $\beta = 0$. We will also place the magnetic field in the x-direction and thus $M_y = 0$.

We assume now that the distance L between the two superconducting electrodes is so large that the solution for the anomalous Green's function in the ferromagnetic bridge will consequently be the superposition of the Green function in two systems with only one effective superconducting node. In this way, we only need to solve the anomalous Green's function in a lateral geometry with one effective superconducting node with spin-orbit coupling present. Thus, we start by solving a system with only one effective superconducting node including spin-orbit coupling in the region $x \leq 0$ and a region with only the ferromagnetic film $x \geq 0$. Far into the semi-infinite regions the solutions will converge to zero, and we only take into account the boundary conditions at $x = 0$ in Eqs. (15) and (16) with the addition of continuity of the anomalous Green's functions. We will also assume that the Rashba coupling is weak, $\alpha^2 \ll |M|/D$, so that we can remove any second order term in α in the differential equation. The general solution of the differential equations then becomes

$$f_s = -\frac{2\alpha k}{K_p^2 - k^2} C_4 e^{kx} + C_5 e^{K_p x} + C_6 e^{K_m x} + \frac{k^2}{K_p^2\left(2k^2 - K_p^2\right)} h e^{i\phi_1} \tag{23}$$

$$d_x = C_5 e^{K_p x} - C_6 e^{K_m x} - \frac{K_p^2 - k^2}{K_p^2\left(2k^2 - K_p^2\right)} h e^{i\phi_1} \tag{24}$$

$$d_y = 0 \tag{25}$$

$$d_z = C_4 e^{kx} - \frac{2\alpha K_p}{K_p^2 - k^2} C_5 e^{K_p x} - \frac{2\alpha K_m}{K_p^2 - k^2} C_6 e^{K_m x} \tag{26}$$

when $x < 0$. Here, $k = \sqrt{-2i\epsilon/D}$, $K_{p(m)} = \sqrt{-2i(e + (-)M_x)/D}$ and $h = \sinh(\theta)/\zeta(W + d)^2$ and in the ferromagnetic bridge when $x > 0$ the solution is

$$f_s = -C_1 e^{-K_m x} + C_2 e^{-K_p x} \tag{27}$$

$$d_x = C_1 e^{-K_m x} + C_2 e^{-K_p x} \tag{28}$$

$$d_z = C_3 e^{-kx}. \tag{29}$$

As expected, only d_z has any long-ranged triplet components in the purely ferromagnetic region, and thus we are mostly interested in finding C_3. Applying the boundary conditions at $x = 0$, we get to the first order in α,

$$C_3 = -\frac{3K_p^4 - kK_p^3 + (kK_m - 6k^2)K_p^2 + 2k^3 K_p + k^4}{\left(4kK_p^6 - 12k^3 K_p^4 + 8k^5 K_p^2\right)} \times \frac{d}{W + d} \alpha h e^{i\phi_L}, \tag{30}$$

which clearly shows that we only get a long-ranged triplet component if we have Rashba spin-orbit coupling present. Letting $|M_x| \gg \epsilon$, we get $|K_{(m/p)}| \gg |k|$ and

$$C_3 = -\frac{3d\alpha h e^{i\phi_L}}{4(W + d)kK_p^2}. \tag{31}$$

We now place a second superconducting electrode at $x = L/2$ and push the first electrode back to $x = -L/2$. We solve the differential equations for the second node and assume that total condensate function $\underline{f}$ is a superposition of the two solutions and that the superconducting nodes are so far apart that the overlap between the two solutions is small. The complete solution for the long-ranged component is thus

$$d_z = C_3^- e^{-k(x+L/2)} + C_3^+ e^{k(x-L/2)}. \tag{32}$$

Here, C_3^- is the coefficient for the left superconducting node and C_3^+ for the other node. C_3^- will be the coefficient found in Eq. (30), while C_3^+ will be similar except with the sign of k, $K_{(p/m)}$ changing sign since the anomalous Green's functions are propagating in the opposite direction. We also have to remember to use a different macroscopic phase ϕ_R for C_3^+. Entering this LRT component into the formula for the supercurrent, we get

$$I_Q = 4N_0 De \int_0^\infty d\epsilon \tanh(\beta\epsilon/2) \tag{33}$$

$$\times \Re\left(k\left(C_3^+ \tilde{C}_3^- - C_3^- \tilde{C}_3^+\right) e^{-kL}\right). \tag{34}$$

Here the tilde conjugation is as mentioned just doing the transformation $\epsilon \to -\epsilon$ and $i \to -i$. Using the approximated C_3 in Eq. (31), the long-ranged supercurrent becomes

$$I_Q = 8N_0 De \sin(\Delta\phi) \int_0^\infty d\epsilon \tanh(\beta\epsilon/2) \left(\frac{3d\alpha}{4(W + d)}\right)^2 \times \Re\left(-i\frac{h\tilde{h}}{kK_m^2 K_p^2} e^{-kL}\right), \tag{35}$$

where $\Delta\phi = \phi_R - \phi_L$. Therefore, this long-ranged triplet component also gives a long-ranged supercurrent that is proportional to α^2 for small α. In this expression for the supercurrent, we have used the simplified C_3 solution which amounts to the approximation that the main contribution to the integral for the supercurrent comes from the region $\varepsilon \ll |M_x|$. Numerically, we have confirmed that the main contribution indeed comes from the region near $\varepsilon = \Delta$. Alternatively, and

more accurately, we could simply use the whole solution for C_3 in equation (30) which results in a much longer expression for I_Q. The point is nevertheless that we get a long-ranged supercurrent when $\alpha \neq 0$. As previously argued, if we rotate the exchange field from a pure x-direction to lie along the y-axis, the long-ranged component will become zero. An in-plane rotation of the exchange field from $\boldsymbol{M} = M\boldsymbol{e}_x$ to $\boldsymbol{M} = M\boldsymbol{e}_y$ with Rashba coupling should therefore result in a significant drop in the magnitude of the supercurrent.

As mentioned above, the system is invariant under the transformation $d_x \leftrightarrow d_y, \alpha \leftrightarrow \beta, M_x \leftrightarrow M_y$ and hence we get the same expression for the long-ranged supercurrent with β instead of α if we set $\alpha = M_x = 0$ and keep β and M_y nonzero. This means that pure Dresselhaus spin-orbit coupling would also be sufficient to get a long-ranged supercurrent.

C. Numerical results

The weak proximity approximation is only valid if the magnitude of the elements of $\underline{f}$ are much smaller than unity which limits the choice of parameter values that can be explored. We will solve the full proximity effect Usadel equation numerically in this section, which is free from this restriction.

We will solve the problem by using the Riccati parameterization with spin-orbit coupling derived in Ref. [12],

$$\begin{aligned} D\left(\nabla^2\gamma + 2\left(\nabla\gamma\right)\tilde{N}\tilde{\gamma}\left(\nabla\gamma\right)\right) &= -2i\epsilon\gamma - i\boldsymbol{M}\cdot\left(\boldsymbol{\sigma}\gamma - \gamma\boldsymbol{\sigma}^*\right) \\ &+D\left(\underline{\boldsymbol{A}}^2\gamma - \gamma\left(\underline{\boldsymbol{A}}^*\right)^2 + 2\left(\underline{\boldsymbol{A}}\gamma + \gamma\underline{\boldsymbol{A}}^*\right)\tilde{N}\left(\underline{\boldsymbol{A}}^* + \tilde{\gamma}\underline{\boldsymbol{A}}\gamma\right)\right) \\ &+2iD\left(\left(\nabla\gamma\right)\tilde{N}\left(\underline{\boldsymbol{A}}^* + \tilde{\gamma}\underline{\boldsymbol{A}}\gamma\right) + \left(\underline{\boldsymbol{A}} + \gamma\underline{\boldsymbol{A}}^*\tilde{\gamma}\right)N\left(\nabla\gamma\right)\right). \end{aligned} \tag{36}$$

The corresponding equation for $\tilde{\gamma}$ can be found by tilde conjugating the equation above. Here, the Green's functions are given as $\underline{g} = N(1+\gamma\tilde{\gamma})$ and $\underline{f} = 2N\gamma$. And $N = (1-\gamma\tilde{\gamma})^{-1}$, and thus we need to solve for γ and $\tilde{\gamma}$. We will still be approximating the system to be one dimensional with the KL boundary conditions in the two nodes working as two sources of singlet states. The KL boundary conditions are

$$\frac{\partial}{\partial z}\gamma = \frac{1}{L\zeta}\left(1-\gamma\tilde{\gamma}_S\right)N_S\left(\gamma-\gamma_S\right) + i\underline{A}_z\gamma + i\gamma\underline{A}_z^* \tag{37}$$

where ζ is the ratio between the barrier resistance and the bulk resistance of the heavy metal, and L is the width of the normal metal and ferromagnetic layer which is $L = W + d$. γ_S and N_S are the Riccati parameters for the BCS bulk superconductor. Since the width W of the heavy metal and the ferromagnetic film is small, we will neglect the inverse proximity effect and use the bulk BCS Green functions in the superconductors. We will as in the last section use this boundary condition between the heavy metal and the superconductor an effective source of singlet state pairs. Since the normal vector of the interface points in the z-direction, we get $\underline{A}_z = 0$. The z-component of $\nabla^2\underline{\gamma}$ will be non-zero when averaged over the z-direction, and the effective Usadel equation becomes:

$$\begin{aligned} &D\Bigg[\frac{\partial^2}{\partial x^2}\gamma + \frac{1}{(W+d)\zeta}\left(1-\gamma\tilde{\gamma}_S\right)N_S\left(\gamma-\gamma_S\right) \\ &+2\left(\frac{\partial}{\partial x}\gamma\right)\tilde{N}\tilde{\gamma}\left(\frac{\partial}{\partial x}\gamma\right)\Bigg] \\ &= -2i\epsilon\gamma - i\boldsymbol{M}\cdot\left(\boldsymbol{\sigma}\gamma - \gamma\boldsymbol{\sigma}^*\right) \\ &+D\frac{d}{W+d}\Bigg[\underline{\boldsymbol{A}}^2\gamma - \gamma\left(\underline{\boldsymbol{A}}^*\right)^2 \\ &+2\left(\underline{\boldsymbol{A}}\gamma + \gamma\underline{\boldsymbol{A}}^*\right)\tilde{N}\left(\underline{\boldsymbol{A}}^* + \tilde{\gamma}\underline{\boldsymbol{A}}\gamma\right)\Bigg] \\ &+2iD\frac{d}{W+d}\Bigg[\left(\frac{\partial}{\partial x}\gamma\right)\tilde{N}_F\left(\underline{\boldsymbol{A}}^* + \tilde{\gamma}\underline{\boldsymbol{A}}\gamma\right) \\ &+\left(\underline{\boldsymbol{A}} + \gamma\underline{\boldsymbol{A}}^*\tilde{\gamma}\right)N\left(\frac{\partial}{\partial x}\gamma\right)\Bigg]. \end{aligned} \tag{38}$$

The corresponding equation for $\tilde{\gamma}$ can be found by tilde conjugation the equation above. By using the bulk BCS Green's function, we can easily calculate N_S and γ_S.

D. Parameters

We consider the system depicted in Fig. 1. We will assume that the the correlation length of the superconductor is $\xi_S = \sqrt{D/\Delta} = 25$ nm, where Δ is the superconducting gap energy. We will have the lengths $W = d = 2$ nm and $L = 25$ nm. This will give the ratio $\xi_S/L = 1$. We will also let the length of the spin-orbit coupled region be 5 nm, which gives us $G/L = 0.7$. The interface transparency will be $\zeta = 5$, and the exchange field is placed in the xy-plane $\boldsymbol{M} = M(\cos(\theta), \sin(\theta), 0)$. We normalize ϵ and M to the gap energy Δ. We choose a strong ferromagnet $M_F = 50\Delta$ and with $W = d$, the effective exchange field will be $M = 25\Delta$ in the two superconducting electrodes and $M = 50\Delta$ in the middle region. The value of the exchange field is reasonable considering an ultra-thin strong ferromagnet like cobalt in contact with a heavy metal like platinum [15]. The macroscopic phase difference has been set to $\Delta\phi = \phi_R - \phi_L = \pi/2$, while the temperature is $T = 0.5T_C$, and in addition, we will now only assume a pure Rashba coupling which we will normalize to the length of the ferromagnetic bridge L such that αL will be a dimensionless quantity. The spin-orbit coupling term is then

$$\underline{\boldsymbol{A}} = -\alpha\underline{\sigma}_y\boldsymbol{e}_x + \alpha\underline{\sigma}_x\boldsymbol{e}_y. \tag{39}$$

The supercurrent is plotted as a function of the exchange field angle θ and Rashba coupling in Fig. 2 and 3, respectively, where $I_0 = N_0DAe$. With Rashba coupling, we clearly see an enhanced supercurrent when the exchange field points in the x-direction ($\theta = 0$). There also seems to be a certain magnitude of the Rashba constant where the supercurrent is peaked when $\theta = 0$, namely at $\alpha L \approx 5$. Interestingly, we also

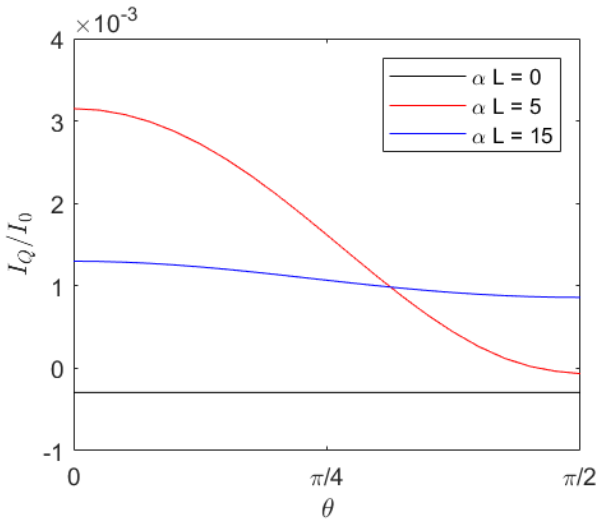

Figure 2. The supercurrent is plotted as a function of exchange field θ. When $\theta = 0$ the exchange field points along the x-direction, while $\theta = \pi/2$ corresponds to the exchange field pointing in the y-direction.

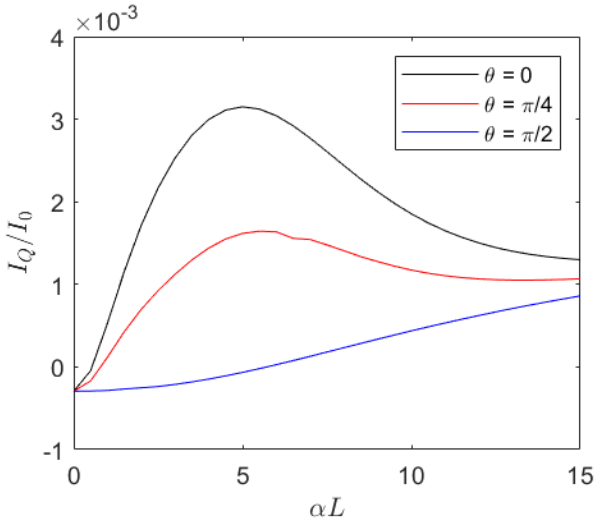

Figure 3. The supercurrent is plotted as a function of Rashba coupling α in the heavy metals.

see from Fig. 3 that we are able to create $0-\pi$ transitions when the strength of the Rashba coupling is $\alpha L \leq 6$. Thus, there exists an angle close to $\theta = \pi/2$ where the current is zero as long as $\alpha L < 6$. It also seems that the supercurrent becomes independent of θ when $\alpha L \to \infty$. This is, as we explained in the weak proximity limit, because the energy of the LRTs get an imaginary part which destroy the coherence of these components.

The supercurrent is also plotted as a function of the length of the ferromagnetic region in Fig. 4 where we have set $\alpha\xi = 5$. This choice corresponds to the maximum supercurrent in Fig. 3 when $L/\xi = 1$. We see that the supercurrent in the case of a pure x-directed exchange field ($\theta = 0$) decays much slower than in the case where the exchange field points along the y-axis ($\theta = \pi/2$). This is precisely due to the fact that the supercurrent is now carried by long-ranged triplet Cooper pairs. Note that the supercurrent rapidly changes sign when $\theta = \pi/2$ due to 0-π oscillations. In contrast, for $\theta = 0$ there is no $0-\pi$ transitions in the interval $0.5 < L/\xi < 2$. This allows for an interesting observation, namely that there exists several possible intervals of L/ξ where a 90 degree in-plane rotation of the magnetization essentially turns the supercurrent on and off.

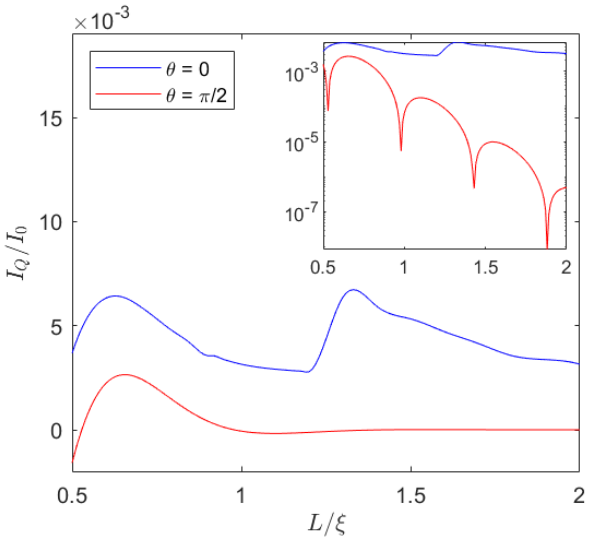

Figure 4. The supercurrent plotted as a function of the length of the ferromagnetic bridge L. The inset is a log-plot of the absolute value of the current and shows how vastly different the exponential decay is for the two in-plane directions of the exchange field are. The sharp dips in the log graph shows where the short ranged current switches sign.

IV. CONCLUDING REMARKS

We have shown that a lateral Josephson junction with spin-orbit coupled contacts to a ferromagnetic film that is magnetized in-plane is able to carry a long-ranged triplet supercurrent. This supercurrent is highly sensitive to the in-plane rotation of the magnetic field, and our system thus effectively acts as a magnetic transistor for the supercurrent. The main merit of our result is that the long-ranged triplet supercurrent is tuned with a single ferromagnetic layer without any requirement for an out-of-plane magnetization. We believe this could provide a way to realize tunable triplet supercurrents via Rashba spin-orbit coupling in a considerably simpler way than previous proposals.

ACKNOWLEDGMENTS

We thank Jabir Ali Ouassou and Morten Amundsen for useful discussions. This work was supported by the Research

Council of Norway through its Centres of Excellence funding scheme grant 262633 QuSpin. N.B. was supported by EPSRC New Investigator Award EP/S016430/1.

[1] K. K. Likharev, Sov. Tech. Phys. Lett. **2**, 12 (1976).

[2] J. Linder, and J. W. A. Robinson, *Superconducting Spintronics*, Nature Physics. **11**, 307 (2015).

[3] M. Eschrig, *Spin-polarized supercurrents for spintronics: a review of current progress*, Rep. Prog. Phys. **78**, 104501 (2015).

[4] J. W. A. Robinson, J. D. S. Witt, and M. G. Blamire, *Controlled Injection of Spin-Triplet Supercurrents into a Strong Ferromagnet*, Science **329**, 5987 (2010).

[5] T. S. Khaire, M. A. Khasawneh, W. P. Pratt, and N. O. Birge, *Observation of Spin-Triplet Superconductivity in Co-Based Josephson Junctions*, Phys. Rev. Lett. **104**, 137002 (2010).

[6] X. L. Wang, A. Di Bernardo, N. Banerjee, A. Wells, F. S. Bergeret, M. G. Blamire, and J. W. A. Robinson, *Giant triplet proximity effect in superconducting pseudo spin valves with engineered anisotropy*, Phys. Rev. B **89**, 140508(R) (2014)

[7] P. V. Leksin, N. N. Garifyanov, I. A. Garifullin, Ya. V. Fominov, J. Schumann, Y. Krupskaya, V. Kataev, O. G. Schmidt, and B. Bchner, *Evidence for Triplet Superconductivity in a Superconductor-Ferromagnet Spin Valve*, Phys. Rev. Lett. **109**, 057005 (2012).

[8] F. S. Bergeret, A. F. Volkov, and K. B. Efetov, *Odd triplet superconductivity and related phenomena in superconductor-ferromagnet structures*, Rev. Mod. Phys. **77**, 1321 (2005).

[9] N. Banerjee, J.W.A. Robinson, and M. G. Blamire, *Reversible control of spin-polarized supercurrents in ferromagnetic Josephson junctions* Nature Communications **5**, 4771 (2014).

[10] M. Houzet, *Ferromagnetic Josephson Junction with Precessing Magnetization*, Phys. Rev. Lett. **101**, 057009 (2008).

[11] F. S. Bergeret, and I. V. Tokatly, *Spin-orbit coupling as a source of long-range triplet proximity effect in superconductor-ferromagnet hybrid structures*, Phys. Rev. B. **89**, 134517 (2014).

[12] S. H. Jacobsen, J. A. Ouassou, and J. Linder, *Critical temperature and tunneling spectroscopy of superconductor-ferromagnet hybrids with intrinsic Rashba-Dresselhaus spin-orbit coupling*, Phys. Rev. B. **92**, 024510 (2015).

[13] N. Satchell, and N. O. Birge, *Supercurrent in ferromagnetic Josephson junctions with heavy metal interlayers*, Phys. Rev. B. **97**, 214509 (2018).

[14] N. Satchell, R. Loloee, N. O. Birge, *Supercurrent in ferromagnetic Josephson junctions with heavy metal interlayers. II. Canted magnetization*, arXiv:1904.08798

[15] N. Banerjee, J. A. Ouassou, Y. Zhu, N. A. Stelmashenko, J. Linder, and M. G. Blamire, *Controlling the superconducting transition by spin-orbit coupling*, Phys. Rev. B. **97**, 184521 (2018).

[16] S. Jacobsen, I. Kulagina, and J. Linder, *Controlling superconducting spin flow with spin-flip immunity using a single homogeneous ferromagnet*, Sci. Rep. **6**, 23926 (2016)

[17] E. Nakhmedov, O. Alekperov, F. Tatardar, Y. M. Shukrinov, I. Rahmonov, and K. Sengupta, *Effect of magnetic field and Rashba spin-orbit interaction on the Josephson tunneling between superconducting nanowires*, Phys. Rev. B. **96**, 014519 (2017).

[18] A. Costa, P. Högl, and J. Fabian, *Magnetoanisotropic Josephson effect due to interfacial spin-orbit fields in superconductor/ferromagnet/superconductor junctions*, Phys. Rev. B. **95**, 024514 (2017).

[19] A. Buzdin, *Direct Coupling Between Magnetism and Superconducting Current in the Josephson φ_0 Junction*, Phys. Rev. Lett. **101**, 107005 (2008).

[20] J. Arjoranta, T. T. Heikkilä, *Intrinsic spin-orbit interaction in diffusive normal wire Josephson weak links: Supercurrent and density of states*, Phys. Rev. B. **93**, 024522 (2016).

[21] W. Belzig, F. K. Wilhelm, C. Bruder, G. Schn, . D. Zaikin, *Quasiclassical Greens function approach to mesoscopic superconductivity*, Superlattices and Microstructures. **25**, 56 (1999).

[22] J. Rammer and H. Smith *Quantum field-theoretical methods in transport theory of metals*, Rev. Mod. Phys. **58**, 323 (1986).

[23] K. D. Usadel, *Generalized Diffusion Equation for Superconducting Alloys*, Phys. Rev. Lett. **25**, 507 (1970).

[24] M. Yu. Kupriyanov, and V. F. Lukichev, *Influence of boundary transparency on the critical current of "dirty" SS'S structures*, Zh. Eksp. Teor. Fiz. **94**, 139 (1988).

[25] I. Gomperud, and J. Linder, *Spin supercurrent and phase-tunable triplet Cooper pairs via magnetic insulators*, Phys. Rev. B. **92**, 035416 (2015).

[26] A. J. Leggett, *A theoretical description of the new phases of liquid 3He*, Rev. Mod. Phys. **47**, 331 (1975).

Bibliography

[1] M. Y. Kupriyanov, and V. F. Lukichev, *Influence of boundary transparency on the critical current of "dirty" SS'S structures*, Zh. Eksp. Teor. Fiz. 94, 139 (1988).

[2] B. D. Josephson, *Possible new effects in superconductive tunnelling*, Phys. Lett. 1, 7 (1962).

[3] M. Tinkham, *Introduction to Superconductivity*, (Dover Publications, 1996).

[4] V. Ambegaokar, and A. Baratoff, *Tunneling Between Superconductors*, Phys. Rev. Lett. 11, 104 (1963).

[5] A. F. Andreev, *The Thermal Conductivity of the Intermediate State in Superconductors*, Sov. Phys. JETP. 19, 1228 (1964).

[6] J. P. Morten, *Spin and Charge Transport in Dirty Superconductors*, Master's Thesis, Norwegian University of Science and Technology, (2003).

[7] M. Houzet, *Ferromagnetic Josephson Junction with Precessing Magnetization*, Phys. Rev. Lett. 101, 057009 (2008).

[8] S. H. Jacobsen, J. A. Ouassou, and J. Linder, *Critical temperature and tunneling spectroscopy of superconductor-ferromagnet hybrids with intrinsic Rashba-Dresselhaus spin-orbit coupling*, Phys. Rev. B. 92, 024510 (2015).

[9] R. Holm, and W. Meissner, *Messungen mit Hilfe von flüssigem Helium. XIII*, Z. Phys. 74, 715 (1932).

[10] A. T. Filippov, *The Versatile Soliton*, page 213-214, (Birkhäuser Basel, 2010).

[11] A. J. Leggett, *A theoretical description of the new phases of liquid 3He*, Rev. Mod. Phys. 47, 331 (1975).

[12] H. Bruus, and K. Flensberg, *Many-Body Quantum Theory in Condensed Matter Physics - An Introduction*, (Oxford Graduate Text, 2016).

[13] T. Yokoyama, and Y. Tserkovnyak, *Tuning odd triplet superconductivity by spin pumping*, Phys. Rev. B. 80, 104416 (2009).

[14] M. V. Costache, M. Sladkov, S. M. Watts, C. H. van der Wal, and B. J. van Wees, *Electrical Detection of Spin Pumping due to the Precessing Magnetization of a Single Ferromagnet*, Phys. Rev. Lett. 97, 216603 (2006).

[15] T. Moriyama, R. Cao, X. Fan, G. Xuan, B. K. Nikolic, Y. Tserkovnyak, J. Kolodzey, and J. Q. Xiao, *Tunnel Barrier Enhanced Voltage Signal Generated by Magnetization Precession of a Single Ferromagnetic Layer*, Phys. Rev. Lett. 100, 067602 (2008).

[16] S. H. Jacobsen, J. A. Ouassou, and J. Linder, *Advanced Magnetic and Optical Materials*, Chapter: 1 - Superconducting Order in Magnetic Heterostructures, (Wiley, 2016).

[17] M. N. Baibich, J. M. Broto, A. Fert, F. Nguyen Van Dau, F. Petroff, P. Etienne, G. Creuzet, A. Friederich, and J. Chazelas, *Giant Magnetoresistance of (001)Fe/(001)Cr Magnetic Superlattices*, Phys. Rev. Lett. 61, 2472 (1988).

[18] J. Linder, and J. W. A. Robinson, *Superconducting Spintronics*, Nature Physics. 11, 307. (2015).

[19] V. Chandrasekhar, *An introduction to the quasiclassical theory of superconductivity for diffusive proximity-coupled systems*, arXiv:cond-mat/0312507v2 (2004).

[20] A. Schmid, and G. Schön, *Linearized kinetic equations and relaxation processes of a superconductor near Tc*, J. Low. Temp. Phys. 20, 207 (1972).

[21] J. A. Ouassou, T. D. Vethaak, and J. Linder, *Voltage-induced thin-film superconductivity in high magnetic fields*, Phys. Rev. B. 98, 144509 (2018).

[22] J. A. Ouassou, https://github.com/jabirali/GENEUS .

[23] F. S. Bergeret, A. F. Volkov, and K. B. Efetov, *Odd triplet superconductivity and related phenomena in superconductor-ferromagnet structures*, Rev. Mod. Phys. 77, 1321 (2005).

[24] M. Eschrig, *Spin-polarized supercurrents for spintronics*, Physics Today. 64, 1 (2011).

[25] P. Fulde, and R. A. Ferrell, *Superconductivity in a Strong Spin-Exchange Field*, Phys. Rev. 135, A550 (1964).

[26] A.I Larkin, and Y. N. Ovchinnikov, Zh. Eksp. Teor. Fiz. 47, 1136 (1964).

[27] I. Gomperud, and J. Linder, *Spin supercurrent and phase-tunable triplet Cooper pairs via magnetic insulators*, Phys. Rev. B. 92, 035416 (2015).

[28] F. S. Bergeret, A. F. Volkov, and K. B. Efetov, *Josephson current in superconductor-ferromagnet structures with a nonhomogeneous magnetization*, Phys. Rev. B. 64, 134506 (2001).

[29] F. S. Bergeret, and I. V. Tokatly, *Spin-orbit coupling as a source of long-range triplet proximity effect in superconductor-ferromagnet hybrid structures*, Phys. Rev. B. 89, 134517 (2014).

[30] G. Dresselhaus, *Spin-Orbit Coupling Effects in Zinc Blende Structures*, Phys. Rev. 100, 580 (1955).

[31] E. Rashba, Sov. Phys. Solid State. 2, 1109 (1960).

[32] N. Banerjee, J. A. Ouassou, Y. Zhu, N. A. Stelmashenko, J. Linder, and M. G. Blamire, *Controlling the superconducting transition by spin-orbit coupling*, Phys. Rev. B. 97, 184521 (2018).

[33] J. Rammer, and H. Smith, *Quantum field-theoretical methods in transport theory of metals*, Rev. Mod. Phys. 58, 2 (1986).

[34] M. Amundsen, *Quasiclassical Theory Beyond 1D: Supercurrents and Topological Excitations*, Master's Thesis, Norwegian University of Science and Technology, (2016).

[35] W. L. McMillan, *Transition Temperature of Strong-Coupled Superconductors*, Phys. Rev. 167, 331 (1968).

[36] F. S. Bergeret, and I. V. Tokatly, *Singlet-Triplet Conversion and the Long-Range Proximity Effect in Superconductor-Ferromagnet Structures with Generic Spin Dependent Fields*, Phys. Rev. Lett. 110, 117003 (2013).

[37] I. V. Bobkova, and A. M. Bobkov, *Long-Range Proximity Effect for Opposite-Spin Pairs in Superconductor-Ferromagnet Heterostructures Under Nonequilibrium Quasiparticle Distribution*, Phys. Rev. Lett. 108, 197002 (2012).

[38] G. Annunziata, M. Cuoco, C. Noce, A. Sudbø, and J. Linder, *Spin-sensitive long-range proximity effect in ferromagnet/spin-triplet-superconductor bilayers*, Phys. Rev. B. 83, 060508 (2011).

[39] W. Belzig, F. K. Wilhelm, C. Bruder, G. Schön, and A. D. Zaikin, *Quasiclassical Green's function approach to mesoscopic superconductivity*, Superlattices and Microstructures. 25, 5 (1999).

[40] P.G. de Gennes, *Superconductivity Of Metals And Alloys*, (Benjamin, 1966).

[41] F. Altomare, and A. M. Chang, *One-Dimensional Superconductivity in Nanowires*, (Wiley, 2013).

[42] G. Eilenberger, *Transformation of Gorkov's equation for type II superconductors into transport-like equations*, Z. Phys. 214, 195 (1968).

[43] K. D. Usadel, *Generalized Diffusion Equation for Superconducting Alloys*, Phys. Rev. Lett. 25, 507 (1970).

[44] J. Rammer, *Quantum Field Theory of Non-equilibrium States*, (Cambridge University Press, 2007).

[45] S. Shapiro, *Josephson Currents in Superconducting Tunneling: The Effect of Microwaves and Other Observations*, Phys. Rev. Lett. 11, 80 (1963).

[46] S. Strogatz, *Sync: The Emerging Science of Spontaneous Order*, (Hyperion, 2003).

[47] T. Yamashita, K. Tanikawa, S. Takahashi, and S. Maekawa, *Superconducting π Qubit with a Ferromagnetic Josephson Junction*, Phys. Rev. Lett. 95, 097001 (2005).

[48] M. A. Nielsen, and I. L. Chuang, *Quantum Computation and Quantum Information*, (Cambridge University Press, 2000).

[49] Y. Nakamura, C. D. Chen, and J. S. Tsai, *Spectroscopy of Energy-Level Splitting between Two Macroscopic Quantum States of Charge Coherently Superposed by Josephson Coupling*, Phys. Rev. Lett. 79, 2328 (1997).

[50] J. M. Martinis, and K. Osborne, *Superconducting Qubits and the Physics of Josephson Junctions*, arXiv, arXiv:cond-mat/0402415v1 (2004).

[51] J. Bardeen, L. N. Cooper, and J. R. Schrieffer, *Microscopic Theory of Superconductivity*, Phys. Rev. 106, 162 (1957).

[52] L. N. Cooper, *Bound Electron Pairs in a Degenerate Fermi Gas*, Phys. Rev. 104, 1189 (1956).

[53] S. Hikino, M. Mori, S. Takahashi, and S Maekawa, *Ferromagnetic Resonance Induced Josephson Current in a Superconductor/Ferromagnet/Superconductor Junction*, J. Phys. Soc. Jpn. 77, 053707 (2008).

[54] A. Ikushima, and T. Mizusaki, *Superconductivity in Niobium and Niobium-Tantalum Alloys*, J. Phys. Chem. Solids. 30, 873 (1969).

[55] M. Eschrig, A. Cottet, W. Belzig, and J. Linder, *General Boundary Conditions for Quasiclassical Theory of Superconductivity in the Diffusive Limit: Application to Strongly Spin-polarized Systems*, New J. Phys. 17, 083037 (2015).

[56] Y V.. Nazarov, *Novel circuit theory of Andreev reflection*, Superlattices and Microstructures. 25, 5 (1999).

[57] C. W. J. Beenakker, *Random-matrix theory of quantum transport*, Rev. Mod. Phys. 69, 731 (1997).

[58] Y. V. Nazarov, and Y. M. Blanter, *Quantum transport*, (Cambridge University Press, 2009).

[59] J. C. Cuevas, J. Hammer, J. Kopu, J. K. Viljas, and M. Eschrig, *Proximity effect and multiple Andreev reflections in diffusive superconductor–normal-metal–superconductor junctions*, Phys. Rev. B 73, 184505 (2006).

[60] K. S. Tikhono, and M. V. Feigel'man. *AC Josephson effect in the long voltage-biased SINIS junction*, JETP Letters, 89, 4 (2009).

[61] A. A. Jara, C. Safranski, I. N. Krivorotov, C. T. Wu, A. N. Malmi-Kakkada, O. T. Valls, and K. Halterman, *Angular dependence of superconductivity in superconductor/spin-valve heterostructures*, Phys. Rev. B. 89, 184502 (2014).

[62] Z. Nussinov, A. Shnirman, D. P. Arovas, A. V. Balatsky, and J. X. Zhu, *Spin and spin-wave dynamics in Josephson junctions*, Phys. Rev. B. 71, 214520 (2005).

[63] R. C. Dynes, J. P. Garno, G. B. Hertel, and T. P. Orlando, *Tunneling Study of Superconductivity near the Metal-Insulator Transition*, Phys. Rev. Lett. 53, 2437 (1984).

[64] T. Wakamura, H. Akaike, Y. Omori, Y. Niimi, S. Takahashi, A. Fujimaki, S. Maekawa, and Y. Otani, *Quasiparticle-mediated spin Hall effect in a superconductor*, Nature Materials. 14, 675 (2015).

[65] H. Yang, S. H. Yang, S. Takahashi, S. Maekawa, and S. S. P. Parkin, *Extremely long quasiparticle spin lifetimes in superconducting aluminium using MgO tunnel spin injectors*, Nature Materials. 9, 586 (2010).

[66] S. Kolenda, M. J. Wolf, and D. Beckmann, *Observation of Thermoelectric Currents in High-Field Superconductor-Ferromagnet Tunnel Junctions*, Phys. Rev. Lett. 116, 097001 (2016).

[67] V. V. Ryazanov, V. A. Oboznov, A. Yu. Rusanov, A. V. Veretennikov, A. A. Golubov, and J. Aarts, *Coupling of Two Superconductors through a Ferromagnet: Evidence for a* Π *Junction*, Phys. Rev. Lett. 86, 2427 (2001).

[68] L. D. Landau, and E. M. Lifshitz, *Theory of the dispersion of magnetic permeability in ferromagnetic bodies*, Phys. Z. Sowjetunion. 8, 153 (1935).

[69] M. Amundsen, and J. Linder, *General solution of 2D and 3D superconducting quasiclassical systems: coalescing vortices and nanoisland geometries*, Scientific Reports. 6, 22765 (2016).

[70] C. Holmqvist, S. Teber, and M. Fogelström, *Nonequilibrium effects in a Josephson junction coupled to a precessing spin*, Phys. Rev. B 83, 104521 (2011).

[71] S. H. Jacobsen, I. Kulagina, and J. Linder, *Controlling superconducting spin flow with spin-flip immunity using a single homogeneous ferromagnet*, Scientific Reports. 6, 23926 (2016).

[72] A. Manchon, H. C. Koo, J. Nitta, S. M. Frolov, and R. A. Duine, *New perspectives for Rashba spin–orbit coupling*, Nature Materials. 14, 871 (2015).

[73] M. Eschrig, *Distribution functions in nonequilibrium theory of superconductivity and Andreev spectroscopy in unconventional superconductors*, Phys. Rev. B. 61, 9061 (2000).

[74] B. Pannetier, and H. Courtois, *Andreev Reflection and Proximity effect*, arXiv, arXiv:cond-mat/9912024v2 (1999).

[75] K. Fossheim, and A. Sudbø, *Superconductivity: Physics and Applications*, (Wiley, 2004).

[76] L. L. Li, Y. L. Zhao, X. X. Zhang, and Y. Sun, *Possible Evidence for Spin-Transfer Torque Induced by Spin-Triplet Supercurrents*, Chinese Physics Letters. 35, 7 (2018).

[77] C. Bell, S. Milikisyants, M. Huber, and J. Aarts, *Spin Dynamics in a Superconductor-Ferromagnet Proximity System*, Phys. Rev. Lett. 100, 047002 (2008).

[78] S. Teber, C. Holmqvist, and M. Fogelström, *Transport and magnetization dynamics in a superconductor/single-moleculemagnet/superconductor junction*, Phys. Rev. B. 81, 174503 (2010).

[79] K. R. Jeon, C. Ciccarelli, A. J. Ferguson, H. Kurebayashi, L. F. Cohen, X. Montiel, M. Eschrig, J. W. A. Robinson, and M. G. Blamire, *Enhanced spin pumping into superconductors provides evidence for superconducting pure spin currents*, Nature Materials. 17, 499 (2018).

[80] M. Amundsen, and J. Linder, *The quasiclassical theory for interfaces with spin-orbit coupling*, arXiv, arXiv:1904.11986v1 (2019).

[81] J. A. Ouassou, J. W. A. Robinson, and J. Linder, *Controlling spin supercurrents via nonequilibrium spin injection*, arXiv, arXiv:1810.08623v2 (2019).

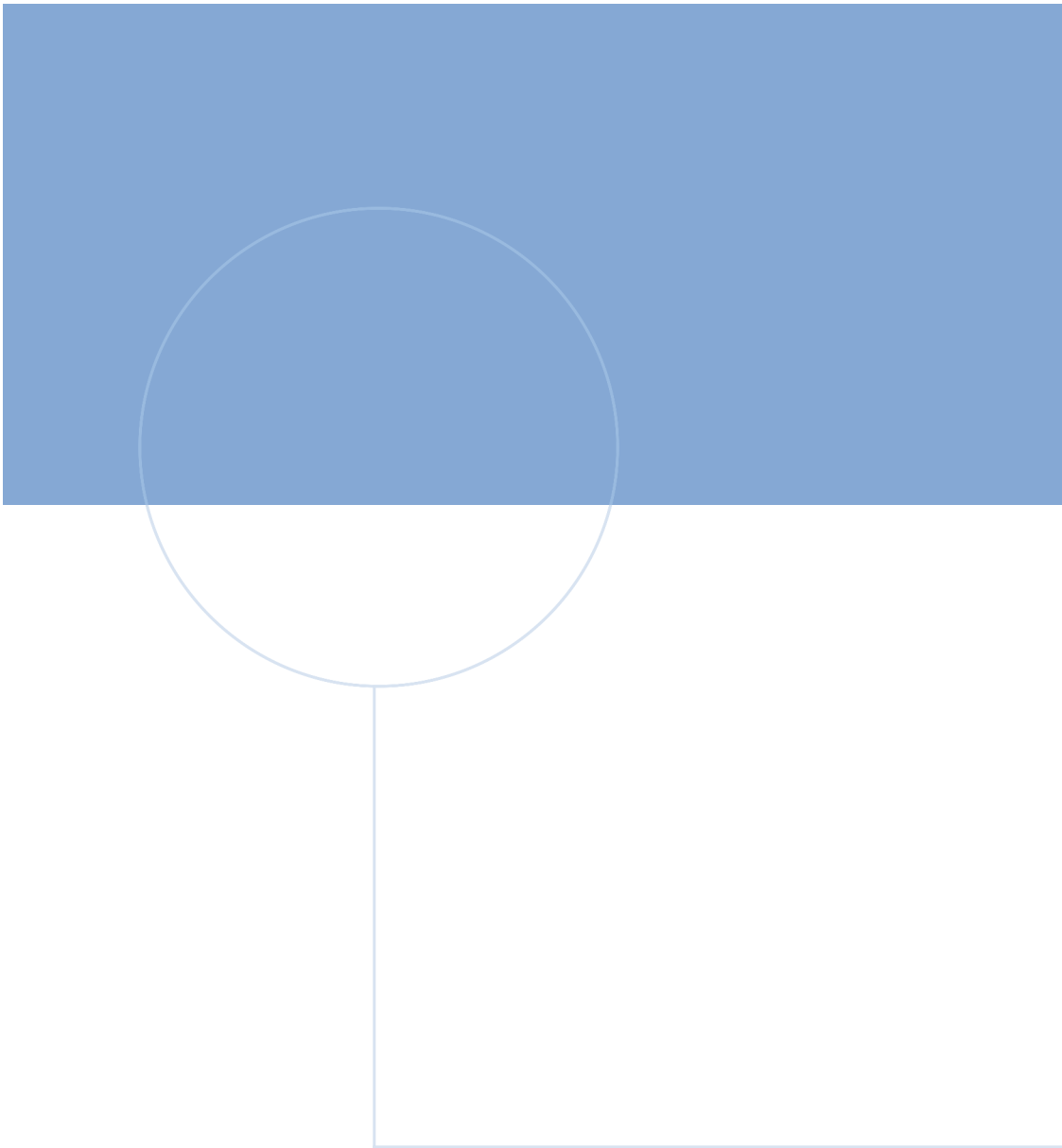

NTNU
Norwegian University of
Science and Technology